Technical Report Documentation Page

1. Report No.	2. Government Accession No.	3. Recipient's Catalog No.
CG-D-37-82	AD A120824	

4. Title and Subtitle	5. Report Date
Study of Reradiation of Loran-C in a Harbor Environment	8 June 1982
	6. Performing Organization Code

7. Author(s)	8. Performing Organization Report No.
Valdis V. Liepa and Robert L. Frank	018958-1-F

9. Performing Organization Name and Address	10. Work Unit No. (TRAIS)
Radiation Laboratory (ECE) The University of Michigan Ann Arbor, MI 48109	11. Contract or Grant No. DTCG23-81-C-20012

12. Sponsoring Agency Name and Address	13. Type of Report and Period Covered
U.S. Department of Transportation United States Coast Guard Office of Research and Development Washington, DC 20590	Final Report April 1981 to June 1982
	14. Sponsoring Agency Code

15. Supplementary Notes

Robert L. Frank was subcontractor to the University of Michigan. His address is 30795 River Crossing, Birmingham, MI 48010

16. Abstract

A study is made of the degradation of Loran-C accuracy near overhead conductors such as bridges and power lines. Using a small scale model of the Golden Gate Bridge, amplitude and phase measurements were performed for numerous illumination and position bearings at a variety of distances from the bridge. By sweeping frequency over a 5:1 range, one model simulated a 5:1 range of bridge sizes. The data confirm that up to resonance the large structures can produce large errors (the Golden Gate and Verrazano Narrows bridges are only ten percent below resonant size at 100 kHz) and the smaller bridges produce much smaller errors. The directions of wave incidence and measurement relative to the bridge greatly affect the error, with broadside incidence being worst. The data are compared with full scale measurements. To improve the understanding of how the errors occur, measurements were carried out using (modified) bridge models with insulators replacing metallic portions. The relationship between reradiation from bridges and power lines is discussed and similarities noted. Some preliminary suggestions for reducing the errors are made, with suggestions for future work. An extensive literature review and bibliography are included.

17. Key Words		18. Distribution Statement
Loran-C	Radio navigation	Document is available to the U.S. public through the National Technical Information Service, Springfield, Virginia 22161
Reradiation	Radio propagation	
Scattering	Model measurements	

19. Security Classif. (of this report)	20. Security Classif. (of this page)	21. No. of Pages	22. Price
Unclassified	Unclassified	237	

Form DOT F 1700.7 (8-72) Reproduction of completed page authorized

AE 483-2-69

PROJECT UMPIRE

University of Michigan Probe for Interplanetary

Research and Exploration

A Student Design Project

Department of Aerospace Engineering

University of Michigan

Winter Term 1969

FOREWORD

Project UMPIRE is the ninth in a series of preliminary design feasibility studies conducted in Aerospace Engineering 483. Previous studies have included a Mars probe, solar probe, polar-orbiting meteorological and earth resources satellites and a geostationary communications satellite.

In this senior elective course, over a period of fifteen weeks, the students are given a problem statement with specific constraints. In the current problem a Jupiter fly-by probe, Atlas/Centaur launched, was specified for initial exploratory measurements in the Jovian environment. The interplay between sensors, data handling, trajectory, communications, power, weight and volume, etc., was then investigated and the spacecraft configuration determined.

The students set up their project organization and meet two afternoons a week as a team and during weekends as sub-groups to coordinate the critical interface between all groups. The emphasis is on team effort and team results with a high degree of mutual interdependence.

Guest lectures by the faculty, university research specialists, industry and government specialists are given and supplemented with small group conferences. The student is given the opportunity to apply his previous theoretical and analytical course work to the highly redundant field of preliminary design. He is also in active contact with professional experts in the field. Despite the short time available, it has been found possible to select current problems of national interest and make significant progress--as this report will demonstrate.

Wilbur C. Nelson
Professor

ABSTRACT

Project UMPIRE (University of Michigan Probe for Interplanetary Research and Exploration) is an engineering proposal for a deep-space Jupiter fly-by probe. The goals of the probe are two-fold: the primary mission objective will be achieved as the spacecraft flies by Jupiter and a rather detailed investigation of the planet is made, and the secondary objective will be realized as various measurements of the vast interplanetary region are made during the journey from Earth to Jupiter and in the post-encounter trajectory.

The 51.5 pound scientific package includes a magnetometer, a set of low energy radiation experiments, a micrometeoroid detector, a plasma probe, a radio propagation experiment, an infrared radiometer, a cosmic ray detector, a photometer, and an astronomy experiment.

The communications system is compatible with the Deep Space Instrumentation Facility (DSIF), and will use the 85 foot dish antennas during launch and cruise, and the 210 foot antennas during the critical encounter phase. A sixteen foot parabolic high gain antenna will be the main transmission antenna from the spacecraft. At encounter with Jupiter approximately 79 minutes are required for transmission of commands from Earth to the spacecraft and back to Earth, and at five astronomical units communications is capable of transmitting 1664 bits per second with the 210 foot DSIF antennas receiving.

During period when transmission to the DSIF network is impossible due to excessive solar interference, Jovian radio noise, and the approximately 90 minute encounter occultation, data will be stored for future transmission. Onboard magnetic tape recorders will provide a data storage element with a capacity of 3.5×10^9 bits. Assuming the 210 foot antennas will be available for 16 hours a day, it will take 9.2 days following encounter with Jupiter to transmit the stored data, using data compression.

The instrument package of UMPIRE is cylindrically shaped (62 inches in diameter and 17 inches high, including micrometeoroid protection) and is constructed of aluminum alloy; the total weight of the spacecraft is 462 pounds. The spacecraft will be spin-stabilized with the spin axis pointing toward Earth about one day after the launch. Onboard power will be supplied by three SNAP-19 Radioisotope Thermoelectric Generators with TAGS-2N thermoelectrics, using $^{238}PuO_2$ as the energy source. An active system of three bimetallic louvers will be used for thermal control. The spacecraft need not have sterilization or germicidal constraints imposed since it will not be impacting Jupiter.

As presently planned, the Atlas SLV-3C/Centaur/Burner II-SS launch system will thrust the spacecraft into space from the Eastern Test Range early in 1972, with the nominal launch date 4 March 1972.

TABLE OF CONTENTS

1
INTRODUCTION

1.1 SCIENTIFIC GOALS OF DEEP SPACE INVESTIGATIONS

Deep space investigations ultimately seek to provide a greater understanding of the origin, operation, and evolution of our solar system and of the galactic medium. Since successful missions have already been flown to Venus and Mars, our nearest neighbors, it is considered highly desirable to extend our investigations farther into the solar system by means of a deep-space Jupiter fly-by probe. The goals of such a probe would be twofold: as the spacecraft flew by Jupiter the primary mission objective would be achieved as a detailed investigation of the planet would be made, and during the journey from the Earth to Jupiter a secondary objective would be fulfilled as various measurements of the vast interplanetary region would be made.

Jupiter itself is an extremely interesting planet. It is the largest planet in our solar system, and is the innermost of the nonterrestial type planets, located approximately five astronomical units (A. U.) from the sun (Figure 1. 1). Jupiter occupies more than twice the total volume of the other planets. Its large mass (more than three hundred times the mass of Earth) and low mean density (only about one-fourth the density of Earth) indicate that the present chemical composition of Jupiter may be very similar to the composition prevalent at the time of formation of the planet, and that the chemical abundancies of Jupiter may be more solar-like than Earth-like. Finally, Jupiter is the only other planet in our solar system besides Earth which is suspected to have a large magnetic field and magnetosphere, perhaps similar to Earth.

Earth-based observations of Jupiter have only whetted scientific appetite for knowledge concerning Jupiter. A close study of Jupiter (with the initial fly-by probe affording preliminary data, and later missions yielding more definitive data) could help to answer such queries as the cause of the wandering Great Red spot, and whether magnetic anomalies are associated with such observable features; the prediction of the erratic decameter radio noise storms, and the nature of the influence of the satellite I_o on the decametric radiation; the existence or nonexistence of a solid planetary surface; the nature of the magnetic field; the characteristics of the trapped radiation belts; and the possible presence of an internal heat source. In addition, information could be obtained concerning the composition of the Jovian atmosphere; the nature of the Jovian biosphere, if it exists; and the Jovian ionosphere, and its distribution of thermal plasma at great distances from the planet.

Investigations of the interplanetary region can be made between Earth and Jupiter and in all post-encounter trajectories. It should be possible to obtain information on questions such as the termination point of the solar wind; the variation of interplanetary particle fluxes and magnetic fields with the distance from the sun and with time; the path of solar cosmic rays through interplanetary space; the effect of interstellar and interplanetary magnetic fields on galactic cosmic rays; the distribution and physical characteristics of micrometeoroids in interplanetary space; and the magnitude of the hazards posed to spacecraft by cosmic dust and asteroid belts.

In addition to the previously mentioned investigations, the Jupiter probe would also allow improved determination of solar system physical constraints and planetary ephemerides. Precision tracking data from such flights should yield information valuable in deriving improved mass determinations and ephemerides for Jupiter and for the Earth-moon system, an improved value for the astronomical unit, and other physical determinations of scientific and practical significance. This should significantly reduce the current space navigation problems resulting from an inadequate knowledge of planetary motions and gravitational effects, and the new information may be of sufficient precision to permit testing of basic physical theories.

1.2 DESIGN PHILOSOPHY

1.2.1 Definition of Mission

Project UMPIRE is a preliminary feasibility and design study for a Jupiter fly-by deep-space probe. Our intent is to formulate a system for the first such mission, and hence the function of the mission is envisioned as both the acquisition of a broad range of scientific data, and the establishment of boundaries within which subsequent missions can make more accurate measurements. In order to meet our projected launch date, within a launch window from the latter part of February to the middles of March in 1972, we must necessarily work as much as possible within the state-of-the-art; little or no development should be required. Since this is an initial probe, and there is some risk concerned with the success of the mission, the spacecraft should be of low cost and should be compatible with a relatively inexpensive launch vehicle. Finally, in order to assure the highest possible reliability, we must seek to use simple concepts.

1.2.2 Constraints

We have placed the following constraints on our system:

1) Be compatible with the Atlas SLV-3C/Centaur/Burner II-SS launch vehicle,

2) Be compatible with the Deep Space Instrumentation Facility (DSIF),
3) Provide sufficient thermal control to assure operating temperature for the scientific instruments,
4) Operate in space for at least three years,
5) Provide a data system to sample radings from the instrumentation and to transmit the information to Earth, and
6) Provide a command system to permit changes in operating modes of onboard equipment by ground command.

Compatibility with the Atlas SLV-3C/Centaur/Burner II-SS launch system imposes further restrictions upon the system. First, the weight of the spacecraft and scientific instruments must not exceed 500 lb. Second, the vibration, acceleration, and shock loads induced by the launch vehicle will place requirements on the mechanical integrity of the spacecraft and scientific instruments.

Compatibility with the DSIF space network requires that the communication system operate at S-band frequencies. In addition, the downlink frequency must be able to operate at a fixed ratio of the uplink frequency, so that accurate Doppler measurements can be made and the spacecraft velocity relative to the Earth can be measured for trajectory determination.

The constraint of a minimum lifetime in space of three years has been imposed in order to allow sufficient time for the journal from Earth to Jupiter, which requires 590 days from the nominal launch date of 4 March 1972, and time for transmission of data following the encounter with Jupiter. Additional time has been allotted as a safety factor and to allow additional interplanetary measurements to be made.

1.3 GENERAL DESCRIPTION OF MISSION

As presently planned, the probe will be launched from the Eastern Test Range early in 1972, with a launch window extending from the latter part of February until the middle of March. The next available launch window is in April of 1973, since an opposition of Earth and Jupiter occurs only every thirteen months.

The launch vehicle will be the Atlas SLV-3C/Centaur/Burner II-SS launch system. The spacecraft itself is cylindrically shaped. The spacecraft will be spin-stabilized with the spin axis pointing toward Earth about one day after the launch. Thermal control is provided by superinsulation and by an active system of bimetallic louvers. The DSIF space network will be used to communicate with the spacecraft during the mission, and a sixteen foot parabolic high gain antenna will be used as the main transmission antenna.

Onboard power will be furnished by three SNAP-19 Radioisotope Thermoelectric Generators (RTG's) with TAGS-2N thermoelectrics, using $^{238}PuO_2$ as the energy source; these will be mounted on booms and folded below the spacecraft and then deployed after ejection and separation of Burner II-SS. It was decided to use RTG's rather than solar panels because of the long duration of the mission and the distance to be travelled from the sun (5 A. U.). RTG's are compact, reliable, and provide for direct conversion power for extended periods of time; in addition, the RTG's have no unusually vulnerable areas which would be susceptible to meteoroid or asteroid damage in space, such as would be encountered in the Jupiter probe. Since Project UMPIRE is an initial probe, it is especially suited for testing of the RTG power system (since the RTG system has been flown only once); should the RTG's prove effective and reliable on Project UMPIRE, it would then be possible to employ them with greater assurance in future interplanetary explorations.

Since Project UMPIRE is an initial probe, the scientific package has been chosen to obtain abroad sampling of data from both the interplanetary region and the Jovian environment. Experiments which have been chosen as most meaningful and which integrate most readily with the spacecraft system are: a magnetometer, a set of low energy radiation experiments, a micro-meteoroid detector, a plasma probe, a radio propagation experiment, an infrared radiometer, a cosmic ray detector, a photometer, and an astronomy experiment.

1.4 REFERENCES

Clark, J. F., E. W. Hymowitz, and J. H. Trainor, "Galactic Jupiter Probes, Goddard Space Flight Center, NASA Document No. X-100-67-211, March 1967.

"Experimenter Planning Document for Proposed Pioneer F/G Missions," Ames Research Center, NASA Document No. P-200, October 18, 1968.

"Galactic Jupiter Probe Program Concept," Goddard Space Flight Center, NASA, March 1967.

"Handbook of the Physical Properties of the Planet Jupiter," NASA Document No. SP-3031, 1967.

"Phase A Report, Galactic Jupiter Probe," volume 1, Goddard Space Flight Center, NASA Document No. X-701-67-566, November 1967.

"Preliminary Progress Report, Galactic/Jupiter Probe Study," Lockheed Missiles and Space Company, LMSC-A848035, June 30, 1967

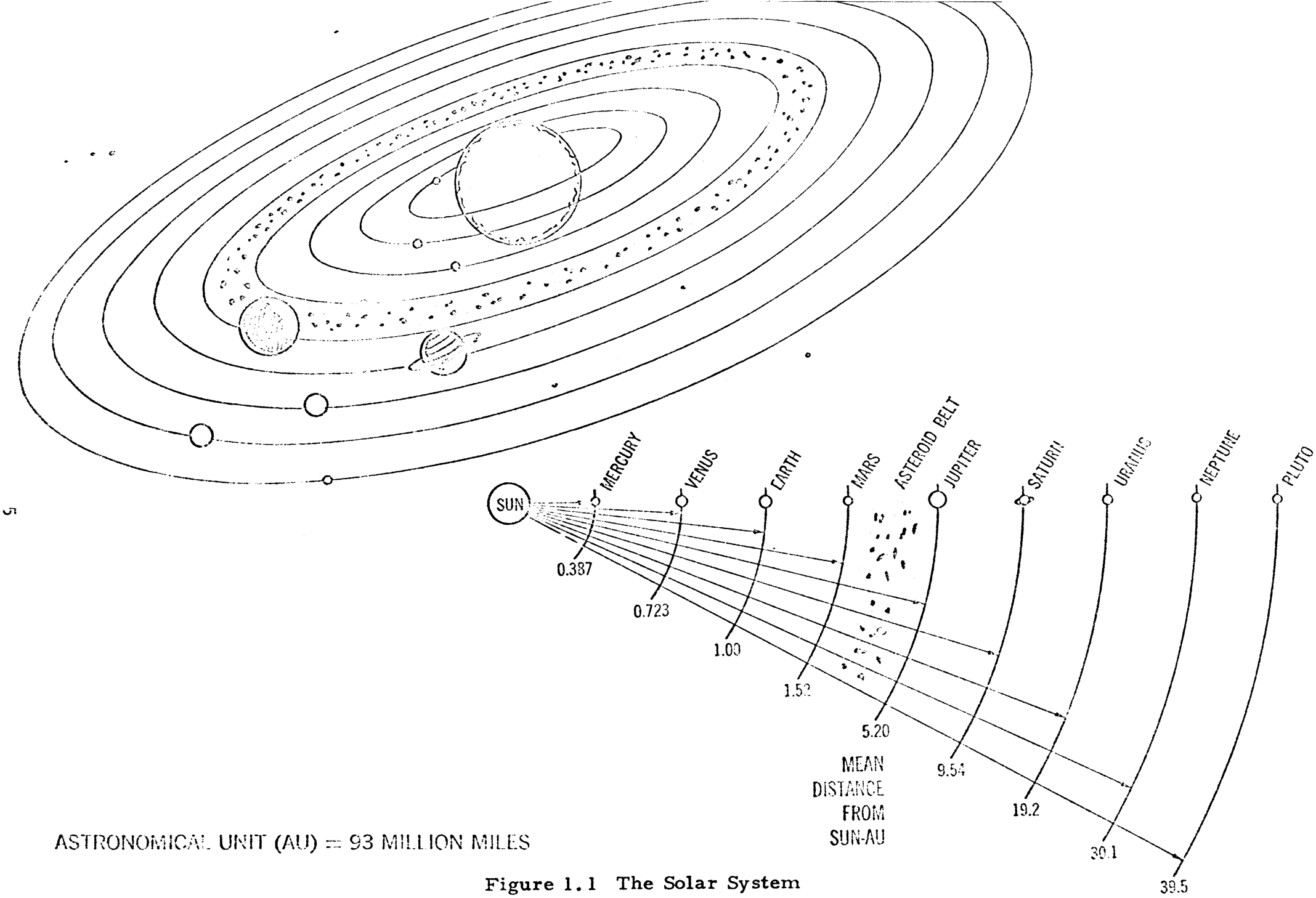

Figure 1.1 The Solar System

2
SCIENCE PAYLOAD

2.1 INTRODUCTION

Since Project UMPIRE will be the first Jupiter Fly-by probe, the selection of the science payload has been governed by two major objectives: (1) Determination of the conditions and phenomena occurring in deep space and (2) Measurements of the Jovian environment. All but one of the scientific experiments chosen for this mission has the capability of fulfilling both objectives. The exception is the infrared radiometer, used for temperature measurements at Jupiter. UMPIRE's science payload will require a minimum amount of integration complexity with the spacecraft and will gather a broad sampling of scientific data throughout the entire flight. A primary purpose of these scientific measurements will be to provide guidelines for future experiments to follow in making more accurate investigations of the phenomena involved.

2.1.1 Experiments

A specific set of instruments has been selected to achieve the mission outlined above. These instruments are:

1) A triaxial fluxgate magnetometer to measure the interplanetary magnetic field and the Jovian magnetosphere.
2) A set of low-energy radiation sensors to study the occurrence of low-energy electrons and protons in space and in the Jovian Van Allen belts.
3) A set of high-energy radiation sensors to study high-energy radiation and solar and galactic cosmic rays.
4) A radio propagation detector to determine the velocity of propagation of radio waves in space and determine characteristics of the Jovian atmosphere.
5) A radio astronomy experiment to study the source of emission of radio frequency transmissions from Jupiter, solar burst activity, and the ambient plasma density in space.
6) A plasma probe to study characteristics of the solar wind, and its interaction with the Jovian magnetosphere.
7) A micrometeoroid detector to determine the distribution of micrometeoroids in deep space and near Jupiter.
8) An infrared radiometer to make temperature measurements of Jupiter.
9) An ultraviolet photometer to determine the presence of Lyman Alpha radiation in space and near Jupiter.

Each of the above areas is discussed in greater detail in sections 2.2 to 2.10.

2.1.2 Constraints

An important decision made by the science payload subsystem was the choice of the trajectory. The UMPIRE mission will follow a clockwise trajectory with a nominal closest approach of 5 Jupiter radii (R_J). The clockwise trajectory was chosen for the viewing conditions it affords for UMPIRE's science payload. Its advantages include viewing a larger surface area of the planet, and two observations of the terminator. The clockwise trajectory will also provide a means to check the scientific measurements taken during the cruise to Jupiter, because the post encounter trajectory comes back in toward the Sun. The closest approach distance of $5R_J$ was chosen in order to provide a safe margin between the spacecraft and the Jovian trapped radiation belts located at about $3R_J$.

2.2 MAGNETIC FIELDS

Measurement of the magnetic fields is one of the prime mission objectives. The two areas of interest are the interplanetary magnetic field and the Jovian magnetosphere. Not only are these measurements of great scientific interest in themselves, but they would also be correlated with the trapped radiation and solar wind experimental results to obtain a more complete picture of the phenomena involved.

The magnitude of the interplanetary magnetic field near the Earth ranges from about 3 to 30 gamma with its direction along spiral magnetic field lines radiating from the Sun (Figure 2.1). Different components of the field vary according to both $1/R$ and $1/R^2$. Therefore, the field strength could fall off to less than 1 gamma at 5 AU (Reference 1). It is for this reason that the effects of the spacecraft's magnetic field must be kept to a minimum. However, measurement of the interplanetary magnetic field is not considered as important as measurement of the Jovian magnetosphere.

The Jovian magnetosphere is assumed to be large in both magnitude and extent. Estimates of the magnetic field strength are based upon radio emissions at decimeter wavelengths from Jupiter. Davis and Chang's estimates (Reference 2) of the magnetic field assume that synchrotron radiation of relativistic electrons is the source of Jupiter's radio emissions. For this mission's region of closest approach of from 4 to 6 R_J, Davis and Chang predict an upper limit of 4 to 6 gauss (1 gauss = 10^5 gamma). On the other hand, Warwick's estimate (Reference 2) of the magnetic field strength, which is based upon the Cerenkov radiation mechanism, indicates a maximum field strength of 40,000 gamma for the same region of closest approach. Because of the widely varying theories concerning the relationship of the magnetic field to the radio emissions, direct measurements of the magnetic field will be invaluable in establishing the phenomenon involved in the decimeter radiation from Jupiter.

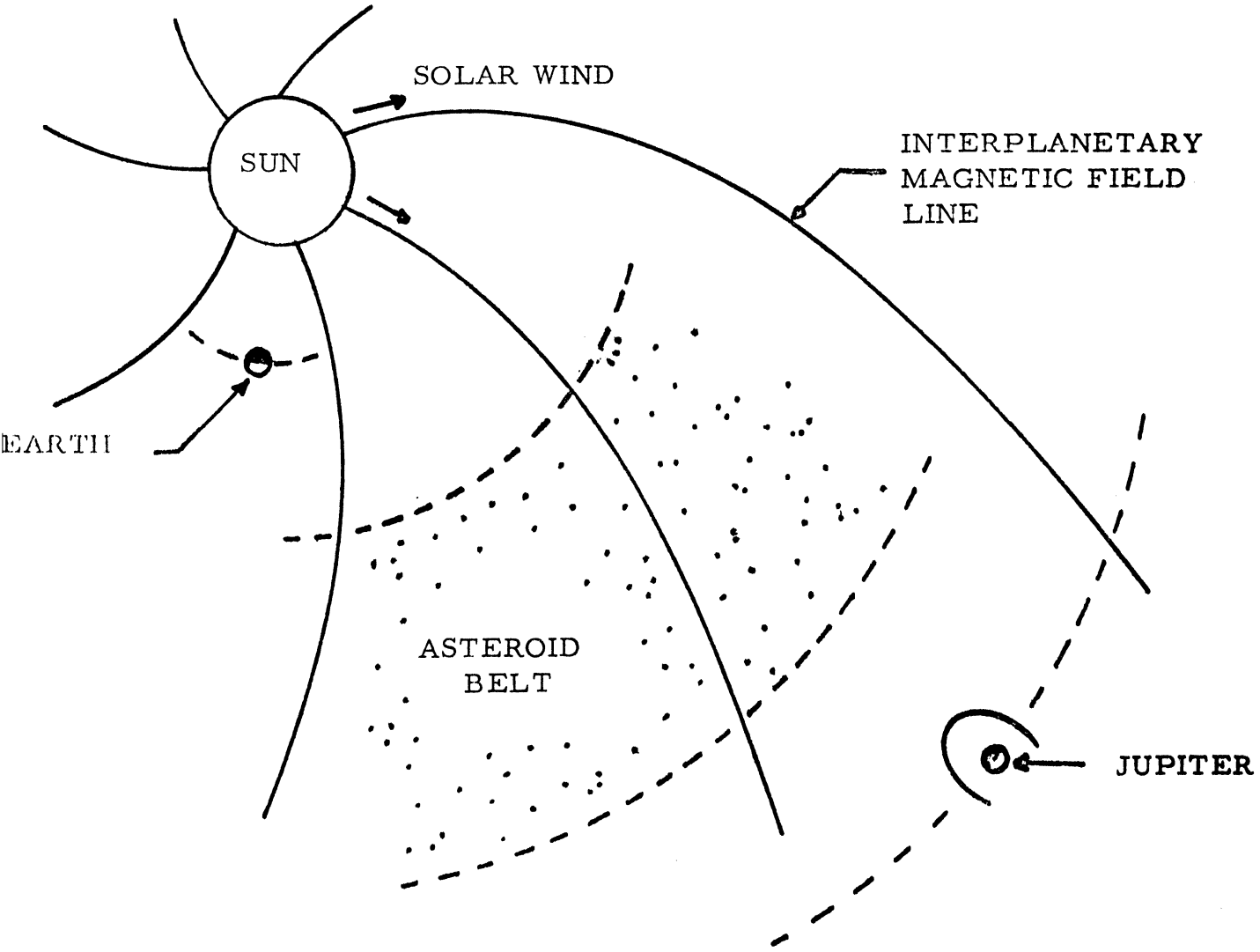

Figure 2.1 The Interplanetary Environment

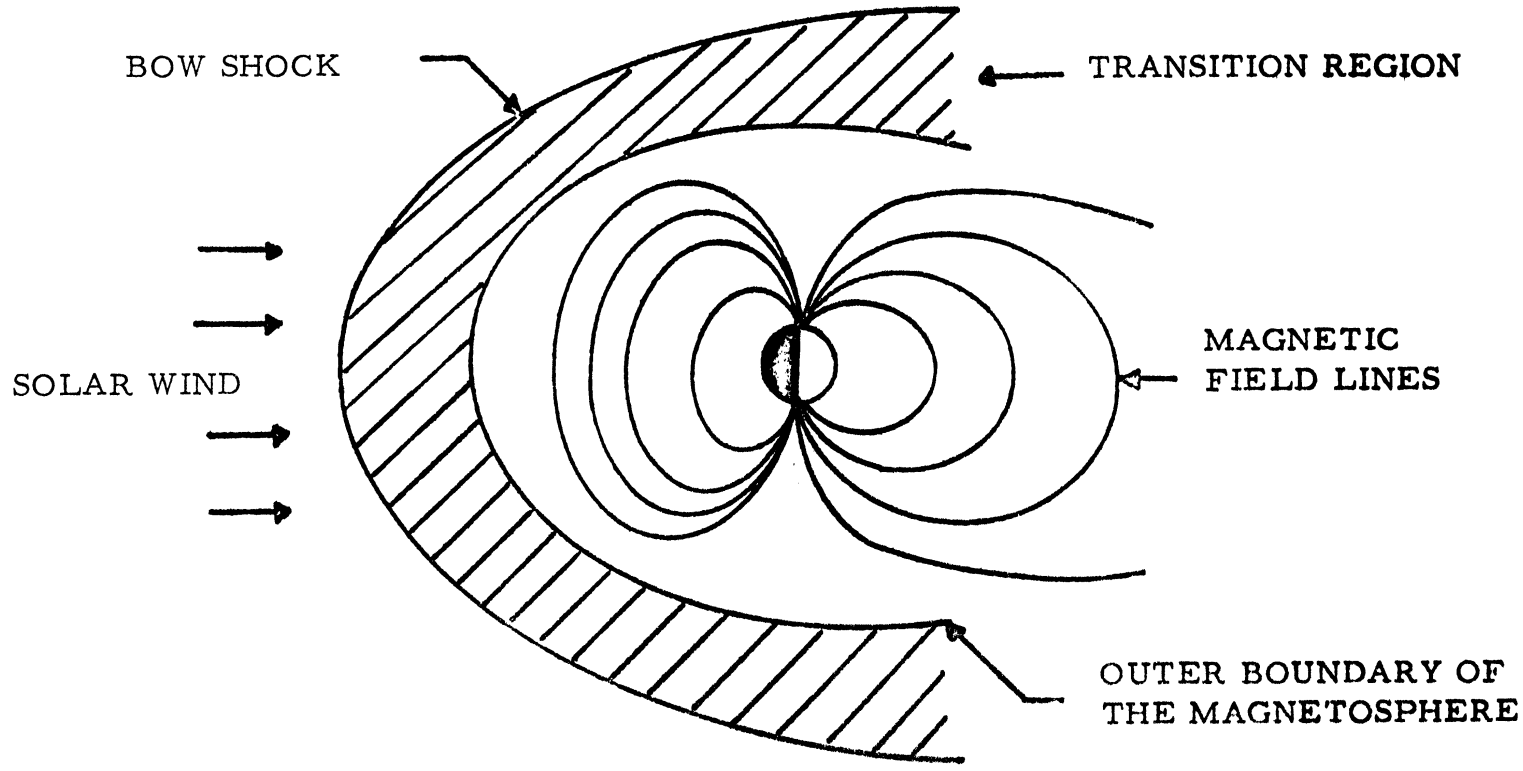

Figure 2.2 The Jovian Environment

The probable extent of the magnetosphere on the sunward side of Jupiter is about 50 R_J, and, assuming that the solar wind extends as far as Jupiter, the magnetosphere will be confined somewhat like that of the Earth, where a shock front of solar plasma builds up and a turbulent transition region is formed between the shock and the magnetosphere (Figure 2.2). Magnetic field measurements in this region correlated with data from the plasma probe experiment will be very useful in determining the exact extent of the Sun's influence on the magnetosphere. The orientation of Jupiter's magnetic field is assumed to result from a magnetic dipole offset from the center of the planet with the magnetic field axis at an angle of about 10 degrees to the rotation axis (Figure 2.3). The feature of greatest uncertainty is the position of the dipole center.

A triaxial fluxgate magnetometer with spin demodulation incorporated has been chosen for measuring magnetic fields. The sensor is mounted on a 14 foot boom where the intrinsic magnetic field of the spacecraft is approximately .3 gamma; however, further development in the design of the spacecraft should attempt to reduce this value to .1 gamma. There are three sensors mounted mutually orthogonal in the sensor envelope with one parallel to the spin axis. For reliability and stability purposes, two sensor envelopes will be mounted on the boom. The experiment will be designed to use automatic scale changes to accommodate a range of measurements from .1 gamma to 6 gauss. The fluxgate magnetometer has the advantages of being durable, simple, and flight proven.

2.3 LOW-ENERGY RADIATION

Measurements of radioactive particles and fluxes in space and in the Jupiter sphere of influence are of the utmost importance. The extent and composition of radiation fields are interesting problems which can only by solved by direct measurements at specific points in space.

There is a broad energy level spectrum of radiation and experiments have been arbitrarily classified as low-energy experiments or high-energy experiments. This is perhaps a rather artificial distinction since there is some overlap in the range of energies studied by each instrument. However, it is a convenient assignment because the two groups are more important in different segments of the flight trajectory. The low-energy experiments are anticipated to yield more information in the asteroid belts and during the Jupiter encounter. The high-energy experiments will be more important in measurements of the interplanetary environment.

The low energy experiments cover the energy spectrum from 0.04 Mev to about 50 Mev (Reference 3). Electronic and nucleonic particles are detected and counted. It is anticipated that Jupiter has two belts of trapped

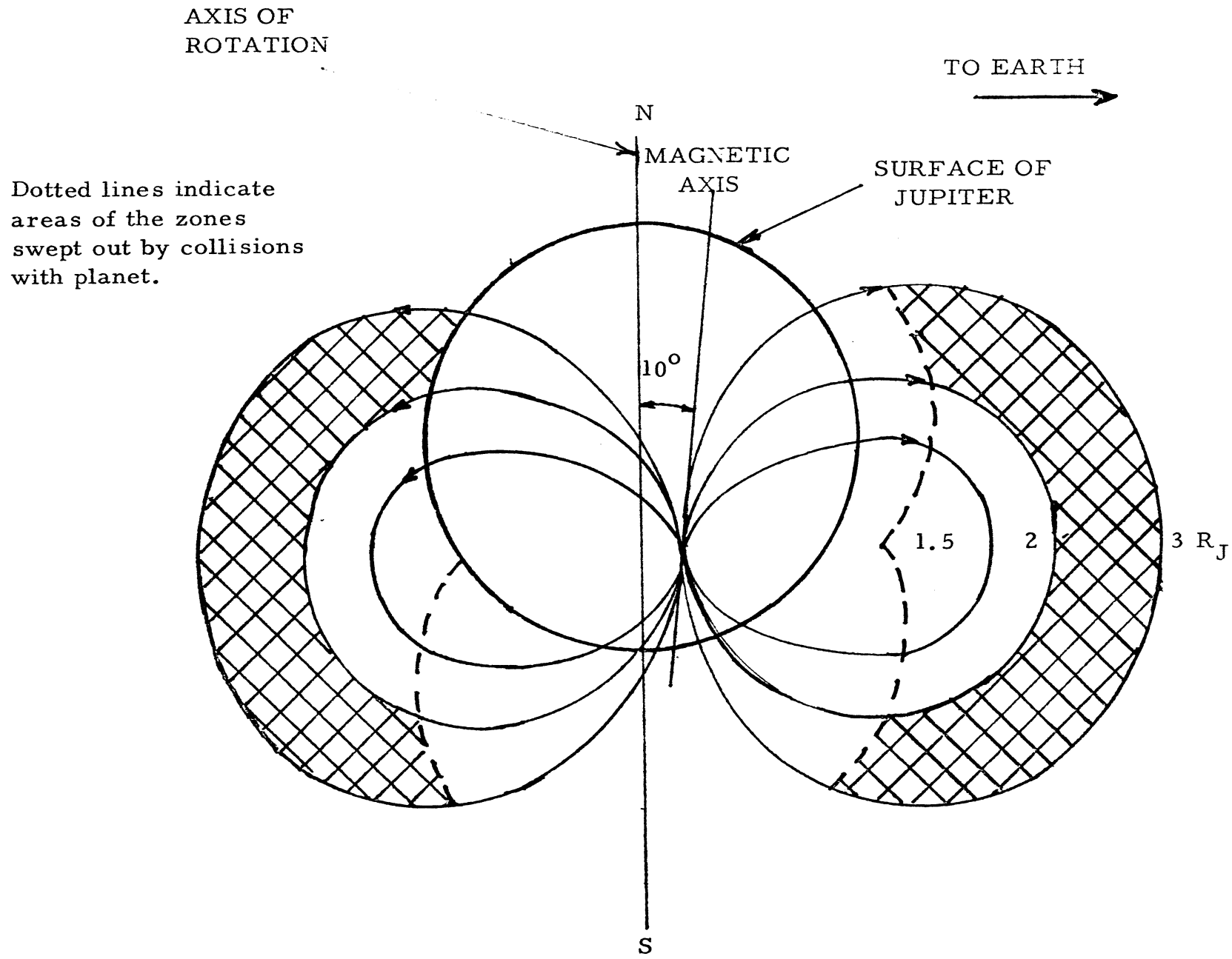

Figure 2.3 Jupiter's trapped radiation belts (Reference 1).

radiation, formed by the interaction of the magnetic field of Jupiter and corpuscular radiation from space (Figure 2.3). Two instrument packages have been included to study low-energy particles: one is an energetic particles detector of the type developed by Van Allen for the study of radiation belts, and the other is an integrating ionization chamber and Geiger-Mueller counter designed to investigate radiation fluxes in space. Both instruments are flight proven and are recommended as complimentary experiments.

The objectives for Van Allen's energetic particles detector include determination of: the magnitude and orientation of magnetic moments of a planet, the radial extent of its atmosphere, possibilities for aurorae and magnetic storms, the interaction of solar plasmas with the magnetosphere, the relationship between solar phenomena and the emission of energetic particles, the propagation of energetic particles in interplanetary space, and the relationship of the occurrence of energetic particles in space to solar and geophysical effects. The objectives of the ionization chamber include: measurement of ionizing radiation in space with stability and accuracy to detect small changes, determining the dependence of radiation intensity on distance from the sun, determination of the relation in changes in radiation between points in space with the distance between the points, observation of the time history of solar radiation, and measurement of energetic magnetically trapped particles (Reference 4).

The energetic particles detector is mounted in the main spacecraft compartment so that its four sensors scan the plan perpendicular to the spin axis. The ionization chamber is rather susceptible to background radiation from the RTG power source; therefore, it will be mounted on one of the fourteen foot booms that extend radially from the body of the spacecraft.

Background radiation from the RTG's can be reduced to a level compatible with the objectives of the radiation experiments by using coincidence techniques to restrict the viewing angles, booms to gain separation distances, and pointing of the RTG's to reduce the effective flux incident on the instruments.

2.4 HIGH-ENERGY RADIATION

The study of high-energy radiation is also of prime importance for an initial space probe of this type. Two instruments have been included for the study of high-energy particles. They will attempt to accomplish a large number of objectives and represent a compromise between expending a large portion of the weight budget and conducting a thorough scientific study.

These instruments will investigate three basic categories of radiation: high-energy radiation particles, solar cosmic rays, and galactic cosmic rays. Cosmic rays are very high-energy nucleonic and electronic particles (usually hydrogen, helium, and alpha particles).

One of the instruments will study the high-energy particles and galactic cosmic rays, and the other will study solar cosmic rays. Objectives for the two instruments include: measurement of the radial gradient of low-energy cosmic ray intensity in the solar system; measurement of the ratio of low-energy protons and helium ions as a function of distance from the sun; searching for trapped protons and electrons at Jupiter; studying the solar and plasma shock fronts at Jupiter; studying the time dependence, composition, and spectra of solar flare particles in space; searching for a persistent solar contribution to the low-energy proton spectrum; and determination of the presence of high-energy electrons in space (Reference 4).

A charged particle telescope will study the galactic cosmic rays and high-energy particles. It is mounted on the spacecraft body so that it scans the plane perpendicular to the spin axis. The solar cosmic ray sensor is mounted on one of the fourteen foot booms and the electronics package is carried in the spacecraft body.

2.5 RADIO PROPAGATION AND OCCULTATION

An important consideration of the science payload is measurement of the velocity of propagation of radio waves through space. The velocity is determined from time delay or Doppler shift techniques, involving radio transmissions sent to the spacecraft and signals returned from the craft. Knowledge of the velocities will yield information on the integrated number of electrons between the craft and the earth. Accurate tracking of the craft is accomplished in view of this information. The effects of the presence of plasmas may also be studied. This experiment is an important requisite for some of the other experiments. The radiation experiments, the radio astronomy experiments, and the plasma studies are all enhanced by this experiment.

The equipment used for velocity measurements can also be used to perform an Earth occultation experiment. This consists of transmitting radio signals from the spacecraft through the Jovian atmosphere. As the spacecraft travels through space the radio path from the spacecraft to the Earth is a straight line and the only Doppler component present is due to the relative velocity between the Earth and the spacecraft. When the geometry is such that the spacecraft begins to transmit through the Jovian atmosphere, then two other components add to the Doppler shift of the radio signal:

(1) The radio ray path will be bent due to the atmosphere's refractive index, and (2) The radio signal will be retarded because of the atmosphere itself. Knowing the Doppler shift and the position and velocity of the spacecraft, a computation of the scale height of the planetary atmosphere can be made. Such a calculation is also useful in supplementing spectroscopic experiments for determining such properties as composition, temperature, and density. The only information available thus far on the planet Jupiter is a study by Baum and Code of the occultation of the star Signa Arietis (Reference 1). This observation yielded a scale height between 8 and 12 kilometers and a mean molecular weight between two and four. An Earth occultation trajectory can provide more accurate data and probe further into the atmosphere; however, the amount of data at lower atmospheric levels will be a function of the signal strength.

The instrument has two small whip antennas which are mounted on the feed assembly of the main communications antenna in the plane perpendicular to the spin axis. The electronics are mounted in the spacecraft body.

2.6 RADIO ASTRONOMY (Reference 5)

The radio astronomy equipment package is designed to handle a number of important questions concerning Jupiter and interplanetary space. One of the most intriguing problems in the study of Jupiter concerns the source of emission of radio waves in the decameter range. The location of the source, its size and form, and its motion are important areas of study. A determination of the complete radio frequency spectrum (especially the lower frequencies) is desirable. The duration of radio emission bursts and the polarization of the decametric waves are other aspects of the Jovian study. A second experiment that can be performed with this instrument concerns low-frequency solar burst activity; the available range of radio frequencies will yield extensive data concerning the solar corona. A third experiment that can be performed deals with the ambient plasma density throughout space. The density and irregularities of the interplanetary medium can be determined, and the effect on these phenomena by the asteroid belt can also be studied. In addition, the effects of a plasma environment on radio frequency noise can be studied. These measurements provide valuable information in addition to that gathered by the experiments geared to solar investigations.

The experiment requires a large dipole antenna. Since it is not possible to mount just two perpendicular antenna stems because of stability problems, three equally spaced antenna stems will be mounted radially out from the spacecraft body in the plane perpendicular to the spin axis. These antennas will be mounted on the three instrument booms to keep them in their proper relative positions and to prevent other stability problems.

2.7 THE SOLAR WIND (Reference 6)

The solar wind is a plasma consisting mainly of hydrogen ions, electrons, and some helium ions. The flow of the plasma is generally in the form of an Archimedes spiral radiating outward from the Sun. There is scientific interest in studying the spatial and temporal characteristics of solar plasma at further distances from the Sun than the Venus-Earth-Mars region, and in studying the interaction of the solar wind with the Jovian magnetosphere. According to Warwick's theory of the magnetic field and the assumption of a solar wind strength of approximately 1/25 that observed near the Earth, a plasma bow shock would be located at about 80 R_J. A turbulent transition region exists between the shock and the confined magnetosphere; this area will be of particular interest in determining the extent of the solar wind's influence on Jupiter's magnetic field. Upon crossing the shock the solar plasma is expected to increase in thermal energy while decreasing in bulk velocity and changing direction by about 40 degrees. This will give a good indication of the bow shock's location.

The plasma probe will be a combination of two highly developed and flight proven detector systems in order to obtain more complete information about the plasma than either detector could obtain alone. Also, if either detector fails, the other would still be able to provide significant data. The two detectors are a Faraday cup and a spherical electrostatic analyzer. The Faraday cup will measure the total flux, flow direction, bulk velocity, and coarse energy spectra of the positive ion content of the solar plasma. This information will determine the region in space where the plasma is concentrated. The electrostatic analyzer will then carry out a high resolution study of the energy spectrum and angular spread of the plasma in this region. This leads to an accurate two-dimensional description of the temperature and energy distribution. The electrostatic analyzer also makes measurements of the electron spectra of the plasma. The two sensors will be located on the feed assembly of the antenna with their longitudinal axis parallel to the spin axis and pointing toward Earth.

2.8 MICROMETEOROIDS

A study of the mass, velocity, and flux of micrometeoroids in deep interplanetary space is of interest for two reasons: (1) These measurements will be of value in the investigation of the origin and evolution of the solar system and (2) They will be important in formulating the design of future spacecraft shielding.

The source and distribution of micrometeoroids within the solar system is poorly understood. Much of the data recorded thus far has come from

microphone experiments which record the number of impacts above a certain threshold and at the same time yield a signal proportional to some yet undetermined function of particle mass and velocity. One hypothesis concerning the origin of micrometeoroids is that they come predominantly from cometary and asteroidal debris, with the interstellar contribution considered negligible (Reference 7). As far as distribution is concerned, there is no direct information on micrometeoroids beyond 2 A. U. The region of primary interest for this mission will be the Asteroid Belt, which extends from about 2 to 4 A. U. (Figure 2. 1). This region must be crossed before any spacecraft can reach the outer planets. Also of interest will be the near Jupiter environment, which due to the large gravitational attraction of Jupiter, is believed to consist of a large dust cloud.

Choosing a specific instrument for studying micrometeoroids is extremely difficult due to the lack of existing experiments capable of satisfying the mission goals. The ideal experiment would have low weight and power requirements, a large dynamic range, and would be capable of yielding more accurate information than the existing piezoelectric microphone types. An instrument similar to the Cosmic Dust Detector used on Mariner IV is suggested for this mission (Reference 4). It could be designed to have a larger dynamic range with increased accuracy if given an additional weight and power allotment. An estimated total weight and power requirement for this instrument is given in Table 2. 1.

The actual sensor will be an impact plate employing both microphone and thin film capacitor detection techniques. It will be located on the outer portion of the base plate. The major parameters measured will be the flux, mass, and particle size distributions of micrometeoroids in space.

2.9 INFRARED RADIOMETER MEASUREMENTS

A thermal history of Jupiter requires knowledge of the way in which the atmosphere affects the transfer of radiation. It will be of great importance to obtain temperature measurements at a variety of wave lengths, which can then be roughly related to the depth at which thermal emission occurs. By making these measurements on both the light and dark sides of Jupiter, it should be possible to determine cooling rates and atmospheric heat capacity. Also, it is important to determine the wavelength dependence of the atmospheric opacity and possible variations over the disk due to temperature effects; this should help to determine whether a large atmospheric greenhouse effect exists. Finally, by correlating variations in temperature on the illuminated disk with ground based studies of the visible features in the cloud layer, understanding of the planet's circulation should be significantly increased.

Jupiter's atmosphere is thought to consist primarily of helium and hydrogen with lesser amounts of methane and ammonia. Infrared (IR) radiometric measurements in the 8 to 14 micron window of the Earth's atmosphere indicate a temperature of about 130° K above the clouds (Reference 1). Temperatures measured in this region of the spectrum refer to ammonia above the visible cloud level. Extension of measurements to wavelengths outside this region would allow investigation of lower levels in the atmosphere. A fly-by mission will afford this opportunity, as well as allowing an increase in angular resolution and observation of the unilluminated hemisphere.

These measurements will be made by an infrared radiometer. It will be mounted in the main spacecraft compartment and will have variable viewing angles. It will scan the infrared region of the spectrum with high resolution measurements made at selected wavelengths.

2.10 ULTRAVIOLET PHOTOMETER MEASUREMENTS (Reference 8)

A single channel photometer experiment has been chosen to map Lyman alpha radiation resulting from auroral activity on the antisolar side of Jupiter. Energetic electrons are expected to travel down lines of force in the Jovian magnetic field and impinge on Jupiter's atmosphere to produce Lyman alpha radiation. Ultraviolet (UV) observations of Jupiter's aurora would help to determine the generation process of decameter radio radiation and the means by which Jupiter's nearest Galilean satellite Io affects the emissions. They may also assist in mapping the magnetic field of Jupiter and identifying atmospheric constituents. The interplanetary portion of the flight will provide an excellent opportunity to map the celestial sphere in Lyman alpha radiation which will provide valuable astronomical information.

The instrument itself is a single channel Lyman alpha sensitive photometer with a .6 degree field of view. During the encounter mode it will operate between 8 and 20 R_J with an on-planet mode so that data is taken as the instrument scans the planet from limb to limb. The photometer will be rigidly fixed to the spacecraft and the angle between the optical aixs and the spin axis will be determined from the trajectory. If possible the time of arrival should be chosen so that Io will be in the field of view of the photometer at some time during the period that the spacecraft is between 8 and 20 R_J.

2.11 ADDITIONAL INFORMATION

Much additional information will be derived from the flight of this probe, and much of it will be useful in the determination of empirical constants used to describe models of various phases of behavior of the planets in space. Such items as the astronomical unit, the Jupiter gravitational constants,

orbital constants, the Jovian mass, and the effects of perturbations by other bodies can be determined by the very accurate and sensitive tracking of the spacecraft in its trajectory.

2.12 SUMMARY OF THE SCIENCE PAYLOAD

2.12.1 Estimated Science Payload

Much of the work done by the group responsible for the science payload was choosing representative instruments to study the phenomena selected for investigation. The group depended heavily on written instrument proposals and project studies already in existence to determine the physical characteristics of the equipment. The characteristics of the payload are estimated in Table 2.1.

2.12.2 Power and Data Profiles

Power and data rate profiles for the science equipment have been developed from the data in Table 2.1. The profiles show the total power and data rate of the instruments operating at all places along the flight path of the spacecraft.

Power (watts)

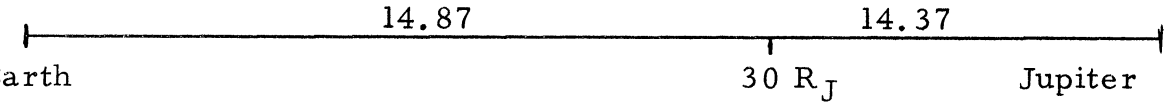

Raw Data Rate (bits per second) (Table 4.1)

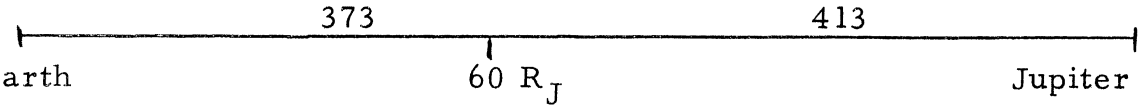

2.12.3 Location of the Instruments

Figure 2.4 has been included to show the relative placement of the science equipment in the spacecraft. In the figure, the instruments are numbered as they are in Table 2.1.

2.13 RECOMMENDATIONS FOR FUTURE MISSIONS

The instruments included in the science payload analyze the fundamental phenomena encountered in deep space flight and measure some of the basic phenomena associated with the planet Jupiter. The experiments were selected so that they would yield a well defined, coherent, and integrated body of information, and redundancies among the experiments increase the validity of the data.

Table 2.1 Estimated Science Payload[1]

Instrument	Weight (lbs)	Power (watts)	Bit Rate (bits/sec)	Mode[2]	Size (in)	Volume (in^3)	Temperature (^oF) Sensor	Electronics	Mounting
1. Fluxgate Magnetometer	8.0	1.5	32 72	C E	3x5x6	90	200(max)	-40 to 140	Sensors on 14 ft boom
2. Low-Energy Radiation									
a. Energetic Particles	2.5	0.4	52	C&E	3x5x6	90		-40 to 140	On spacecraft, sensors exposed
b. Ionization Chamber	3.0	0.5	20	C&E	5x10x13	650			On 14 ft boom
3. High-Energy Radiation									
a. Particle Telescope	2.6	0.6	40	C&E	2x6x6	72		-40 to 140	On spacecraft, sensor exposed
b. Cosmic Ray Detector	6.0	2.0	32	C&E	4x5x6	120	-30 to 100	-4 to 167	Sensor on 14 ft boom
4. Radio Propagation and Occultation	6.5	1.5	52	C&E	4x6x6	144	200(max)	5 to 120	On spacecraft, two small antennas on structure
5. Radio Astronomy	6.0	3.0	40	C&E	7x7x7	343		-20 to 90	Requires three 14 ft antennas
6. Plasma Probe	7.3	3.5	36	C	5x5x7	175		5 to 122	Sensors on antenna structure
7. Micrometeoroids	4.0	1.0	15	C&E	3x8x8	192		-40 to 140	On dark side of craft, sensor exposed
8. IR Radiometer	3.0	3.0	36	E	4x5x7	140		-30 to 140	On spacecraft, sensor exposed
9. Lyman Alpha Photometer	2.6	0.87	24	C&E	4x4x11	176		-4 to 140	On spacecraft, sensor exposed
Total	51.5								

NOTES: 1. (Reference 1-6, 8-16)
2. The modes of operation are either cruise (C) or encounter (E).

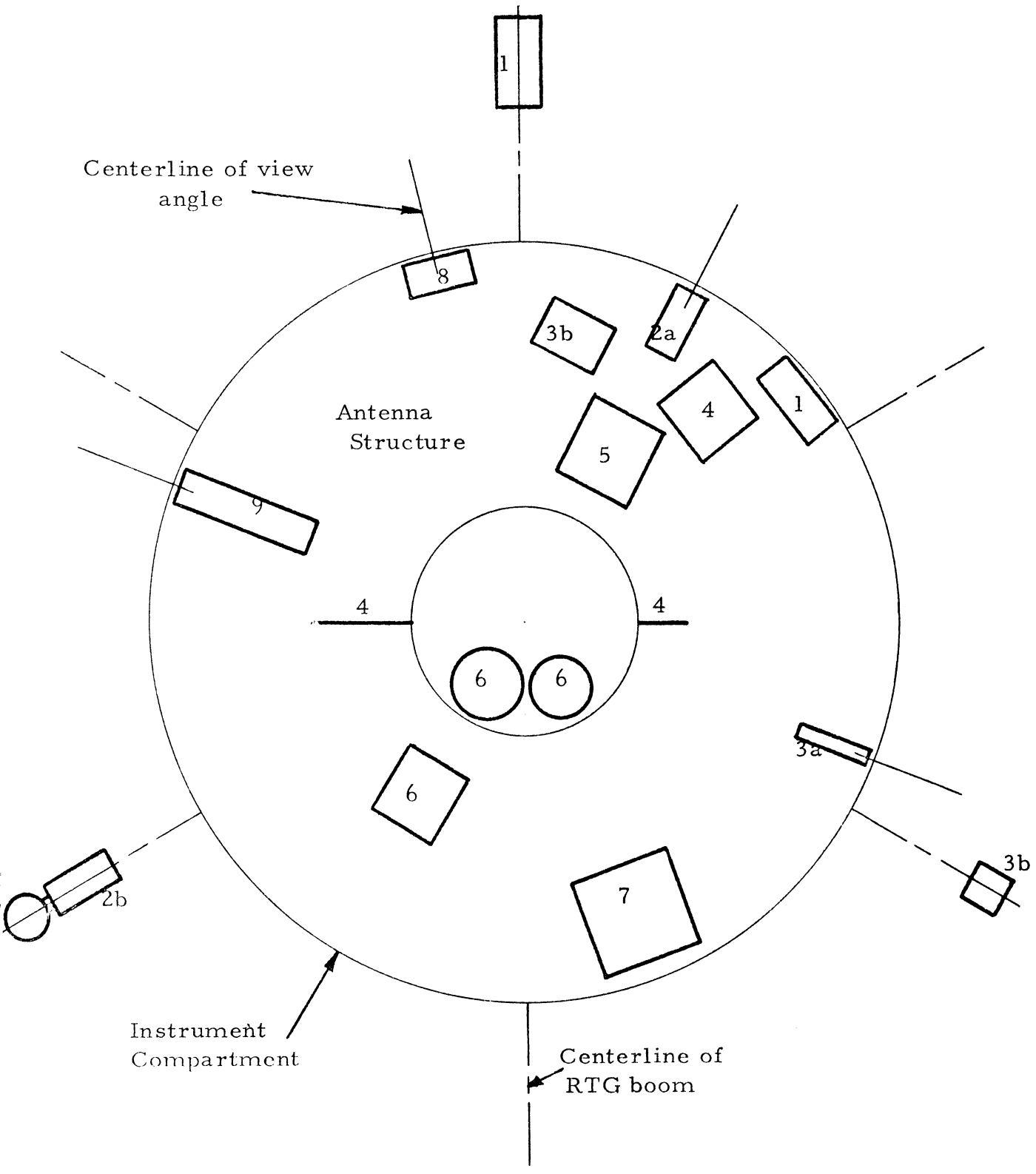

Figure 2.4 Location of the Instruments

With the weight and power allotted for the Project UMPIRE science payload, it is not feasible to devote a majority of the budget to the study of any one phenomenon; furthermore, an initial probe should maintain a broad scope. Through either an increase in the payload or a devotion of more of the payload to a specific objective, each important phenomenon ought to be investigated more thoroughly on subsequent missions. For example, the four pound instrument used to study micrometeoroids on this probe merely records rudimentary data of incident particles on the detector. More extensive instruments have been designed which will yield more complete information about the size, mass, and momentum of such particles, but such instruments are significantly heavier. The heavier weight would be rather restrictive for a fifty pound science payload, but the data obtained from such an instrument would merit its use on a later mission. Similar comparisons can be made about the other phenomena to be studied by the UMPIRE probe.

Experiments which deal solely with the study of the planet are a luxury on this initial exploratory mission. Specific instruments devoted exclusively to the study of Jupiter are of considerable importance, and on future missions (probably of the orbiter type) these should be given high priority. Particularly, electro-optical scanning instruments should be employed because they yield very accurate, high resolution results. Constituents of the atmosphere, relative abundances, depth, and temperature distributions are all important data in the study of the planet. The present atmosphere of Jupiter is similar in composition to the primeval, reducing atmosphere which the Earth is thought to have possessed when the first steps in the origin of terrestrial life must have occurred (Reference 17). There are radiometers, photometers, spectrophotometers, and spectrometers designed to investigate the Jovian atmosphere, but such instruments are quite heavy and provision has been made for only cursory measurements in the UMPIRE payload.

Perhaps the most important single experiment that was omitted from the UMPIRE mission is a television or a photo-television. It was omitted because it has severe weight, power, and data requirements, and would operate only in a relatively small portion of the encounter phase. A satellite designed for the unique problems of a camera would be a valuable tool in the study of Jupiter.

Orbiter and entry flights as well as increased weight, power, and data capabilities offer many exciting possibilities for expanded or specific scientific instrumentation.

2.14 REFERENCES

1. "Phase A Report Galactic Jupiter Probe, Volume I," Goddard Space Flight Center, November, 1967.
2. "Advanced Planetary Probe Jupiter Flyby Application," Jet Propulsion Laboratory, 12 August 1966.
3. "A Study of Jupiter Flyby Missions," General Dynamics, 17 May 1966.
4. Sloan, R.K., "Mariner Mars 1964 Project Report: Scientific Experiments," Jet Propulsion Laboratory, 13 July 1968.
5. Haddock, F.T., et al, "Low-Frequency Radio Astronomy Experiment," The University of Michigan Office of Research, 2 December 1968.
6. "Proposal to NASA for a Plasma Experiment on the Jupiter/Asteroid Missions," Massachusetts Institute of Technology, 26 November 1968.
7. Corliss, W.R., Scientific Satellites, National Aeronautics and Space Administration, 1967.
8. Pearce, J.B., "Technical Proposal to NASA for a Lyman Alpha Sensitive Photometer Experiment on a Jupiter Fly-by Mission," University of Colorado, 2 December 1968.
9. "Preliminary Progress Report Galactic/Jupiter Probe Study," Lockheed Missiles and Space Company, 30 June 1967.
10. "Small Interplanetary Probe Experiments Spacecraft Study," Bendix Systems Division, The Bendix Corporation, 8 August 1966.
11. Frank, L.A., "S.U.I. Experiment for the Eccentric Orbiting Geophysical Observatory," State University of Iowa, 8 August 1964.
12. "Advanced Planetary Probe - Final Technical Report," TRW Systems, 27 July 1966.
13. "Study of Pioneer Missions to Jupiter - Mid Term Briefing," TRW Systems Report, 8 August 1968.
14. Lassen, H.A. and R. A. Park, "Deep Space Probes: Sensors and Systems, Symposium on Unmanned Exploration of the Solar System," TRW Space Technology Laboratories, 10 February 1965.
15. "Experimenter Planning Document for Proposed Pioneer F/G Missions," Ames Research Center, NASA Document No. P-200, 18 October 1968.
16. "JPL Jupiter Mission Study," Presentation to Goddard Space Flight Center, 15 December 1966.
17. "A Study of the UV Spectrum of Jupiter, Part I," Illinois Institute of Technology Research Institute.

Clark, J.F., E. W. Hymowitz, and J.H. Trainor, "Galactic Jupiter Probes," Goddard Space Flight Center, NASA Document No. X-100-67-211, March 1967

"Handbook of the Physical Properties of the Planet Jupiter," NASA Document No. SP-3031, 1967.

"JOVE, Volume II," School of Engineering, Auburn University, Auburn, Alabama, August 1967.

Roberts, D. L., "The Scientific Objectives of Deep Space Investigations, Jupiter," Illinois Institute of Technology Research Institute, 9 March 1964.

"Scientific Objectives of Deep Space Investigations: Jupiter as an Object of Biological Interest," Illinois Institute of Technology Research Institute, May 1967.

Witting, J. M., et al, "Critical Measurements on Early Missions to Jupiter," Illinois Institute of Technology Research Institute, December 1965.

3
COMMUNICATIONS

3.1 INTRODUCTION

The Communications System for UMPIRE is one of the most vital groups of components on board the spacecraft. Basically, the system is involved with, or responsible for providing throughout the course of the mission:

1) Transmission of experimental data on both a real time and delayed time basis.
2) Transmission of vital engineering and housekeeping data on a real time basis.
3) Reception of command signals from the ground stations which provide instructions and information for the other subsystems in the spacecraft.
4) A two way coherent Doppler shift tracking system.
5) Pointing error signals to the attitude control system.

Because practically all of the other phases and subsystems involved in the flight must in some way depend on or utilize the Communications System, efficient and reliable performance is essential for mission success. With this in mind, the system design and component selection was made through a consideration of constraints imposed by the UMPIRE weight and power budgets. Furthermore, the entire system has been chosen to be compatible with the Deep Space Instrumentation Facility (DSIF), using the 85 foot dish antennas during launch and cruise, and the 210 foot dish antennas during the critical encounter phase.

In its present configuration, the total system weighs 78.5 lbs. and requires 33 watts of electrical power throughout the flight. Using the current state-of-the-art, the maximum transmitted bit rate of 5 A. U. is 1664 bits per second (bps). To insure the desired reliability, component redundancy has been provided wherever failure would result in loss of transmission.

3.2 GROUND FACILITIES

Because of the extreme distances involved, and the need for a constant communications link with the ground stations, it will be necessary for UMPIRE to use the existing and/or planned facilities of the DSIF. The DSIF along with the Ground Control System, and the Space Flight Operations Facility, comprise the NASA organized Deep Space Network (DSN). Under

the direction of the Jet Propulsion Laboratory, this complex network is responsible for two-way communication with space vehicles from 10,000 miles ± 30 degrees Earth latitude to interplanetary distances. It is a separate operation, distinct from the other communication and tracking facilities.

In implementing the communication link, the DSN must be able to track the vehicle, and thus calculate the spacecraft's distance, velocity, position, and follow its course. In addition, all necessary data acquired by the probe must be returned to Earth through the DSN. Finally, the Deep Space Network is responsible for relaying commands to the spacecraft to initiate sequences and provide instructions. To date, several deep space missions have been implemented by the DSN. Furthermore, the network currently has the capability to handle a launch while another mission is already in progress, with plans to double this capability in the future.

The DSIF provides the DSN with the actual radio contact link with the spacecraft. It consists primarily of three complexes spaced 120 degrees apart in longitude around the Earth, so that the craft will be in the field of view of at least one station at all times. Each of these sites is equipped with at least two 85 foot dish antennas having a gain of 53 db at 2295 MHz. In addition, the Goldstone center has a 210 foot dish antenna having a gain of 61.81 db ± 32 db at 2295 MHz, with a similar antenna planned for one of the other complexes by 1972. Each of the deep space stations have diplexed low noise transmitters operating at full S-band frequencies. Thus the command control (up-link) for UMPIRE will be at 2110 MHz, while the data reception (down-link) will be at 2300 MHz.

3.3 COMMUNICATION LINK PARAMETERS

System performance is based on the following parameters.

3.3.1 Downlink Power Budget and Link Parameters

Available Signal to Noise Ratio

1) Transmitter power- 12 watt traveling wave tube	10.79 dbw
2) Coupling loss-spacecraft	-1.7 db
3) Spacecraft antenna gain- 55% efficiency	38.45 db
4) Pointing loss (spacecraft antenna)	- .5 db
5) Space loss (5 AU range and 2300 megahertz)	-277.13 db
6) Polarization loss	- .5 db
7) Receiving antenna gain- 210' Dish at Goldstone	61.6 db
8) Pointing loss (receiving antenna)	0
9) Coupling loss	- .2 db

10)	Total received power signal	-169.19 db
11)	Noise spectral density (30^{o} K system temperature available at Goldstone)	-213.8 dbw/hz
12)	Available signal to noise ratio (S/N or SNR)	44.61 db

Required Power Margin

13)	Margin	4.6 db

Maximum Bit Rate for S/N = 40.01 db — 40.01 db

14)	Carrier modulation loss (β = 1.0)	-5.34 db
15)	Carrier to noise density ratio (C/N)	34.67 db
16)	Threshold C/N (for zero db SNR in 2 B_{LO} = 3 hz)	4.77 db
17)	Relative carrier power (db above threshold)	29.90 db
18)	Loop bandwidth 2 B_L = 26.3 hz	14.20 db-hz
19)	Loop SNR	20.37 db-hz
20)	Data modulation loss (β = 1.0)	-1.5 db
21)	Data to noise density ratio (D/N)	38.51 db
22)	Synchronization losses	2.49 db
23)	Required SNR = D/N ratio	3.8 db
24)	Required noise bandwidth	32.22 db
25)	Bit rate transmitted	5 AU 1664 bps 4.74 AU 1856 bps
26)	Data rate possible	5 AU 104 bps 4.74 AU 116 bps

3.3.2 Uplink Power Budget and Link Parameters

Available Signal to Noise Ratio

1)	Transmitter power (10 kw with 85' dish, 100 kw possible with 210' dish at Goldstone)	40.0 dbw
2)	Coupling loss (transmitting)	- .4 db
3)	Transmitter antenna gain (85' dish)	52.5 db
4)	Pointing loss (transmitting antenna)	0
5)	Space loss (5 AU and 2110 megahertz)	-276.34 db
6)	Polarization loss	- .5 db
7)	Spacecraft antenna gain	38.45 db
8)	Pointing loss (spacecraft antenna	- .5 db
9)	Coupling loss (spacecraft)	-1.5 db
10)	Total received power S	-146.53 dbw
11)	Noise density, N, using a noise figure of 10 db	-193.14 dbw/hz
12)	S/N available	46.61 db-hz

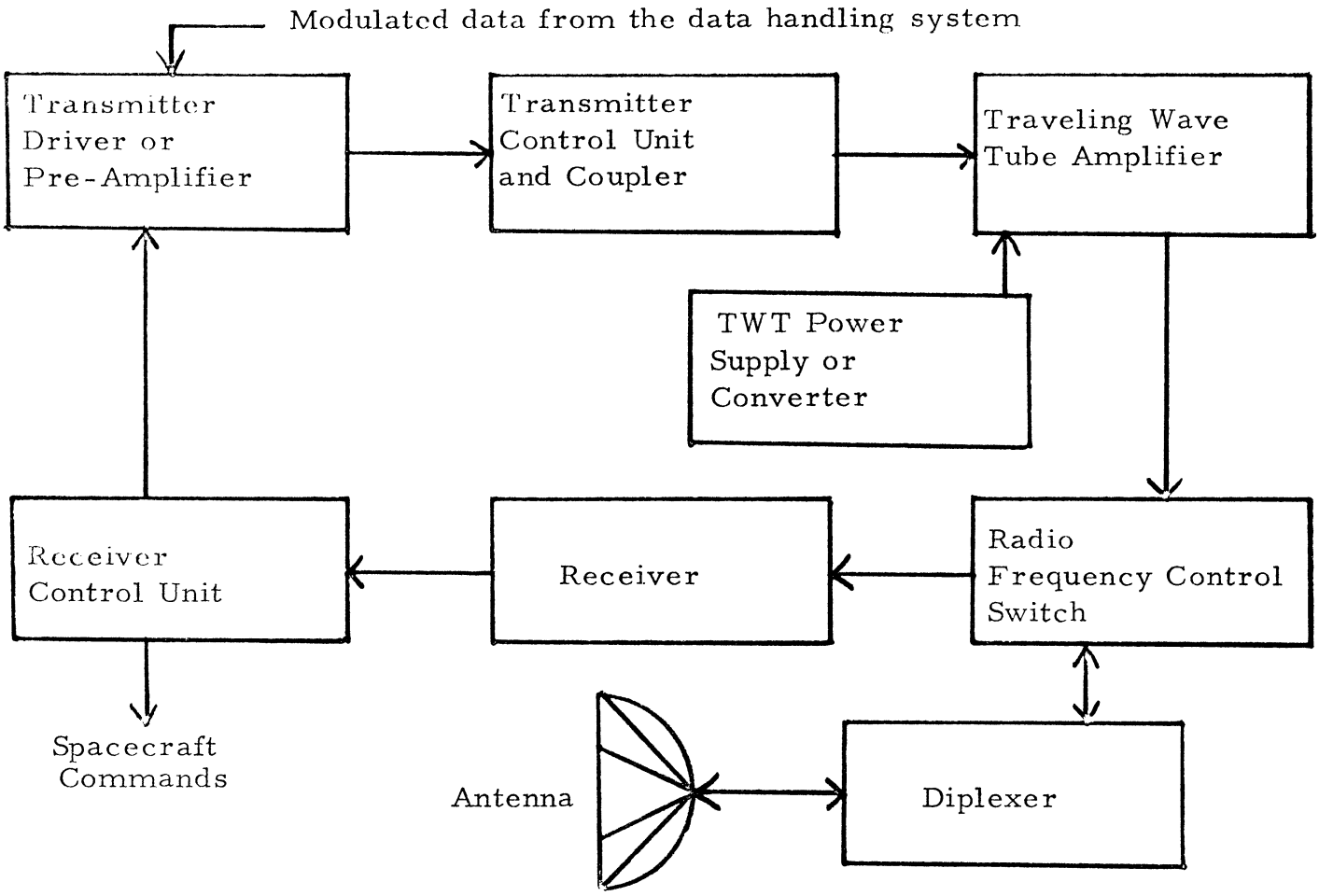

Figure 3.1 Basic Communications System

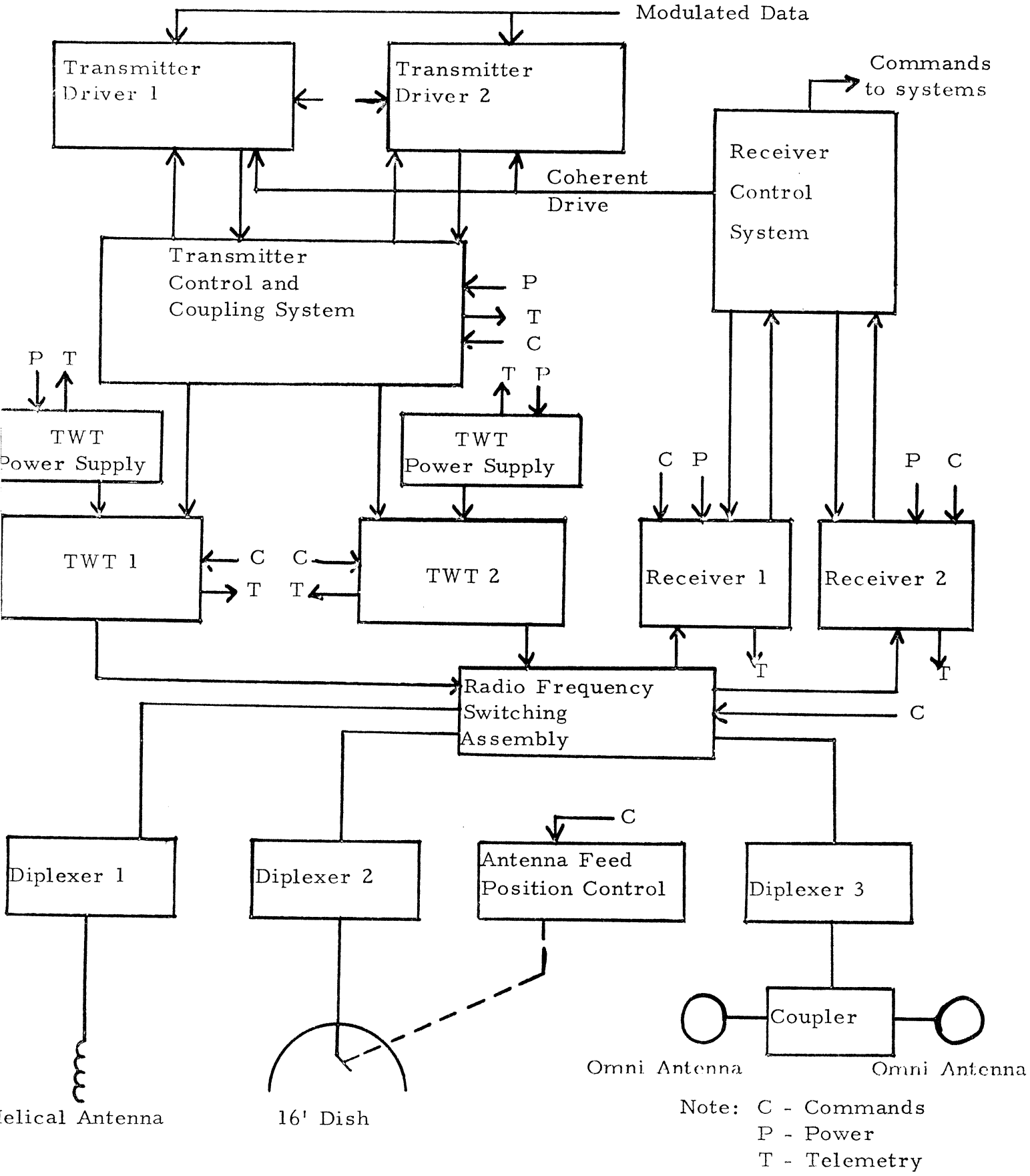

Figure 3.2 Complete Communications System

Required S/N at Command Rate of 9.16 Bits/Sec

13)	Ideal SNR for error probability = 10^{-5}	13.4 db
14)	Synchronization and limiter degradation	8.0 db
15)	Required SNR	21.4 db
16)	Bit rate (9.16 bits/sec)	9.62 db
17)	Required data power/noise ratio	31.02 db-hz
18)	Data modulation loss (β = 1.2)	3.01 db
19)	Required S/N	34.03 db-hz
20)	Power margin	12.18 db

Carrier Performance with the Phase Lock Loop at S/N = 34.03 db-hz

21)	Carrier modulation loss	-3.47 db
22)	C/N = Carrier to noise ratio	30.56 db-hz
23)	Threshold C/N (6 db in 2 B_{LO} = 20 hz)	19.03 db-hz
24)	Relative carrier power (db above threshold)	11.53 db

For a more detailed breakdown of the link parameters and how they were obtained see Appendix A.

3.4 SYSTEM DESCRIPTION

The basic functional block diagram for UMPIRE is given in Figure 3.1. To perform these functions, UMPIRE will need a large high gain antenna, a medium gain conical scan antenna, two essentially zero gain omni-directional antennas, two transmitters, two amplifiers, two receivers, and a combination of diplexers, switches, and control units to provide the different modes of operation. Figure 3.2 is a diagram of the component integration.

3.4.1 Components and Criteria

High Gain Antenna. The key element in this system is the 16 foot high gain, Cassegrain-fed, parabolic reflecting antenna. It will be the primary antenna at Jupiter distances, and will also be used for fine earth pointing. Because of the size restriction imposed by the Centaur booster shroud, the antenna must be of a deployable nature. During launch it will be furled and inoperative--to be deployed after the shroud has been released. Use of such a large diameter was predicated by the need for as much real time transmission as possible, requiring high gain in the down-link. Since transmitter output could not be increased, the gain had to be provided through the antenna. In its present Cassegrain-fed configuration, assuming 55% efficiency, the gain is 38.45 db. The dish is rigidly attached to the space-craft body at its base. Lockheed Missiles and Space Company has done considerable research on the unfurling mechanism and structure, and can collapse such a 16 foot dish into an 18 inch furled diameter with a weight of 21 lbs.

The choice of the Cassegrain feed system shown in Figure 3.3 was motivated by the need for simple placement of the movable horn feed (section 3.4.2), and by the need to place an instrument package on the feed support structure of the antenna. Placing a movable feed at the apex results in a much longer focal length, higher line loss, and complicated mounting. A Cassegrain feed allows aperture blockage because of the subreflector, as well as placement of the horn feed much closer to the vertex of the parabolic dish. Basically, a Cassegrain feed employs a hyperbolic subreflector located between the focal point and the vertex of the dish. It is placed such that its two foci coincide with the actual focus of the dish and the phase center of the horn feed. The result is as if the feed were apex centered. Proper positioning and design of the suberflector, attained through experimental optimization, can result in efficiencies on the same order as ordinary feed systems.

Medium Gain Conical Scan Antenna. To provide coarse earth pointing reference data to the attitude control system for the large antenna, a helical scan antenna having 15 db gain and a beamwidth of 25 degrees is mounted behind the subreflector of the main antenna. It is skewed 11 degrees from the spin axis, or bore-sight of the main antenna. The spinning motion of the spacecraft causes the offset helix to produce a cone of beamwidth of 48 degrees.

Omni-Directional Antennas. Two omni-directional antennas must be used on UMPIRE to provide radio contact whenever the main dish is not earth pointed. One must be placed on the subreflector instrument package to cover the earth pointed hemisphere, and the other on the spacecraft bottom. A true omni-directional antenna is impossible to achieve. Nearly complete coverage has been assumed, however, using a turnstile of crossed dipoles with circular polarization. Such turnstiles have essentially no gain, and will be used primarily for command reception, being coaxially coupled.

Diplexers. Three passive S-band diplexers have been provided to permit simultaneous transmission and reception through each type of antenna.

Amplifiers. Within the current state-of-the-art, there are two basic ways to provide final output amplification: solid state and vacuum tube devices. Keeping development to a minimum, it was decided to use existing amplification devices capable of producing approximately 10 watts at S-band frequencies. This focuses attention on tube devices: triodes, voltage tunable magnetrons, klystrons, amplitrons, and traveling wave tubes (TWT). For deep space applications such criteria as low noise, frequency stability, length of operation, high efficiencies, and wide bandwidth make TWT's the only feasible source for RF amplification. A lifetime of 30,000 hrs. and, according to Figure 3.4, an efficiency of 41% can be assumed with a 12 watt TWT. Two TWT's with integral power supplies will be used for UMPIRE. Only one will be operative, while the other will merely provide reliability.

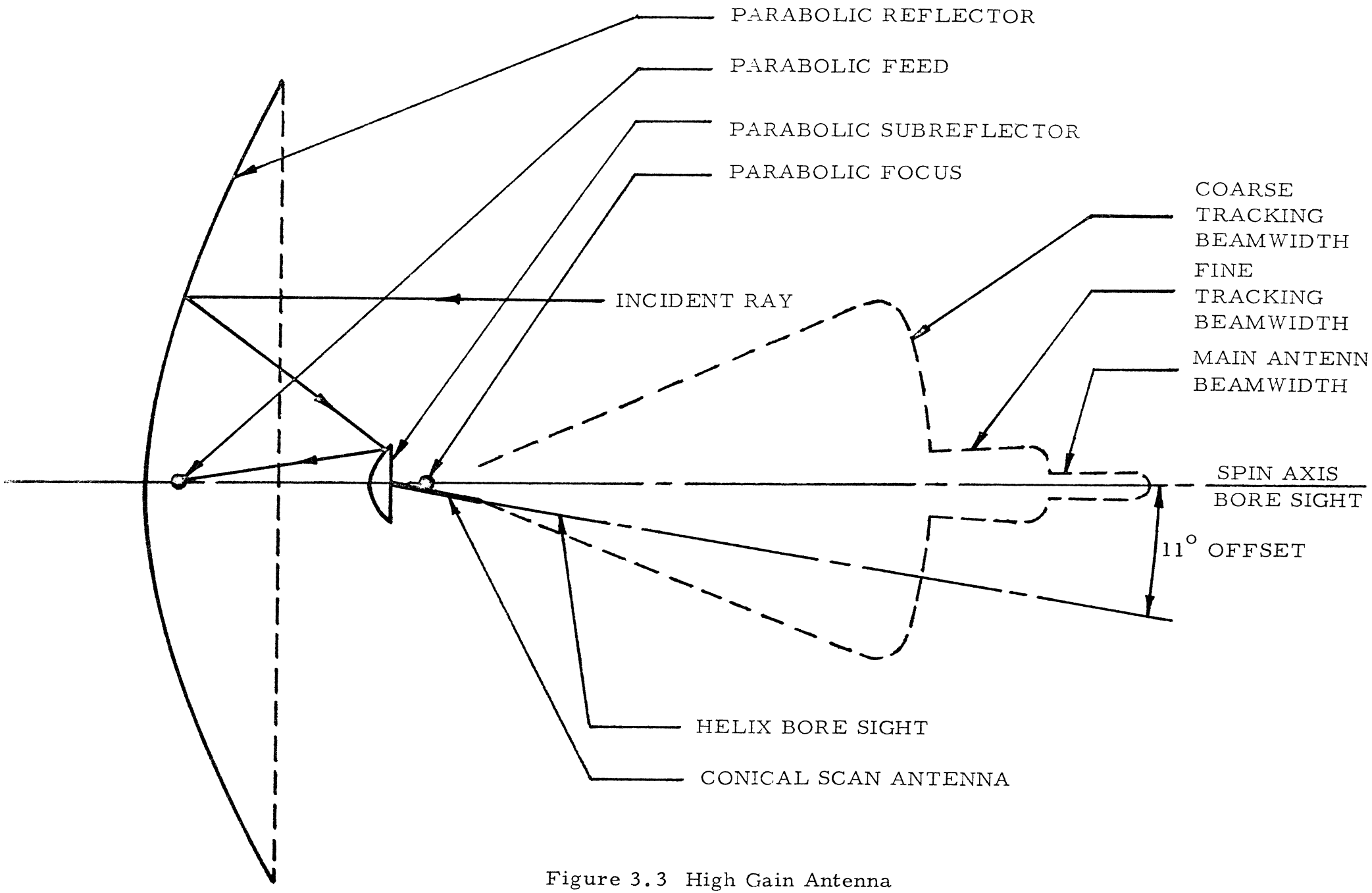

Figure 3.3 High Gain Antenna

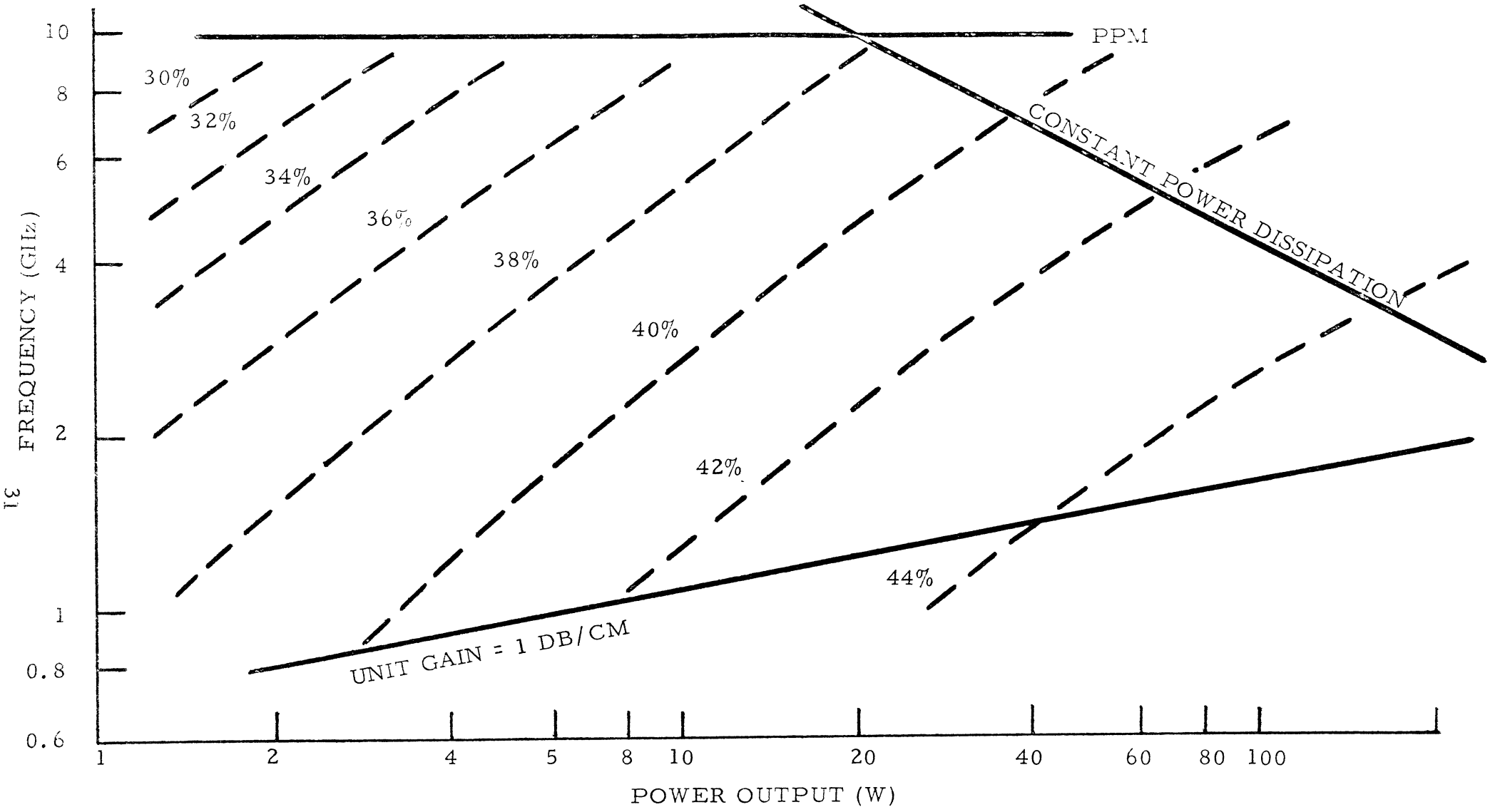

Figure 3.4 Efficiency of a Family of Traveling Wave Tubes (Reference 1)

Transmitter Driver. The transmitter driver is essentially a pre-amp for the TWT and is actually a low power, 50 mw S-band transmitter. It accepts modulated data from the data handling system, converts it to an S-band RF signal and supplies this to the TWT. There will be two on board; one operative, and the other providing a back-up.

Receiver. UMPIRE will use two redundant S-band receivers. Both will operate concurrently for the total duration of the mission, and together provide and/or receive the command signals, conical scan information for the attitude control system, and the coherent reference for the two-way Doppler tracking. Hence, they must be of the multiple conversion type, and employ phase-lock loop reception.

Control Units. The output of both receivers and the input as well as the matching of the drivers to the TWT's will be controlled by two switching units. The transmitter control unit will be operated strictly by ground command. The receiver control unit will have ground over-ride, but will esentially operate with its own built-in logic. Both devices are solid state multiple switches.

RF Switching Assembly. The switching assembly is actually a set of sub-miniature circulator coaxial switches. Six of these are employed to connect the various antennas to the transmitters and receivers for the desired modes of operation.

3.4.2 Operation

Telemetry. Whenever the main dish is not earth pointed, most communication is of the command nature through either omni antenna or the helix antenna. The use of diplexed coupling allows transmission during these periods; however, bit rates will be low. Full Earth coverage can be provided with the 85 foot antennas. After the dish pointing has been accomplished any of the antennas are capable of two-way operation, the ground control making the selection by the proper setting of the circulatar switches. The 16 foot dish will do most of the data transmission and at encounter it must use the 210 foot DSIF antennas.

Phase Lock and Doppler Shift Tracking. Information describing the spacecraft velocity and position will be attained by using the doppler shift phenomenon. Initially, the ground antenna is pointed at the spacecraft and adjusted until it attains and locks onto the spacecraft carrier. It then transmits to the spacecraft receiver which then locks onto the ground signal. The receiver, through the receiver control unit, then assumes control of the on board transmitter. The down-link frequency is then compared with the up-link from the DSIF and any shift yields the range rate.

This system is known as two-way coherent PM. In a similar manner comparison of a ground transmitted pseudo noise signal which is received and retransmitted will provide very accurate range measurement.

Earth Pointing. Because of the small beamwidth (2 degrees) of the 16 foot antenna, very accurate earth pointing of the spacecraft will be required to prevent excessive losses. A 1/10 of a beamwidth error in pointing results in a 1 db loss (Reference 2. This type of accuracy cannot be achieved by the conical scan helix alone. A three to four foot diameter parabolic dish has the desired ability, but is impractical for the UMPIRE configuration. Hence, the 16 foot dish must be used with a larger beamwidth on the order of 6 to 8 degrees for fine earth pointing (Reference 3. . This can be accomplished by an offset feed. Two discrete feeds are not feasible, and a permanently offset horn results in too great an efficiency loss. Hence, the horn will be pivoted on its waveguide and controlled by an electro-mechanical feed positioner. Normal operation will be on-axis, and by ground command the feed will be flipped to its offset position for fine pointing. The RF carrier transmitted from the ground is tracked by whichever antenna mode is being used, and the pointing error signals are relayed to the attitude control system.

3.5 CAPABILITY

The bit rate capability for the communication system is given in Figure 3.5, as a function of distance from the Earth. Shown are the 16 foot dish operating with the 85 foot and 210 foot dishes, and the omni antenna operating with the 210 foot dish.

3.6 ALTERNATIVES AND FUTURE DEVELOPMENTS

In its present configuration, the communications system requires little if any development. If certain technological advances are assumed for the early 1970's, system performance could be improved. To increase reliability, hybrid switching could replace the circulators by varying the DC control voltages. Solid state advances indicate that even greater than 10 watts will be available at S-band frequencies with efficiencies of 50%. This, along with sophisticated feed techniques, and the introduction of hydrogen masers at the ground stations, could provide enough gain so that the main antenna could be made of a smaller, fixed diameter, eliminating any problems associated with the deployable dish.

3.7 INTEGRATION WITH DATA HANDLING

It has been decided to have the communications system handle only the telemetry aspects of the data management. The data handling system is responsible for modulating, encoding, and decoding all of the information. The communications receivers will provide the demodulation of all incoming signals.

Figure 3.5 Communications Capability

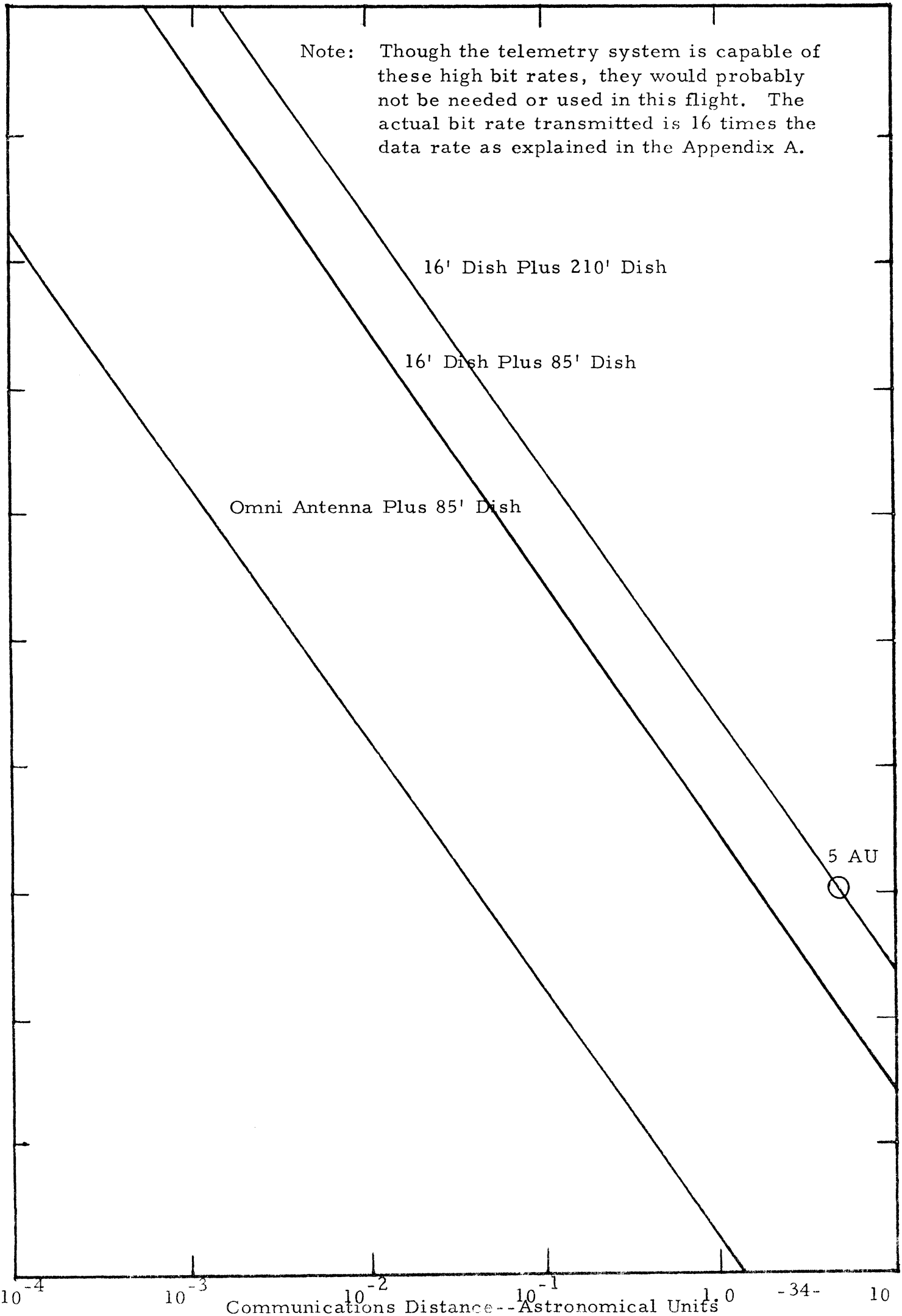

1. Schindler, M. J., "Advances in Traveling-Wave Tubes for Spacecraft Communications Systems," AIAA Paper No. 66-301.
2. Balakrishnan, A. V., Space Communications, McGraw-Hill, New York, 1965.
3. "Advanced Planetary Probe-Final Technical Report," TRW Systems Report, 27 July 1966.
4. "Study of Pioneer Missions to Jupiter - Mid Term Briefing," TRW Systems Report, 8 August 1968.

Blake, L. V., Antennas, John Wiley and Sons, New York, 1966.

Hill, J., "How to Select an Aerospace Antenna," Telemetry Journal, Volume 3, No. 3, April/May 1968.

"Jove," Volume I: Mission and System Study, Auburn - Alabama Engineering Systems Design - Summer Faculty Fellows, NASA Report No. CR-61180, August 1967.

"Phase A Report, Galactic Jupiter Probe," Volume II, Goddard Space Flight Center, Preprint X-701-67-566, November 1967.

"Preliminary Progress Report, Galactic/Jupiter Probe Study," Lockheed Missiles and Space Company, LMSC-A848035, 30 June 1967.

"SPECTRUM," Solar Probe Study by the University of Michigan, April 1967.

"The Deep Space Network," JPL Space Programs Summary 37-46, Volume III, 31 July 1967.

4
DATA HANDLING

4.1 INTRODUCTION

The data handling subsystem for Project UMPIRE has two primary functions:

1) Provide an interface to encode scientific sensor and engineering sensor data and transfer this to the communications subsystem.
2) Provide a means of decoding command signals and distributing these signals to the appropriate subsystem at the proper time.

In designing the data handling subsystem to meet these primary functions, seven basic considerations must be taken into account: system flexibility, ground station availability, system reliability, system efficiency, power, weight and size. The first consideration of system flexibility is a result of the importance of engineering data at launch and science data at encounter. The second consideration, ground station availability, is the cost of operating the Deep Space Network (DSN) for long periods of time and the possibility of other probes having to use the DSN. The third consideration, system reliability, is of prime importance in designing a mission of this type due to the nominal life for equipment of two years in deep space. The fourth consideration is efficiency and is usually a trade off with flexibility and reliability. The last of these considerations, power, weight, and size, are becoming less critical due to microminiature circuits; but they are still valid considerations in design of a system.

These seven considerations are met in this design. Flex format is used for system flexibility along with command selectable data rates and modes. Ground station use is minimized by use of tape recorders to store data for up to seven days in the interplanetary portion of the flight and then dumping it at a high bit rate. System reliability is obtained by use of redundancy in critical components that could fail. Efficiency has been slightly sacrificed due to reliability and flexibility, but it is kept in mind at all times. Power, weight and size are minimized by the use of microminiature circuits.

The data handling subsystem will consist of a Data Formating Element (DFE), a Data Encoding Element (DEE), two Data Storage Elements (DSE), and a Command Decoder Element (CDE) (Figure 4.1).

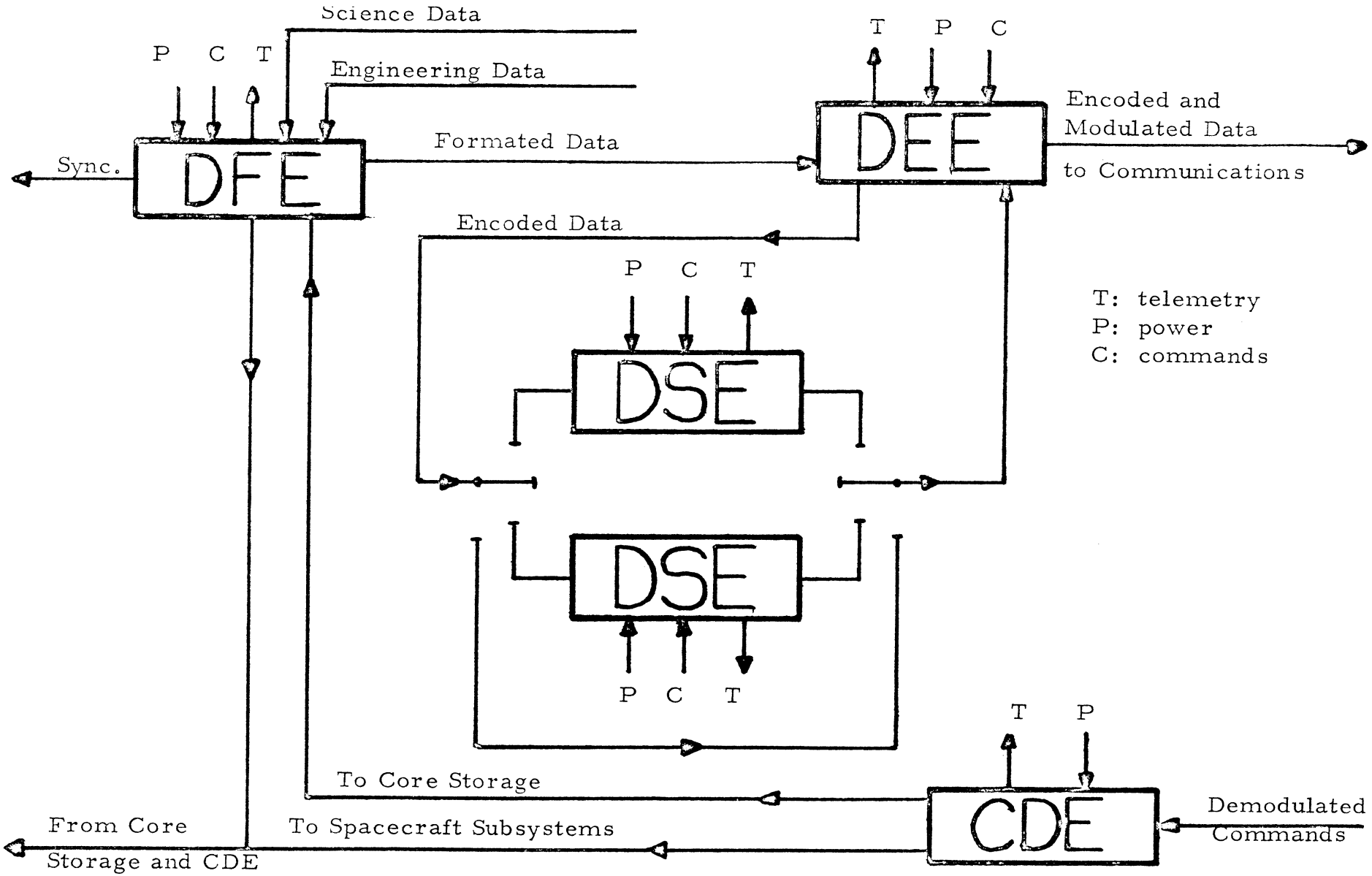

Figure 4.1 Data Handling Block Diagram

4.2 DATA FORMATING ELEMENT

The DFE performs the following functions:

1) Provide the necessary sampling rate for obtaining meaningful data.
2) Formating of the scientific and engineering data.
3) Provide time signals to the spacecraft and execute the stored sequences in the DFE sequencer.
4) Transfer data to the DEE and DSE.

There are ten science and five engineering inputs into the science main frame. Only ten of the eleven science inputs operate at any one time. Choice of the frame size should be reasonably long so that frame synchronization, frame identification, and frame time result in a low percentage of the total bit rate capacity. A 64 word science main frame is chosen, based on these considerations. This allows four samplings of each input and four words for frame synchronization, identification, and timing.

The engineering subframe will have the capability for 63 engineering inputs allowing one word for subframe synchronization.

A crystal oscillator will provide a stable pulse train for clocking purposes. A spacecraft clock will be operated by the crystal oscillator to provide a means of executing on-board sequences.

The DFE will also contain a small core storage device of 10^4 bits capacity. It will be programmed before launch to deploy the experiment booms, deploy the RTGs, enter engineering telemetry format, and enter maximum data rate. This small core storage will have capability to be programmed from the ground and execute the stored sequences upon command or by synchronization with the spacecraft clock. After sampling and formating, the data will be transferred to the DEE.

4.3 DATA ENCODING ELEMENT

The DEE will perform the following functions:

1) Conversion and coding of all spacecraft data.
2) Provide data compression for all data.
3) Provide for the various command selectable data rates.
4) Provide for the various command selectable data modes.
5) Provide Pseudo-Noise Synchronization.
6) Provide for modulation of the data onto the carrier frequency.

Data entering the DEE, which is not of a digital nature already, is converted in the DEE to a digital form. The data is then Convolutional Pulse Code Modulated (PCM) using an 8 bit code. PCM is used for the following reasons (References 1 and 2):

1) Binary data is easier to transmit than analog data.
2) Noise does not degrade the system as much as with other systems.
3) More information can be transmitted over a given bandwidth within a given time period than with other systems.
4) It uses relatively little power.
5) Data can be repeated many times without significant degradation of the signal.

Two types of error are introduced by using PCM encoding. Due to quantizing, there is a quantizing Root Mean Square (RMS) error which is 0.11% (Appendix B). Because of additive noise, digital errors are introduced. With the assumptions that

1) Any bit in a word is equally likely to be in error and
2) only a single bit is in error in a word,

then the digital RMS error is 0.36% (Appendix B). The digital RMS error is based on the assumption of a binary error probability of 1 error in 10^5 bits, which is common with present PCM systems (Reference 2).

Introduction of error to the encoded data is further minimized by the use of one-half Convolutional Encoding. In this system, one parity bit is assigned to each real bit of information. Each parity bit is either a "1" or a "0". Each parity bit is a "1" if some constant arbitrary number of real bits preceding it is odd and each parity bit is "0" if some constant arbitrary number of real bits preceding it is even. This provides a check on each real bit of data to determine whether it is in error or not.

The PCM coding technique will be Bi-Phase Coding. Bi-Phase Coding is very much like Manchester, with either one or two pulses per bit recorded. A polarity direction change always occurs at the beginning of each bit cell; in addition, there is a direction change in the middle of the cell if the bit is a one, and no transition in the middle for a zero. This method is similar to Non-Return to Zero (Mark), but is preferable since this is a self synchronous code and avoids the need for a timing track, when magnetically recording the data. The elimination of the timing track overcomes timing errors due to track-to-track skew or jitter (References 3 and 4).

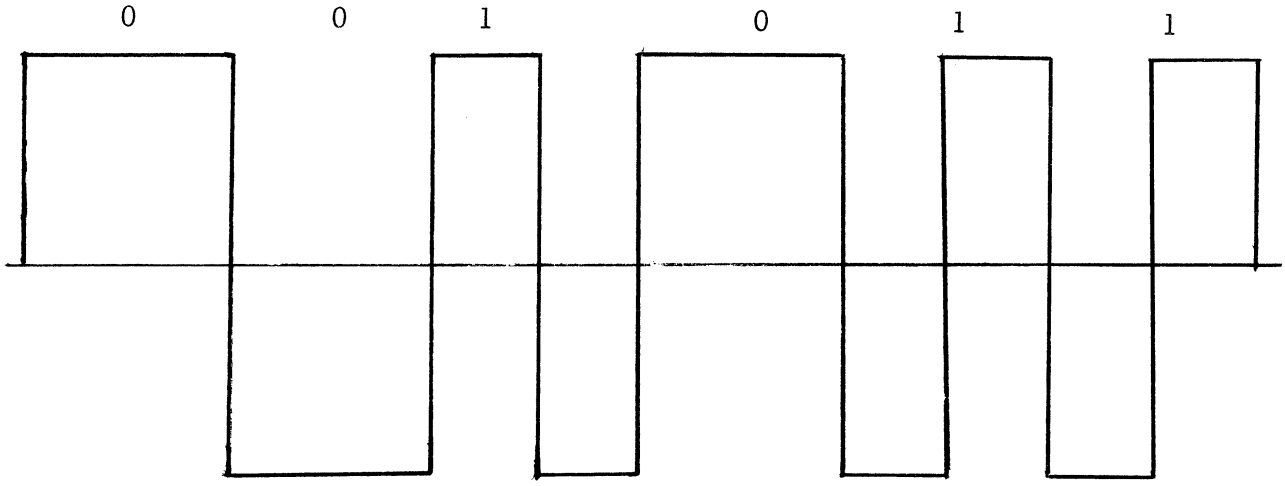

Figure 4.2 Bi-Phase PCM Coding Techniques

The data after encoding either passes through a data compression device or passes to the DSE units.

Data compression is used to enable real-time transmission of all sensor and engineering data at encounter. It also reduces ground processing time and cost. Table 4.1 shows the result of the use of the fan method of data compression. The communications subsystem has the capability of 1664 bits per second at 5 AU. Convolutional PCM encoding, using an 8 bit code and a parity bit for each bit of data results in a data bit rate of 104 bits per second (1664 divided by 16). Using data compression, the data bit rate from the sensors never exceeds 99 bits per second. Thus, real time transmission is possible for all data at any time, using the 210 foot Deep Space Instrumentation Facility (DSIF) antennas. It is probable that only the Goldstone and the proposed Australia antennas will be operating in 1972. In this case, communications will be possible only 16 hours a day.

The fan method of data compression was developed and patented by Radiation Incorporated of Melbourne, Florida. This method of data compression is applicable to all the data types on this mission. Basically, the fan method projects a fan or angle from the last significant value and determines whether the current value is within this angle; the preceding point is discarded and the current value stored until the next point has been tested. If the current value is outside the fan, the preceding value becomes the significant value and it is transmitted. The fan method was chosen due to the high compression ratios possible, even though more complicated than other methods (Reference 5). Two data compression devices will be used for greater reliability.

	DATA RATE (Bits/Sec)					
	INTERPLANETARY			ENCOUNTER		
EXPERIMENT	RAW	COMPRESSED	(FAN)	RAW	COMPRESSED	(FAN)
Fluxgate Magnetometer	32	(10:1)	3.2	72	(10:1)	7.2
Low Energy Radiation	--	----	---	--	----	---
a. Energetic Particles Detector	52	(3:1)	17.3	52	(3:1)	17.3
b. Ion Chamber	20	(10:1)	2.0	20	(10:1)	2.0
Micrometeoroid Detector	15	(1000:1)	0.1	15	(1000:1)	0.1
Plasma Probe	36	(2:1)	18.0	--	----	---
Radio Propagation	52	(3:1)	17.3	52	(3:1)	17.3
Infrared Radiometer	--	----	---	36	(2:1)	18.0
High Energy Radiation	--	----	---	--	----	---
a. Particle Telescope	40	(3:1)	13.4	40	(3:1)	13.4
b. Cosmic Ray Detector	32	(10:1)	3.2	32	(10:1)	3.2
Lyman Alpha Photometer	24	(4:1)	6.0	24	(4:1)	6.0
Radio Astronomy	40	(3:1)	13.4	40	(3:1)	13.4
Engineering and Housekeeping	30	(30:1)	1.0	30	(30:1)	1.0
TOTAL	373	(3.9:1)	94.9	413	(4.2:1)	98.9

Table 4.1 Uncompressed (RAW) Versus Compressed Data Rate

The DEE also performs the function of providing for the various command selectable data rates. Due to the high bit rates of the communications subsystem near Earth and the low bit rates at Jupiter, the capability exists in the Data Handling Subsystem for varying the bit rate. There are four rates: 100, 400, 1600, 6400 bits per second. This gives the capability of transmitting stored data at a high bit rate near earth and yet still being able to empty data storage at Jupiter in case of a data compression failure.

The DEE also has provisions for command selectable data modes: engineering data only, science and engineering data, tape recorder record/playback, and selection of raw or compressed data. At launch the engineering subcom frame would be the main frame, thus allowing the necessary transmission of engineering data following the launch. After establishing the interplanetary trajectory, the main frame would be the science main frame and engineering would return to the subframe role. At midcourse, the engineering frame again would be the main frame. This process of making the subframe the main frame is called flex formating. The third mode of operation is recorder record/playback. On command, data would be real time transmitted and also stored, or data from one recorder would be transmitted while the second recorder is recording real time data. The last mode allows for real time transmission if the redundant compression devices fail.

Redundant Pseudo-Noise generators are also included in the DEE. These provide a pseudo-noise code which supplies bit and word synchronization. The spacecraft data and pseudo-noise code are summed in a binary adder which produces a binary composite waveform as the output.

The DEE also provides for Frequency Modulation (FM) of the encoded data. The system used in Frequency Shift Keying (FSK). In this method of modulation, the carrier is modulated by one of two different frequencies at any instant of time. One of the modulating frequencies represents a "1" and the second modulating frequency represents a "0". Since the carrier is modulated by only one of the two frequencies at any one time, and since the frequency of the two modulating frequencies can be low, the bandwidth of the data is the same after modulation as before. Thus, no increase in bandwidth occurs in using FSK for modulation.

4.4 DATA STORAGE ELEMENT

Data storage is necessary for several reasons. Radio interference in the Jovian Environment could possible interrupt real time telemetry, causing a loss of data without data storage. During the 87.5 minute occultation, valuable data would be lost. Data storage also provides a double check on questionable data points received in real time.

The size of data storage was determined by the maximum bit rate at encounter for 154 hours using 8 bit one-half Convolutional PCM encoding. This is the time within sixty Jupiter radii, which is considered "encounter" for this mission. The resultant DSE capacity is 3.7×10^9 bits (Appendix B). This makes magnetic tape recording the only acceptable means of storage for this mission. It will take approximately 147 hours (6.1 days) after encounter to dump the stored data at a communications bit rate of 1664 bits per second. This is the transmitted data rate (16 times the data bit rate). However, since only 16 hours a day will be available using the 210 foot dish at Goldstone and the 210 foot dish in Australia (to be completed by 1972), it will take 9.2 days to transmit the stored data, using data compression techniques. If data compression should fail there would be no problems in transmitting the stored data, but transmission time would be 38.7 days.

During the early part of February, 1973, the Earth, sun and spacecraft will be directly in line. This precludes receiving any data due to the increase in solar noise when looking directly at the sun. The DSE units will be able to store about 171 hours of data out of the nominal 192 hours of blackout. Data would be lost during the period that storage was filled and before communications is again established.

During the early part of the interplanetary flight, the DSE units will be able to store for periods of time up to seven days and then transmit this to earth at the high bit rate of 6400 bits per second in one 16 hours period. As the mission proceeds, and the communications bit rate decreases, the period between transmissions of stored data decreases. When the earth-spacecraft distance becomes greater than 3.4 AU, data collected during the 8 hours period the DSN is not available cannot be transmitted to earth while also sending real time data during the 16 hours it is available. Therefore, from this point in space to Jupiter, some data out of each 24 hours period will be lost. The DSE units will be clear of stored data prior to encounter.

4.5 COMMAND DECODER ELEMENT

The CDE will provide for decoding of the PCM ground commands. The command word format will consist of the command decoder start bits, address bits, and command bits, followed by the command compliment bits. As the command is received in data handling it will be serially loaded into a shift accumulator whose bit capacity is the same as the number of command bits (Figure 4.3). As the first bit of the compliment enters the shift accumulator, the first bit of the command word is leaving the accumulator. The two are compared in a comparator, and likewise, the next bit in the command and compliment are compared, and so on. If the result of the comparator is that each respective bit in the compliment is

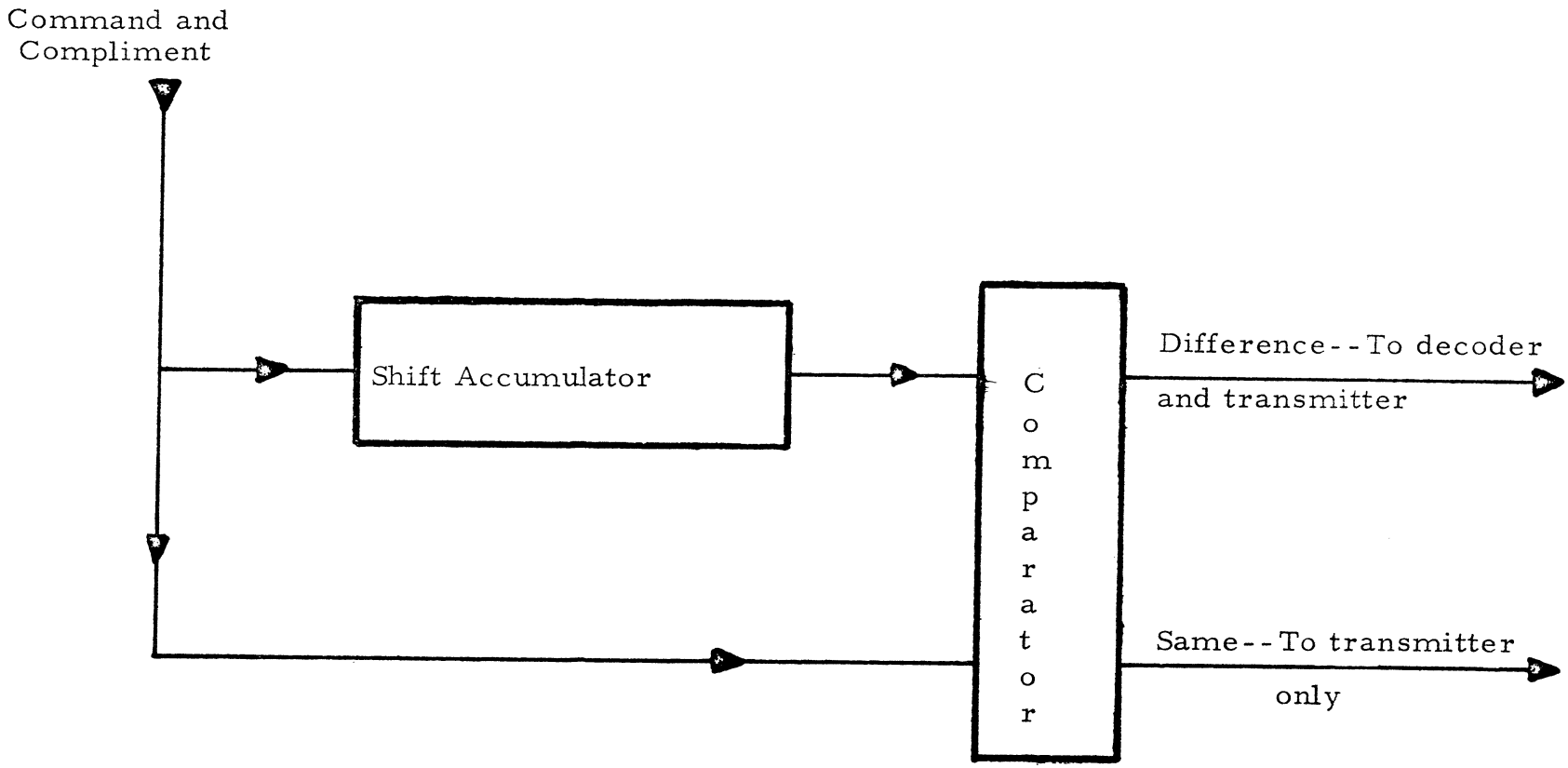

Figure 4.3 Command Verification Block Diagram

opposite to the value of the command bit, the command is executed and the command is retransmitted to earth for further verification. If the result of the comparator is that one or more sets of respective bits are the same value, the command address is transmitted to earth and the command is not executed. Ground command may then retransmit this command. This type of on board verification of a command is necessary due to the time delay in communications at Jupiter. The time delay does not allow ground verification of each command before sending another command. Therefore, blocks of commands will be sent and only those in error will be disregarded.

Commands that are to be executed immediately after decoding will be distributed to the proper subsystem by the CDE. Those to be executed at a later time will be routed to the small core storage in the DFE. One channel of the main frame will sample the core storage for commands to be executed in relation to the spacecraft clock. The CDE must have the capability of decoding 97 discrete commands and three quanitative commands (Table 4.2).

4.6 EQUIPMENT

Equipment for a mission of this type is not generally found off the shelf. Almost everything used would have to be modified or especially designed for this mission. It is possible with present technology to produce a DFE with the capability of a main frame of 64 channels and sub-com frame of 64 channels, crystal oscillator and clocking function, memory control circuitry, power regulation, and spacecraft interfacing. The unit would weigh four pounds, use 0.4 watts, and occupy a volume of 152 in^3. A DEE can be made to provide analog-digital converstion, 8 bit encoding, addition of parity bits, data compression, pseudo-noise generation and FSK modulation. The weight of such a unit would be 4.5 pounds, use 0.62 watts and occupy a volume of 100 in^3. A small core storage of 15,237 bits which is built by Electronic Memories would be suitable for the DFE small core storage. It has been used on Pioneer Deep Space Probes, uses 0.08 watts, weighs 1.7 pounds, and occupies 72 in^3. A command decoder of the size needed for this mission could be designed to use 0.5 watts, weigh no more than 1.8 pounds, and occupy no more than 150 in^3. State of the art in magnetic tape recorders is such that a tape recorder of 1.85×10^9 bits capacity could be developed with the data rates required using 5 watts for recording and 8 watts for playback. The weight would be no more than 9.0 pounds, the volume occupied would be 250 in^3 (Table 4.3). The operating life for this mission is attainable, as is resistance to radiation damage and magnetic interference, with present state of the art technology (Reference 5).

Table 4.2 Spacecraft Commands

	Discrete	Quantitative
Guidance and Control		
ACS electronics on	1	
Step size select	2	
Number of pulses		1
Maneuver select	4	
Start spinup	2	
Stop spinup	1	
Start despin	4	
Stop despin	2	
Spin speed trimmer position		1
Number of pulses for spin		1
Radio frequency tracking (on-off)	2	
Execute maneuver	1	
Data Handling		
Data mode select	8	
Data rate select	4	
Recorder (read-write)	4	
Redundancy switching	4	
Science		
Experiment (on-off)	20	
Mode change	12	
Calibrate	2	
Zero command	1	
One command	1	
Decode	1	
Store	1	
Auto sweep	1	
Stop sweep/step frequency	1	
Start frequency sweep	1	
Communications		
Transmitter/antenna select	6	
Receiver mode select	2	
Receiver (on-off)	2	
Feed Positioner	2	
TWT Positioner	2	
TWT (on-off)	2	
Power		
Converter switching (2 to 1)	1	
TOTAL	97	3

ELEMENT	POWER (watts)	WEIGHT (pounds)	SIZE (in^3)
DFE	0.40	4.0	152
DEE	0.62	4.5	100
CORE STORAGE	0.08	1.7	72
CDE	0.50	1.8	150
DSE	5.00 Record 8.00 Playback		
Each		9.00	250
Total		18.0	500
TOTAL	14.60	30.0	974

Table 4.3 Data Handling Specifications

4.7 REFERENCES

1. Corliss, W., Scientific Satellites, NASA Document No. SP-133.
2. Bauer, L., "Aerospace Engineering 485, Aerospace Communications," University of Michigan, 1969.
3. Instruments Handbook, Leach Corporation, Compton, California, 1967.
4. Treadwell, R. J., "Summary of Paper to be Presented at the Sixth Space Congress - University of Florida," RCA Defense Electronic Products, Astro-Electronics Division, March 1969.
5. "A Study of Jupiter Flyby Missions," General Dynamics, Report No. FZM-4625, 17 May 1969.

"Advanced Planetary Probe Final Technical Report," TRW Systems, 27 July 1966.

Bradbury, H. D., Personal Communication, 13 March 1969. (Manager Business Development, RCA Defense Electronic Products/Astro-Electronics Division)

"Kinelogic Corporation Model RSL Magnetic Recorder," Kinelogic Corporation, 1968.

"Kinelogic Corporation Model LR Magnetic Tape Recorder, " Kinelogic Corporation, 1968.

"Kinelogic Corporation Model RSL Magnetic Recorder," Kinelogic Corporation, 1968.

"Kinelogic Corporation Model HM Magnetic Tape Recorder," Kinelogic Corporation, 1968.

"Leach Bits," Leach Corporation, June 1967.

"Models QRD-2 and QRD-3 OGO Digital Tape Recorders," Specifications, Astro-Electronic Products, RCA, 1969.

"Model QRA-3 HRIR Tape Recorder," Specifications, Astro-Electronics Division, Defense Electronic Products, RCA, 1969.

"Model QRA-2 Video Tape Recorder," Specifications, Astro-Electronics Division, Defense Electronic Products, RCA, 1969.

"OAO Briefing Supplement," Gruman.

"PCM Encoders, Computers, Memory Systems, Analog-to-Digital Converters, Data Processing Systems," Spacetac Inc., 1968.

"Phase A Rerpot, Galactic Jupiter Probe," Volume I, Goddard Space Flight Center, Report No. X-701-67-566, November 1967.

"Pioneer Program," Ames Research Center, NASA Document No. P-200, 18 October 1968.

"Preliminary Progress Report, Galactic/Jupiter Probe Study," Lockheed Missiles and Space Company, Report No. LMSC-A848035, 30 June 1967.

"Preliminary Report of 0V1 Application to U of M Satellite 'Michael'," General Dynamics, Convair Division, Report No. GDC-DCJ67-002, 14 February 1967.

"Proceedings of the NASA - University Conference on the Science and Technology of Space Exploration," Volume 1, NASA Document No. SP-11, 1-3 November 1962.

"Raymond Magnetic Tape Recorder/Reproducers," Raymond Engineering Laboratory Inc.

Saliga, T. V., "A Comparison of Sequential Decoding Metrics by Computer Simulation," NASA Technical Report TR R-294, January 1969.

Sourcebook on the Space Sciences, Van Norstrand.

5
POWER

5.1 INTRODUCTION

The power source for UMPIRE is three SNAP-19 Radioisotope Thermoelectric Generators (RTG's). RTG's and solar panels were the only feasible alternatives for the power system. Considerable study was made on the conventional solar panel method before RTG's were chosen for UMPIRE. Significant problems which motivated the decision were the relatively large panel area that would be required due to the low solar intensity at Jupiter, the vulnerability of these large panels to damage from micrometeoroids and asteroid debris, the necessity of using the 9-foot antenna rather than the 16-foot antenna because of structural restraints, the rapid decrease in power available as the sun-spacecraft distance increases, and the need for on-board batteries as a secondary power source when the spacecraft goes through occultation at Jupiter. Thus RTG's were chosen because this power system eliminates the need for batteries, is independent of spacecraft sun orientation, provides a relatively constant power supply level, is unaffected by the occultation at Jupiter, is less susceptible to particle damage, and allows the use of the 16-foot antenna.

The RTG system, however, does present several integration problems in that the radiation produced by the isotope fuel can interfere with the radiation experiments carried on the spacecraft, and the magnetic field produced by RTG's restricts the measurement threshold of the magnetometers. However, the radiation damage effects can be eliminated, the radiation interference effects reduced to acceptable levels without shielding, and the effects of the magnetic field reduced significantly by designing the spacecraft to maximize the distances between the RTG units and sensitive components. For this reason the RTG's are boom mounted, the 50 degree angle from the vertical being a compromise for stability purposes.

The basic unit of the RTG system is the SNAP-19 with TAGS-2N thermoelectrics which produces 42 watts of power at 2.7 volts at beginning of life (BOL). This system will provide a power level sufficient to supply all power demands well beyond the rated lifetime of the mission.

Because of the stated advantages, and since the disadvantages of an RTG system can be feasibly reduced, if not eliminated, the RTG power system is the most advantageous system for this spacecraft and mission.

5.2 THE SNAP-19 RTG

The SNAP-19 Radioisotope Thermoelectric Generator is a device which transfers heat energy into electrical energy. The fuel (heat source) is Plutonium 238 isotope in the compound form of PuO_2, of which generally 80% by weight is Plutonium. The heat is produced as a result of the radioactive decay of the isotope. The fuel is in compound form because the temperature within the fuel capsule is above the melting temperature of pure Plutonium 238.

The TAGS-2N thermoelements convert the thermal into electrical energy with approximately 5% efficiency with the hot junction temperature at 975° F and the cold junction temperature at 420° F.

The isotope fuel produces alpha radiation which captures electrons when incident on the surrounding material, forming helium atoms. Over a period of time the pressure of the accumulating helium gas increases in the sealed RTG. If provisions are made to allow the gas to escape, there is the possibility of contamination due to fuel leakage. This threat of contamination is only critical while the RTG is on the ground or still under the dominant influence of the earth. Given the present structure of a SNAP-19, however, the helium gas pressure will exceed the critical pressure before Jupiter encounter. Thus, there must be a pressure release device to reduce the pressure during the cruise mode, where there is no longer a contamination restriction. The simplest pressure release device is a one shot burst diaphragm which, after bursting, allows an immediate exit path for the helium gas as it is produced. A second device is a repetitive pressure valve which is simple itself but still more complex than a burst diaphragm and slightly less reliable for an extended mission.

A simple cutaway diagram of the SNAP-19 RTG is shown in Figure 5.1. The fuel capsule contains 1,603 grams of PuO_2 which produces 625 watts of thermal energy. Most of this energy, 95%, must be dissipated as excess energy and this is accomplished by the fins which radiate the heat into space. The overall length of the SNAP-19 is 11 inches, and the overall diameter is 21 inches, two-thirds of which is radial fin length. The total weight of the fueled SNAP-19 unit is 30.5 lbm.

The SNAP-19 has an integral reentry heat shield that meets the NASA requirements of intact reentry in the event of a mission abort. This capability was demonstrated in May 1968, when the Nimbus B launch, carrying two stacked SNAP-19's, was aborted during the ascent phase and the RTG's were recovered almost unscarred.

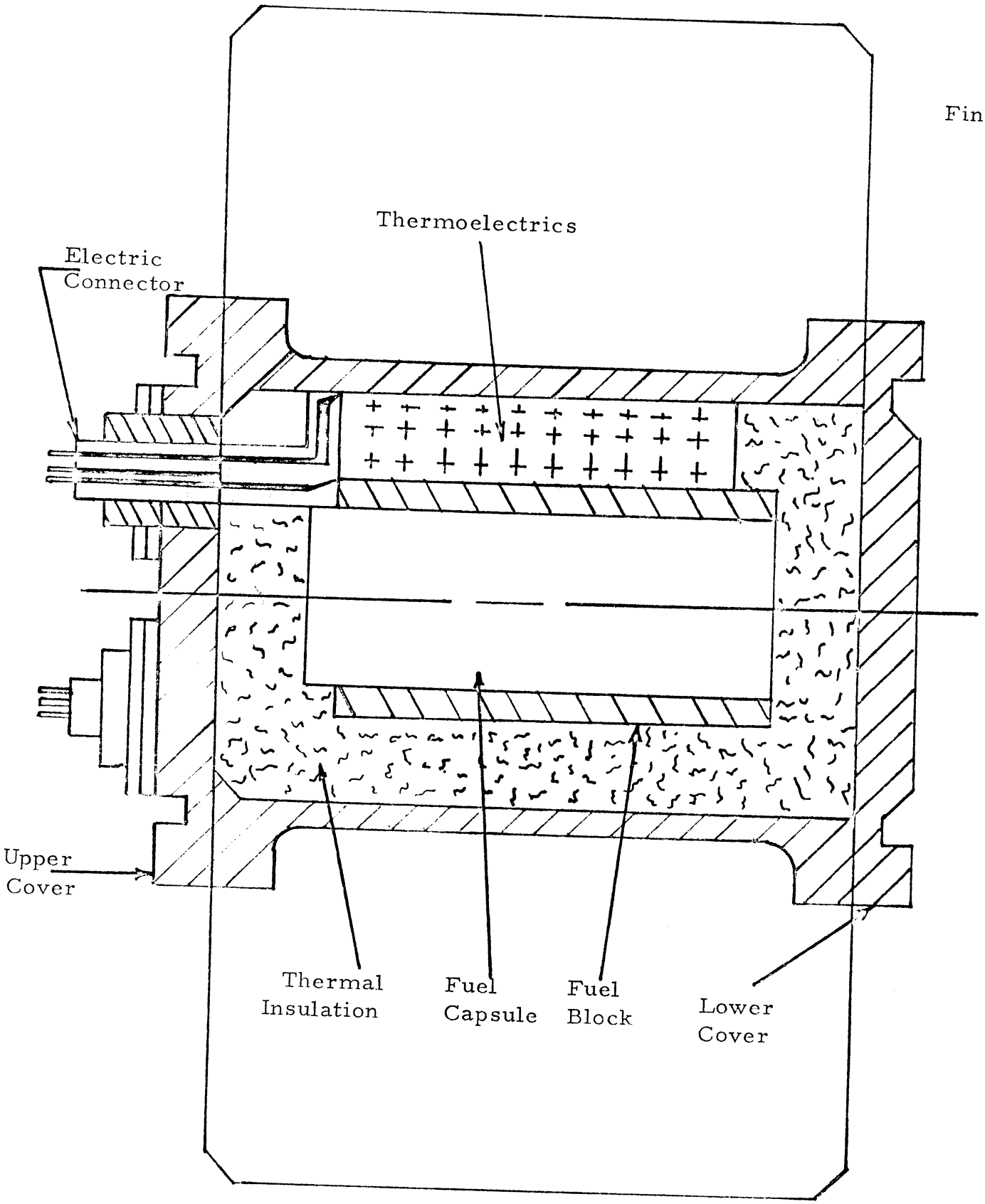

Figure 5.1 SNAP-19 Generator Assembly

5.3 POWER CONDITIONING UNIT

The power conditioning unit (PCU) for this mission should consist of two complete DC-DC converters, a filter for the output to the spacecraft loads, a shunt regulator for each converter, a converter selector relay, and fault sensing and switching circuits (Reference 1). A block diagram of the PCU is shown in Figure 5.2.

The two DC-DC converters and shunt are identical and contain transformer-rectifier systems which produce the unfiltered bus line voltage. The filter is shown separately from the converters because it is common to the output of both converters. The regulators compare load demands with the RTG's supply and control a variable shunt load to protect the RTG's from overheating due to loss of load.

Fault sensing and switching circuits are provided which sense the unfiltered line voltage output and if this voltage becomes too high or too low, cause the converter selector relay to switch the RTG input from the No. 1 to the No. 2 regulator and converter. This is a one-way switch, but there is the capability of switching back to No. 1 by use of a ground signal.

The efficiency of the PCU is approximately 89%. The total weight of the PCU capable of handling the RTG's is 8.5 pounds.

5.4 POWER PROFILE

Each SNAP-19 produces 42 watts of electrical power at BOL, 37.38 watts after converter losses. In addition, the thermal elements degrade with time, reducing the actual usable power as the mission progresses. Figure 5.3 shows the usable power supply curve as a function of mission time. For this analysis it was assumed that the RTG was fueled shortly prior to the start of the mission. At Jupiter encounter, twenty months after launch, there is 98.8 watts available for the spacecraft loads.

The power demand curve for this mission is also shown in Figure 5.3, below which is a breakdown of the power allotment for each different total power value. At Jupiter encounter there is an excess of 27.33 watts available. This margin will allow for the possibility of multiple thermoelement failures.

Since the RTG power system is independent of the sun, the proposed occultation does not affect the spacecraft power system, and since there is always more than sufficient power available for the minimum necessary life-time of the spacecraft, the need for energy storage for this mission has been eliminated.

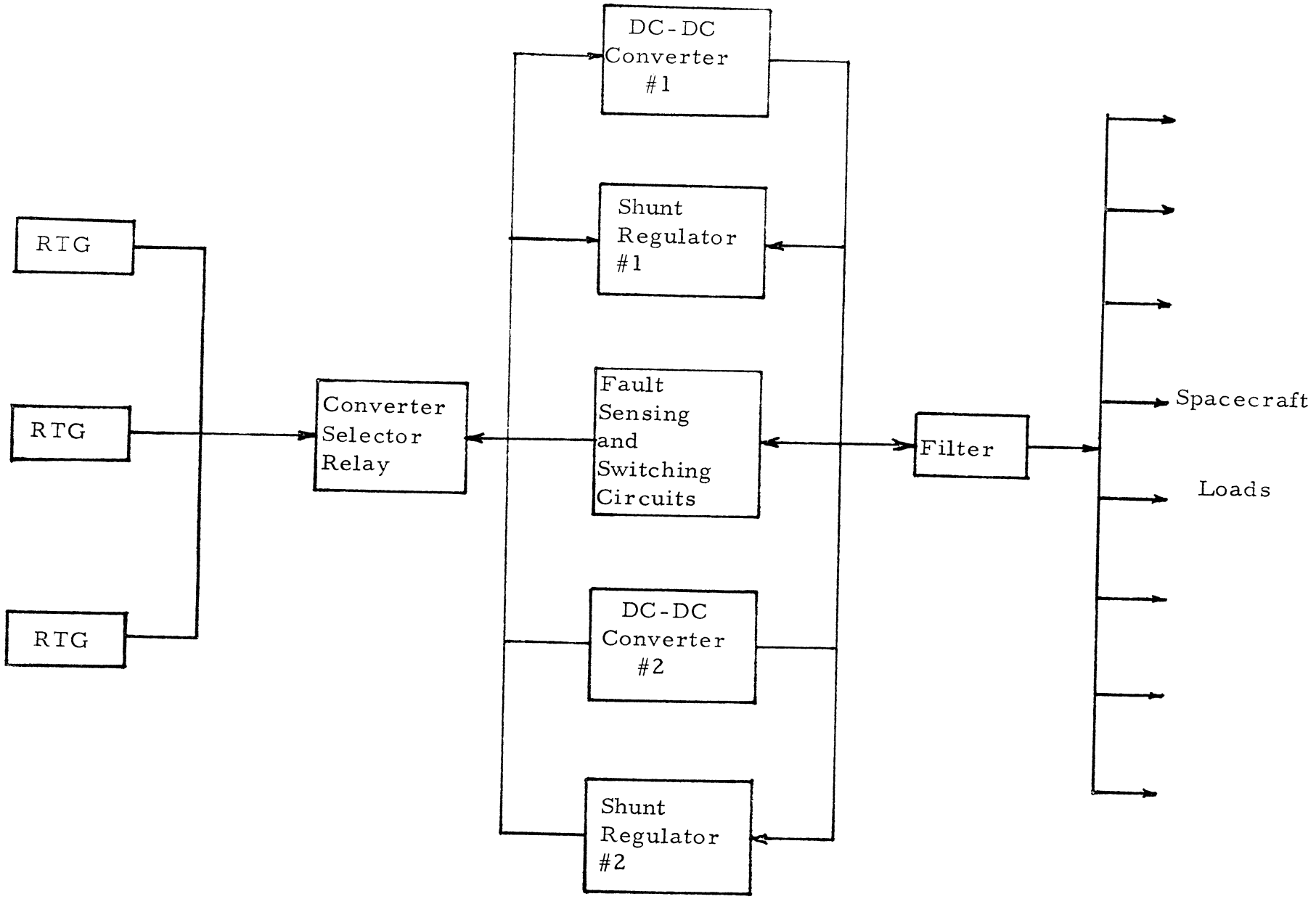

Figure 5.2 PCU Block Diagram

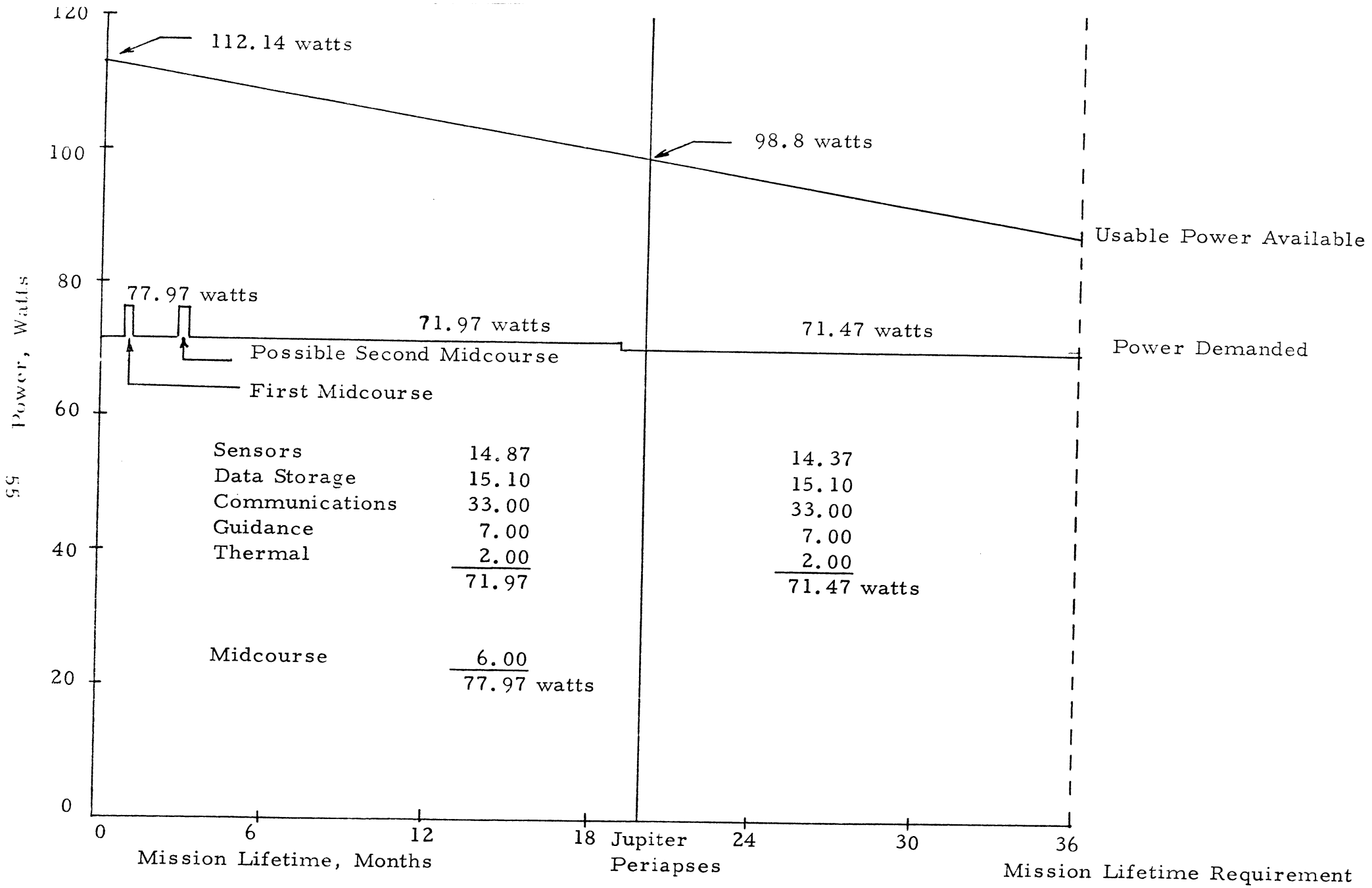

Figure 5.3 Power Supply/Demand Profile

MEASUREMENT	AT CENTER OF BASE PLATE DISK	AT BOOM MOUNTED SENSOR
Gamma Flux	3.425 mrad/hr	0.485 mrad/hr
Neutron Flux	409.0 $\frac{n}{cm^2\text{-sec}}$	57.87 $\frac{n}{cm^2\text{-sec}}$
Magnetic Field	---	0.300 γ
Integrated Gamma Flux: 20 months 36 months	 4.93×10^4 mrad 8.87×10^4 mrad	 6.980×10^3 mrad 1.256×10^4 mrad
Integrated Neutron Flux: 20 months 36 months	 2.12×10^{10} n/cm^2 3.82×10^{10} n/cm^2	 3.0×10^9 n/cm^2 5.40×10^9 n/cm^2

Table 5.1 Radiation and Magnetic Effect Measurements

5.5 POWER SYSTEM WEIGHT SUMMARY

Each SNAP-19 RTG unit weighs 30.5 pounds, which includes the isotope fuel change and the intact reentry heat shield; the three RTG units total 91.5 pounds. This power conditioning unit, which is located on board the spacecraft, weighs 8.5 pounds including the converters, regulators and filter. The total weight of the three SNAP-19 RTG power system is 100 pounds.

5.6 RADIATION AND MAGNETIC CONSIDERATIONS

In the present configuration, each boom mounted sensor is affected the same as the other two. For each sensor, two RTG's are 15.03 feet away and the third RTG is 22.4 feet away (Appendix C). These distances are significant because the radiation flux is inversely proportional to the square of the separation distance, and the magnetic field is inversely proportional to the cube of the separation distance. Table 5.1 shows the radiation flux and/or magnetic field at specific points on the spacecraft, and the integrated radiation dose rate for 20 months and 3 years (Reference 1).

The magnetometer will have a lower limit of 0.3γ on its measurement of interplanetary and Jupiter magnetic fields. The instruments aboard the spacecraft will not be damaged by the radiation, and the radiation sensitive instruments can be oriented to avoid interference from the RTG's.

5.7 REFERENCES

1. Schulz, R.B., "Radioisotope Thermoelectric Generator (RTG) for Improved ALSEP," Aerospace System Division, Bendix Corporation Report No. ETM-087, 18 June 1968.

"Advanced Planetary Probe, Jupiter Fly-by Application," Jet Propulsion Laboratory, Report No. EPD-358, Revision 1, 12 August 1966.

Cosby, W.A., and R.J. Lyle, "The Meteoroid Environment and its Effects on Materials and Equipment," Jet Propulsion Laboratory, NASA Document No. SP-78, 1965.

"Final Report, Voyager Spacecraft, Phase B, Task D, Volume IV, Book 1, Effect of Capsule RTG's on Spacecraft," General Electric Missile and Space Division, Report No. DIN 6750D4379, 16 October 1967.

Heitler, W., The Quantum Theory of Radiation, Clarendon Press, Oxford, 1954.

Memo from K. Wainio, ND-7451, Bendix Systems Division, Ann Arbor, 27 April 1967.

"Preliminary Progress Report, Galactic/Jupiter Probe Study," Lockheed Missile and Space Company, Report No. LMSC-A848035, 30 June 1967.

Sandstom, J.D., "A Method for Predicting Solar Cell Current-Voltage Curve Characteristics as a Function of Incident Solar Intensity and Cell Temperatures," Jet Propulsion Laboratory, Technical Report 32-1142, 15 July 1967.

Strack, W. C. and C. L. Zola, "Solar Electric Propulsion Probes for Exploring the Solar System," Lewis Research Center, Cleveland, Ohio, Report No. TMX-52318, 1967.

"Study and Analysis of Satellite Power Systems Configurations for Maximum Utilization of Power," TRW Systems, NASA Document No. CR-898, October 1967.

Volkoff, J., "Protection Requirements for the Resistance of Material Penetration Damage of Interplanetary Spacecraft Systems," Jet Propulsion Laboratory, Technical Report No. 32-140, 1 July 1964.

6
STRUCTURES

6.1 FACTORS AFFECTING GENERAL CONFIGURATION

This Jupiter flyby probe must meet certain mission requirements. The requirements imposed result mainly from the need to communicate over large distances and the need for a reliable power source during all phases of the mission. The large distance to be traversed by the craft, approximately five astronomical units, makes communication very difficult. To accommodate this constraint a sixteen foot deployable antenna was adopted. The power source consists of three Radioisotope Thermoelectric Generators (RTG's).

All the subsystems of the spacecraft influence the final configuration, though some to a lesser degree than others. The structural design and spacecraft arrangement are influenced primarily by:

1) The high-gain antenna
2) The Radioisotope Thermoelectric Generators
3) Those experiments which are particularly susceptible to radiation and magnetic fields.

6.1.1 Antenna Considerations

To compensate for the free space losses of the large communication distances involved, high gain must be provided. A sixteen foot parabolic antenna utilizing Cassegrain feed will be used to accommodate the desired bit rate. The choice of launch vehicle imposes a constraint of a diameter less than 115 inches, so the antenna must be of a deployable nature.

6.1.2 Radioisotope Thermoelectric Generators

The RTG's represent the heaviest entity on the spacecraft. Since they represent concentrated masses, they have a pronounced effect on the mass properties of the craft. Stability considerations demand that the three RTG's be placed symmetrically about the craft. However, their high level of thermal radiation requires that they have a large solid angle of view. Therefore, they are located on booms. This configuration also removes the RTG's from the radiation-sensitive experiments.

6.1.3 Experiments Sensitive to Radiation and Magnetic Fields

Those experiments sensitive to radiation need to be isolated from the RTG's. Since the RTG's are already boom-mounted, the critical experiments were mounted on booms to further increase their distance from the radiation source. This configuration also allows the experiments sensitive to magnetic fields to be placed at a safe distance from the RTG's.

6.2 GENERAL CONFIGURATION

To meet the requirements described in the previous section, the configuration as shown in Figures 6.1 and 6.2 evolved. The desired transmission rate and large distances required a sixteen foot antenna. To accommodate the launch vehicle constraint as stated earlier, the folding antenna was chosen. Launch vehicle constraints also dictated a folding boom for the RTG system. The science booms are also folding, thus giving a second controlling factor on the moments of inertia. The symmetry of the RTG's about the craft required that the science booms also be placed symmetrically about the craft.

The experimental package is cylindrical in shape, giving maximum volume. The conventional hexagon proved unnecessary as all components are floor mounted to facilitate heat dissipation. The entire package is surrounded by a two-inch micrometeoroid shield. Inside the craft there is superinsulation which provides part of the thermal control. The forward compartment serves as a housing for the omni antenna, plasma probe sensors, conical scan antenna, and mid-course thruster. The subreflector for the antenna is also located in this compartment.

Beneath the instrument compartment there are three sets of louvers which form the active part of the thermal control system. The instruments inside the main compartment are placed so that the temperature gradient on the plate is not excessive. This is accomplished by placing the high heat dissipating devices between the louvers. Such placement assures even heat distribution (Table 6.1 and Figure 6.3).

Adaption of the craft to the TE-364 engine is accomplished by an attachment ring located on the underside of the base plate. This ring mates with the adapter of the injection engine (Figure 6.4).

6.3 STRUCTURAL COMPONENTS

6.3.1 The Main Instrument Compartment

The primary component of this compartment is the center tube which adds compressive and torsional rigidity to the structure. It also serves as a fastening mount for the radial bars and struts. This tube houses the hydrazine tank needed for the mid-course and precession thrusters; mounts are provided inside the tube for fastening the tank. The tube is made of 2024-T4 aluminum alloy, 0.025 inches thick.

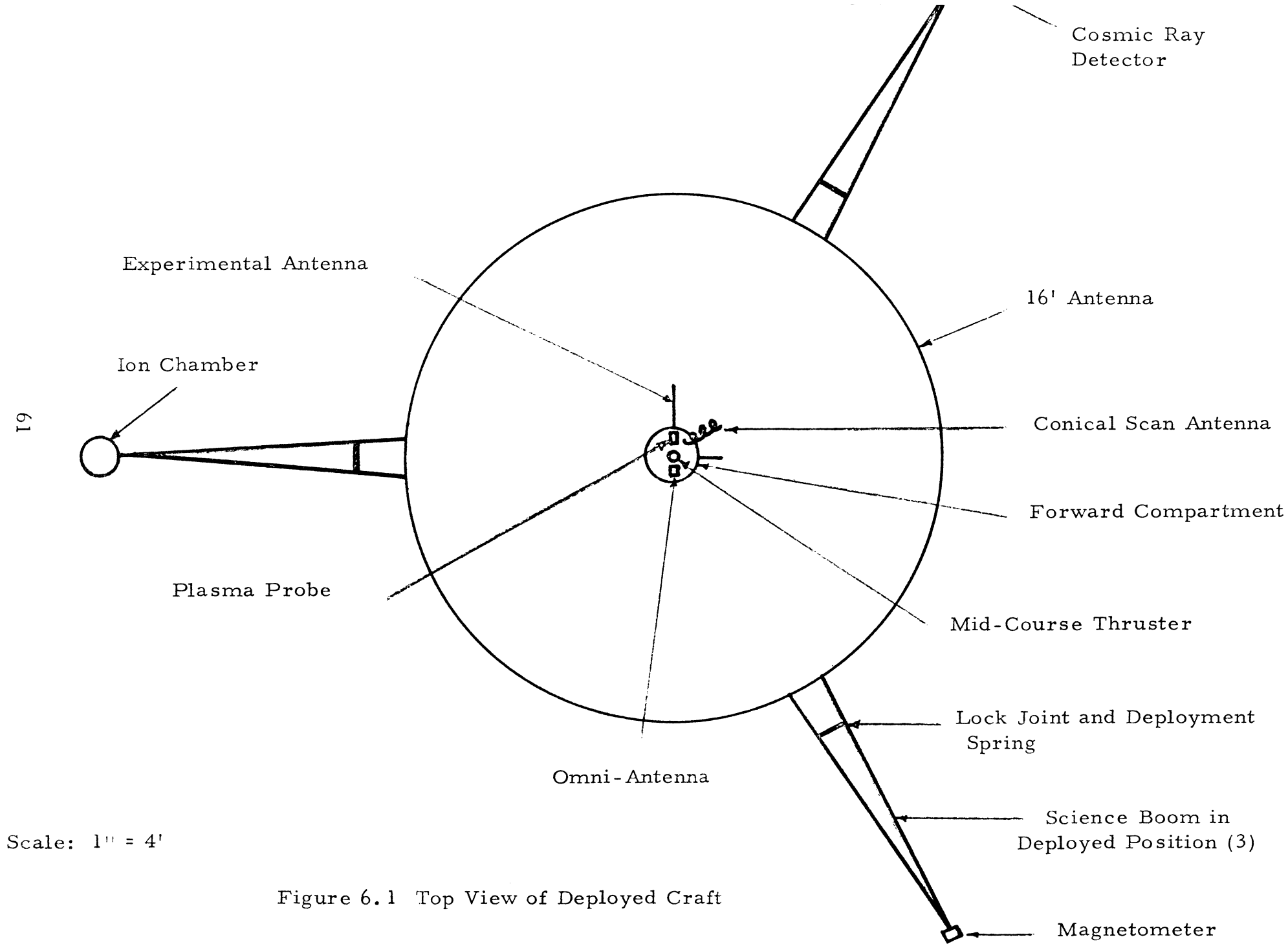

Figure 6.1 Top View of Deployed Craft

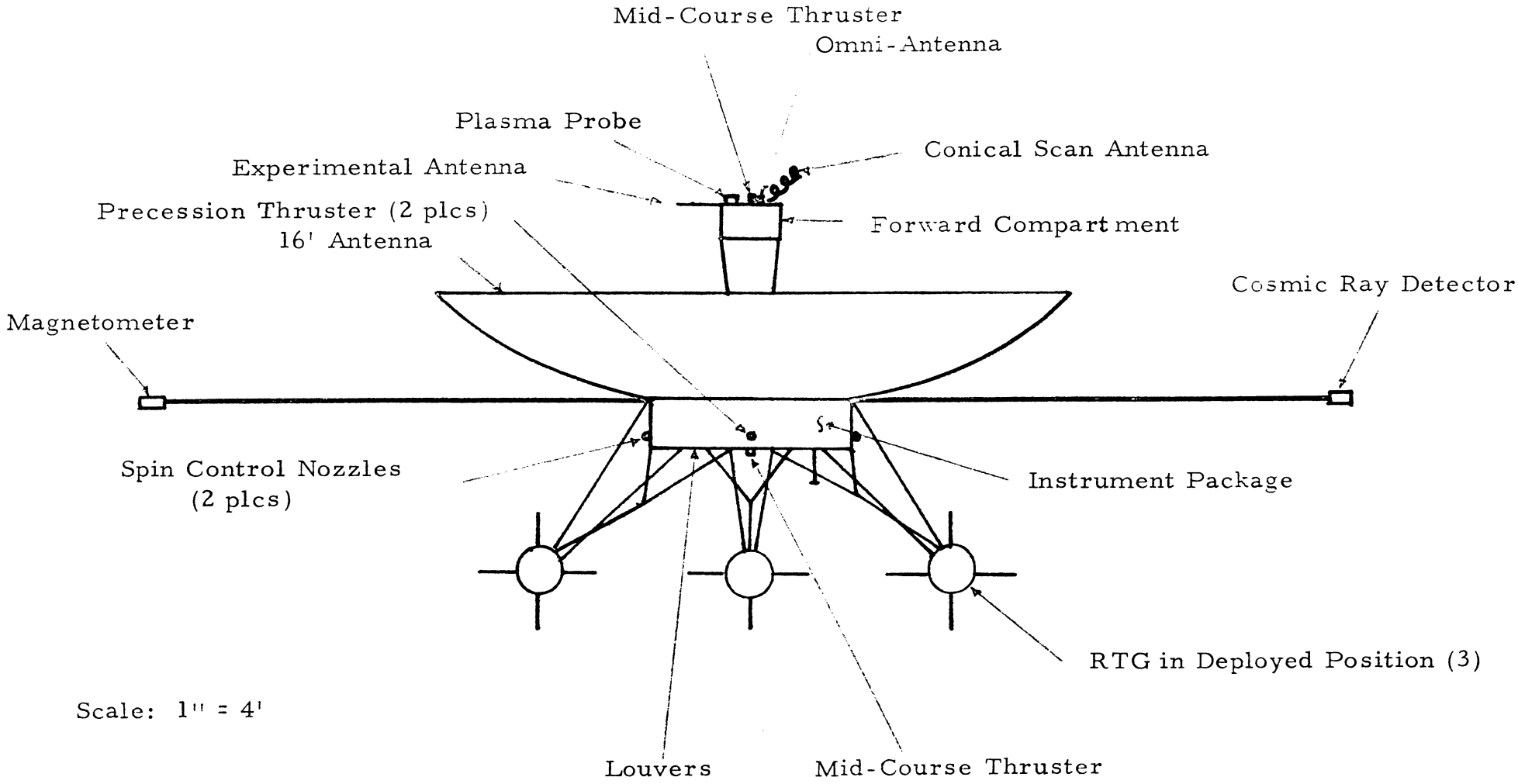

Figure 6.2 Side View of Deployed Craft

Component	Symbol
Fluxgate Magnetometer	S1
Energetic Particles	S2a
Particle Telescope	S2c
Micrometeoroid Detector	S3
Plasma Probe	S4
Radio Propagation	S5
IR Radiometer	S6
Cosmic Ray Detector	S7
Lyman Alpha Photometer	S8
Radio Astronomy	S9
Traveling Wave Tube and Integral Power Supply	C1
Transmitter	C2
PLL Receiver	C3
Diplexers	C4
Omni-Coupler	C5
Switching Mechanisms	C9
Traveling Wave Tube Control Selector	C10
Receiver Control Unit	C11
Decoder and Encoder	D. E.
Tape Recorders	T. R.

Table 6.1 Instruments in Main Compartment

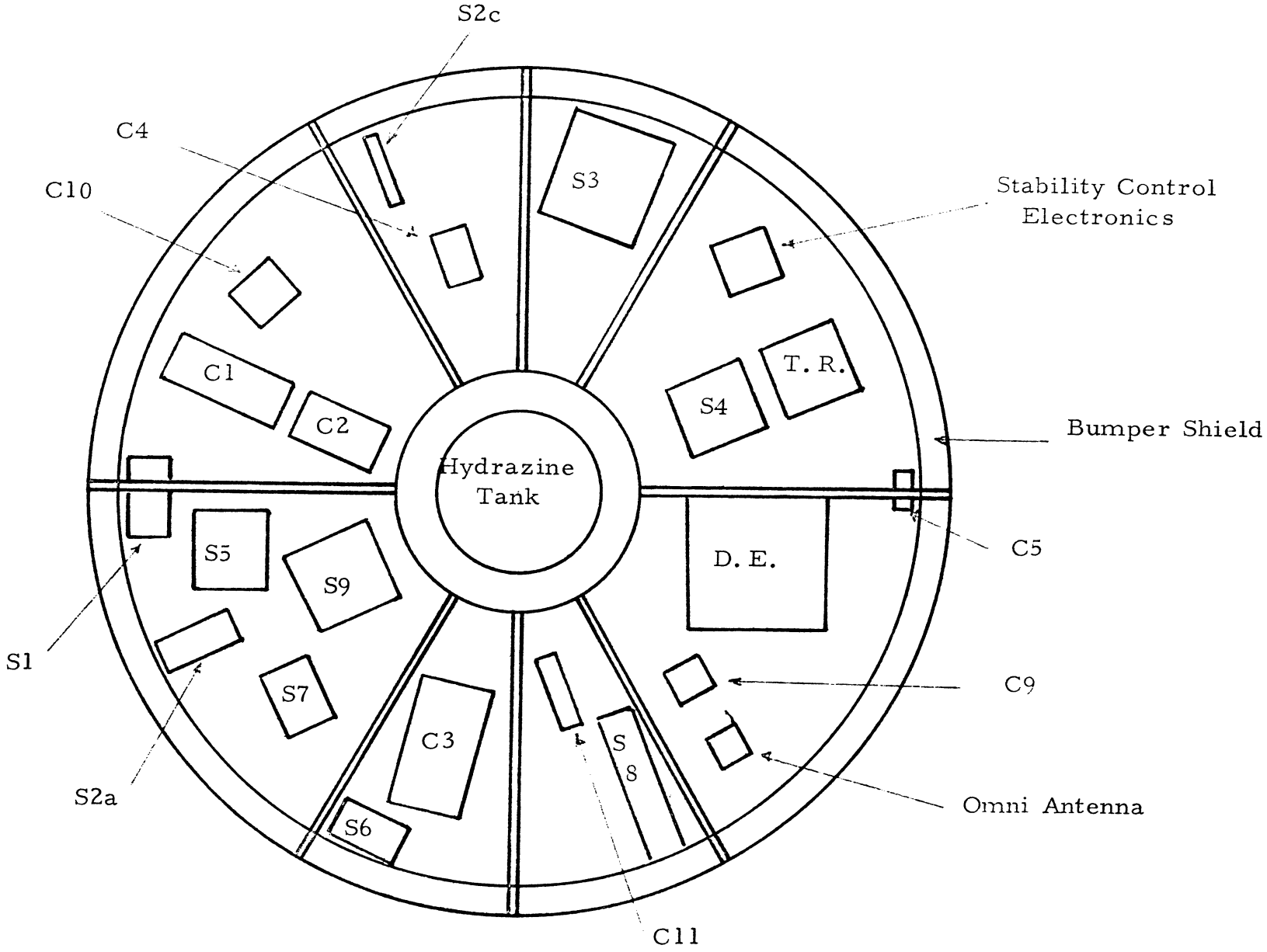

Figure 6.3 Main Compartment

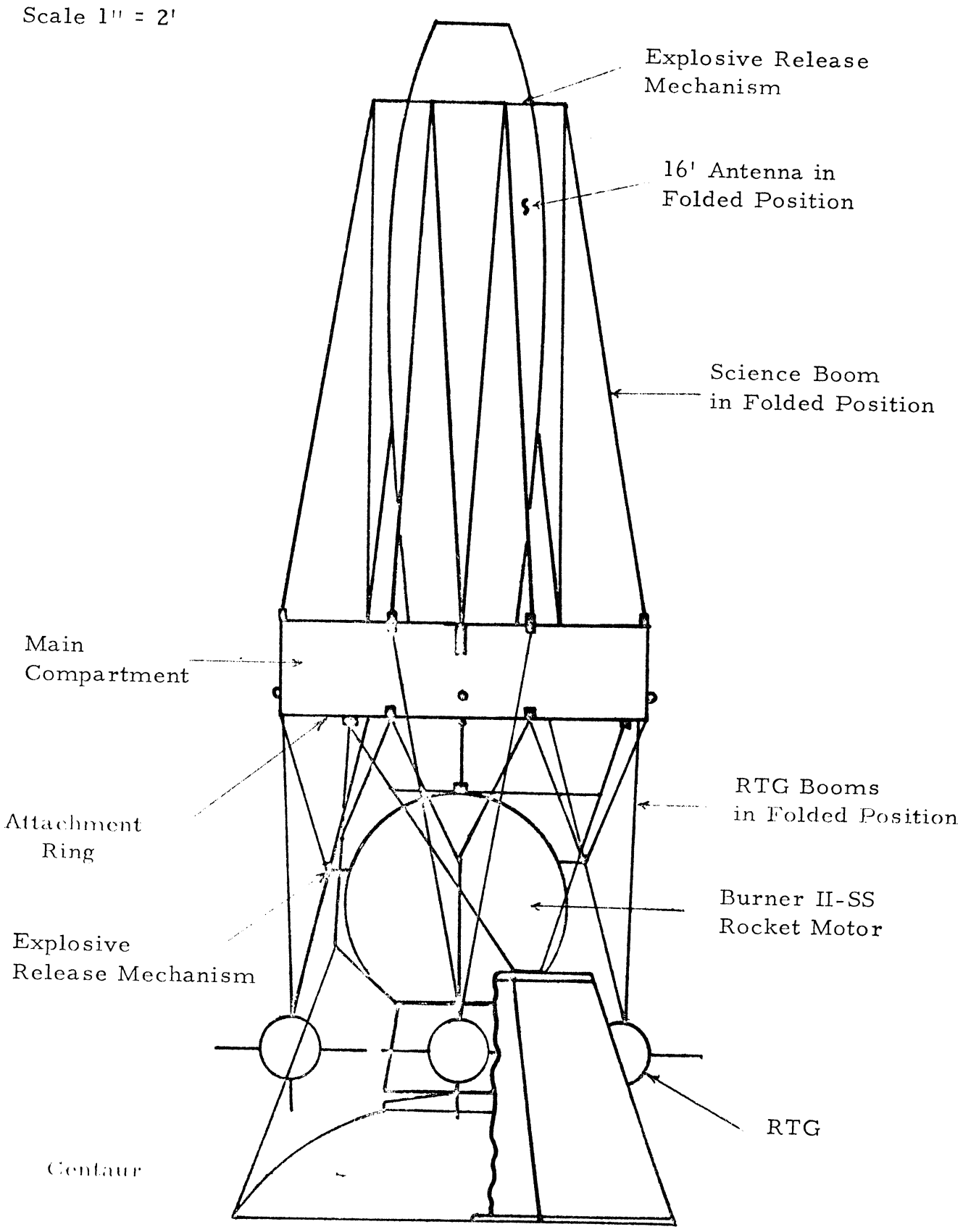

Figure 6.4 Spacecraft in Stowed Position

Protruding radially outward from the center tube are sixteen channel bars made of 2024-T3 machined aluminum alloy. They also are 0.025 inches thick and one inch on each side. These bars give lateral rigidity to the structure while providing a plane on both the top and bottom of the craft to which the main plates may be fastened. Eight channel cross-struts located in pairs ninety degrees apart around the craft add longitudinal rigidity to the spacecraft. These struts are the main load bearing members during launch. The eight channel vertical bars further add to the longitudinal rigidity while also providing attachment points for the thermal and micrometeoroid shielding. Connecting these vertical bars are two 0.025 inch thick, 2024-T4 machined aluminum alloy angle pieces. These function as a mating part for the top and base plates to join the side panels.

The skin of the craft is 2024-T3 aluminum alloy. The actual skin is located two inches inside of a bumper shield. The purpose of this shield is to protect the spacecraft from micrometeoroid puncture. The thickness and weight of these shields is discussed in Section 7.3 (micrometeoroid protection). This bumper shield comes in four units which bolt to the eight vertical bars, thus allowing easy access to the main compartment.

The base plate to which all components are attached is a 0.0935 inch thick, 2024-T4 aluminum alloy plate. The center tube is bolted to this plate along with the bottom set of horizontal channel bars. The top plate is 2024-T3 aluminum alloy which is 0.01 inches thick. It attaches to the angle pieces and bolts to the center tube. Figures 6.5 and 6.6 indicate the major structural components as described above.

6.3.2 The High-Gain Antenna Attachment

The folding antenna to be used is a self-contained unit. No structure is needed to support the dish as its own stiffeners will carry the load. The unit extends from an eighteen inch base plate. This plate will mate with the center tube and be bolted to it. Fiberglass washers are used to lower the heat loss across the joint. The forward compartment housing, the subreflector, and various experiments are specified as part of the unit and no extra structural support is needed.

6.3.3 Science Booms

As described earlier, the magnetometer and energetic particle experiments are located on booms to remove them from the craft and the RTG's. The determination of the boom length proves to be a critical problem. The criteria are: (1) maximize the distance from the RTG's to these packages; (2) keep the booms within an acceptable weight limit; and

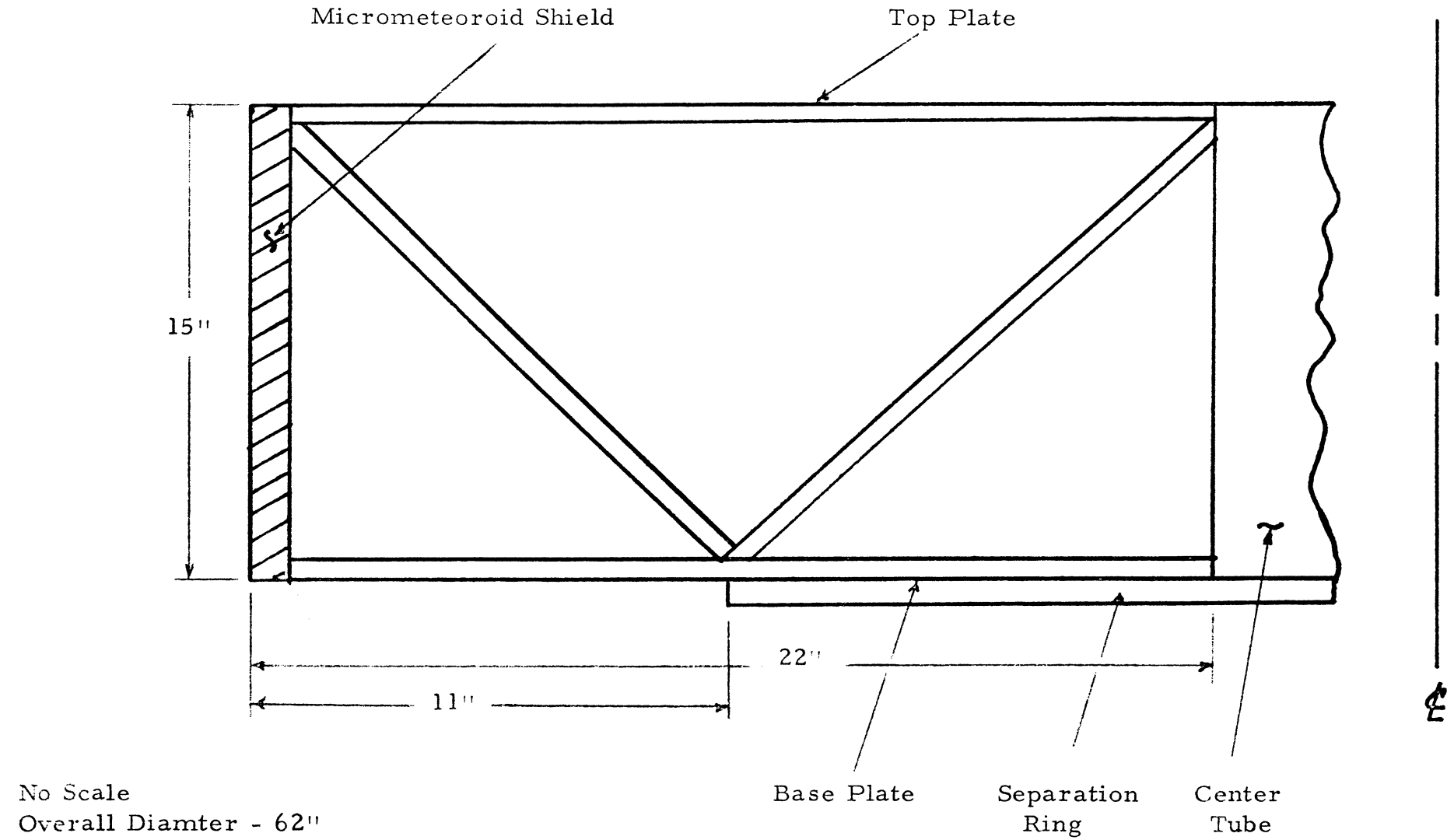

Figure 6.5 Structural Components (Typical Section)

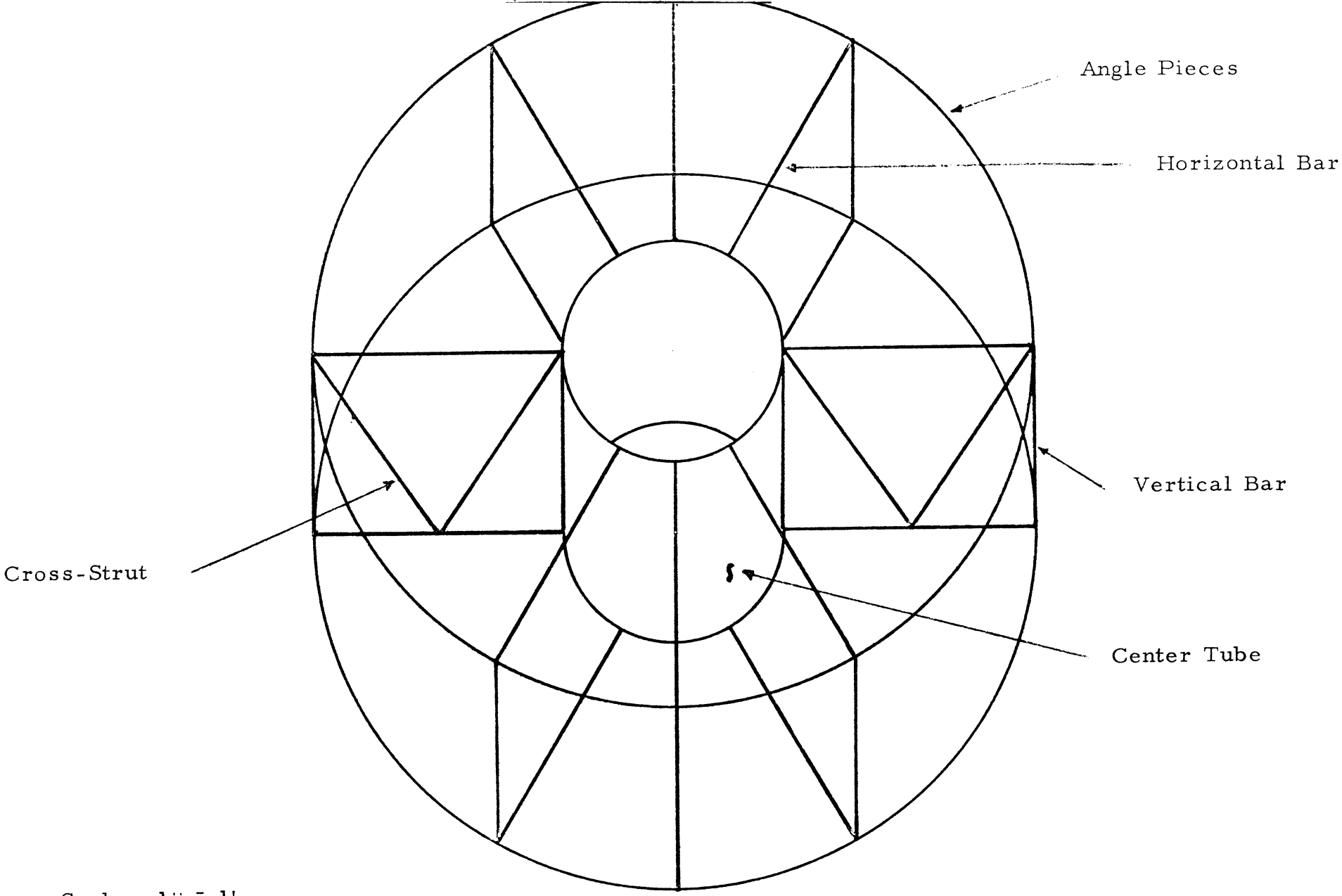

Scale - 1" = 1'

Figure 6.6 Structural Lay-Out

(3) avoid long booms which may cause excessive structural boom loading. Furthermore, the separation distance has to be such that shielding does not become prohibitively heavy. The fourteen foot boom length finally evolved as the one most acceptable to all requirements. Horizontal deployment proves sufficient, thus eliminating excessive structural support necessary for an angled boom.

Several designs were considered for the boom shape. Telescoping booms prove too unreliable and are excessively heavy. Launch constraints require a deployable configuration. The folding boom meets these requirements. Furthermore, because of the spin-stabilized mode, the A-frame design proves to be the most stable. To account for the shock loading at deployment, the booms are rectangular in cross-section. Each boom is hinged at two points on the craft at the top of the instrument package. This placement results from the radiation and stabilization constraints. The booms are made of 2024-T4 aluminum alloy with 2024-T4 aluminum alloy hinges. The folding line is located at the mid-point of the boom. The three booms, when folded, are ten degrees from the vertical. They are connected by an explosive release mechanism. When fired, these mechanisms also release the folding joint to assure smooth deployment. Centrifugal force will most likely assure deployment, but a torsional spring in both hinges provides a back-up system. A lock hinge at the folding line locks the boom in position after it is deployed. Further study may show that velocity limiters are needed to reduce the shock loading at deployment (Reference 1).

6.3.4 RTG Support

The RTG supports consist of a V-shaped frame with a Y-shaped sub-support. In the folded position, the joint of the Y-strut is connected to the TE-364 by an explosive mechanism. When fired, centrifugal force will deploy the booms. A torsional spring located in the bottom two hinges provides the back-up system. The Y-strut will lock in place when the angle from the vertical reaches fifty degrees. This strut is also provided with a shock-absorber to decrease the shock loading at deployment.

The high operating temperatures of the RTG's prohibits the use of aluminum as strut material. Titanium 6Al-4V was decided upon because of its high strength-to-weight ratio in the given temperature range. The struts are 0.025 wall tubing which is 1.25 inches in diameter.

6.3.5 Shielding

The use of small shields at the instruments proves to be superior to the use of large shields near the RTG's. This design uses the $1/r^2$ factor to reduce the shielding weight. Further, the RTG's are pointed toward the ion chamber to reduce the radiation hazard and the particle count. This configuration is based on the fact that the radiation flux is less dense on the ends of the RTG's than on the sides. The large separation distance between the magnetometer and the RTG's is sufficient to keep the magnetic field near the magnetometer at a safe level.

6.3.6 Structural Weight Estimate

Component	Weight (lb)
Experimental Package	
top plate	3.4
base plate	30.1
cross-struts	1.1
vertical bars	0.9
horizontal bars	2.5
center tube	2.4
angle pieces	1.0
RTG Booms	
long struts	3.06
erection struts	1.34
short struts	0.60
brackets, hinges	3.00
Science Booms	
long struts	12.1
short struts	0.5
brackets, hinges	2.0
Misc. Hardware	4.0
TOTAL	68.00

Table 6.2. Structural Weight Estimate

6.4 REFERENCES

1. "Phase A Report, Galactic Jupiter Probe," NASA Document No. X-701-67-566, November 1967.

Osgood, C., Spacecraft Structures, Prentice Hall, Englewood Cliffs, New Jersey, 1966.

7
THERMAL CONTROL

7.1 INTRODUCTION

Project UMPIRE marks the beginning of a new phase of space exploration, that of deep space. Deep space presents many new and more severe environmental constraints on the spacecraft. The thermal subsystem of Project UMPIRE must solve the problem of these new constraints and provide the spacecraft with a suitable environment in which to perform its planned operations. In traveling to Jupiter, the spacecraft must go five times the Earth's distance from the sun, causing a never-experienced extreme in temperature. With temperatures on the skin of the satellite reaching -300° F, the interior must be maintained between 40 and 80° F to assure proper performance of electrical and propulsive equipment. In addition, the thermal control subsystem must keep these low temperatures and the possible resulting thermal gradients from causing dangerous mechanical and structural thermal stresses. Finally, the constraints include the little know meteoroid and radiation fields between Earth and Jupiter; precautions must be taken to assure reasonable protection against the possible damage of meteoroids and degradation due to radiation.

7.2 THERMAL SYSTEM

7.2.1 General

The basic objective of the UMPIRE thermal design is to assure, through environmental control of the internal spacecraft, a maximum long-life reliability of all components against the previously mentioned mission constraints. A temperature control system must maintain an optimum environment in which electronic equipment and experiments can function to design standards.

In all previous missions, the thermal energy for temperature control has primarily come from the sun. Until now, the sun has been an adequate, reliable source of thermal energy. However, because of the nature of this mission, the sun is not considered a feasible source of energy and becomes insignificant during most of the mission. A graph of the variation of solar energy as a function of distance from the sun is shown in Figure 7.1 (Reference 1).

The temperature control design for UMPIRE will utilize the thermal energy dissipated by the electrical equipment to create an isothermal module through an active control system of louvers and superinsulation. Due to the large amounts of heat radiated by the RTG's, additional considerations and precautions must be taken.

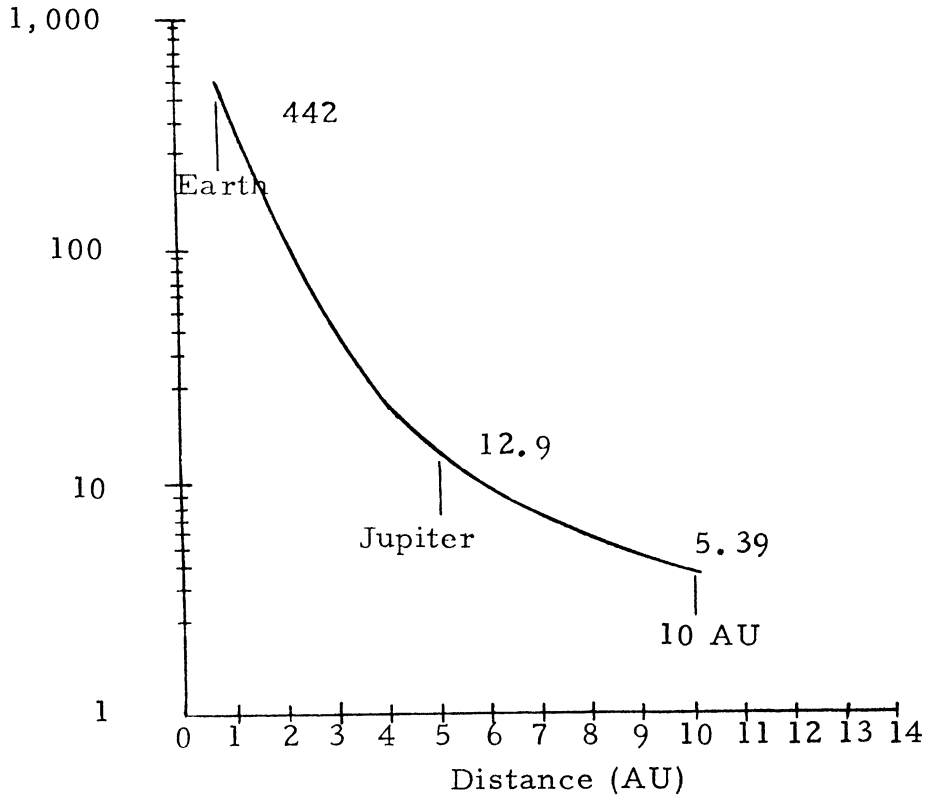

Figure 7.1 Variation of Solar Constant as a Function of Distance from the Sun

The design is separated into two major parts: the main equipment compartment and the separated equipment packages, including any problem areas. Following this is a brief discussion of heat problems associated with the RTG's on the launch pad and in the shroud between the time of launch and injection into Jupiter orbit.

7.2.2 Main Equipment Compartment

Analysis. In designing the temperature control system for UMPIRE, an equation and its terms are needed. Accurate predictions and calculations must be made to keep the internal and entering heat equal to the heat leaving the spacecraft through conduction, convection, and radiation to deep space. Below is the heat balance equation and a brief discussion of the considerations behind each term in regard to this mission. Actual numerical analysis of the equation can be found in the Appendix E.

$$Q_{in} = Q_{out}$$

with $Q_{in} = Q_{environ.} + Q_{internal} + Q_{conduction/RTG's} + Q_{radiation/RTG's}$

and $Q_{out} = Q_{radiation/spacecraft} + Q_{heat\ loss}$

$Q_{environ.}$ - The heat entering the spacecraft due to environmental effects. This term includes direct solar energy, reflected solar energy from planets, and planetary thermal radiation. The latter two are very small due to the distance of the spacecraft from Jupiter and from the sun. The direct solar energy causes a greater problem because the intensity of the solar energy varies from 130 watts/ft^2 at earth to 4.8 watts/ft^2, as previously mentioned. By making the admittance quality of the spacecraft's skin low and/or by superinsulation this term can be considered very small.

$Q_{internal}$ - The heat present due to the dissipation of thermal energy from the experiments and electrical components. This term is the internal power supplied to the spacecraft from the RTG's.

$Q_{conduction/RTG's}$ - The heat that is conducted through the connecting struts between the RTG and spacecraft due to the high surface temperature of the RTG. Thin multi-supported struts with fiberglass insulated joints generally reduce this term to near zero. Utilization of this heat can be obtained by the use of heat pipes (to be explained later).

$Q_{radiation/RTG's}$ - The heat absorbed by the spacecraft due to the radiating heat produced by RTG power sources. The possible uses and effects of this heat will be discussed later in this section.

$Q_{radiation/spacecraft}$ - The heat loss from the spacecraft through convection and radiation of heat to the heat sink of deep outer space. Great changes in this term can be made by changing the effective emittance and/or the surface area of the spacecraft. Superinsulating materials can reduce this figure to an extremely small number.

$Q_{heat\ losses}$ - The heat lost from the conduction and convection of heat out of the spacecraft through sensor openings, propulsive devices, structural components, wires, and cables. Heat loss will be controlled with fiberglass joints and insulation (to be explained later).

Possible Approaches. The simplest method of thermal control would be the passive system. A passive thermal design must maintain a proper energy balance between heat input and energy loss by means of radiation and conduction. Because of the variations in solar energy over the lifetime of the spacecraft and of possible heat losses due to structure or to power failures, the passive system has been eliminated in favor of the more flexible active system.

There are few major methods of active temperature control possible for the mission. They are heat pipes, active louvers, thermal switches, and heaters (electrical or isotope). Each method can be varied according to the source of thermal energy. The only two feasible sources of heat are the RTG's and the electrical equipment package.

The waste heat from the RTG's presents a favorable approach for the use of an active control device. However, the use of this heat places limitations on a number of the spacecraft design configurations. With the RTG deployed away from the spacecraft, radiation heat-transfer could be used. The side of the spacecraft viewing the RTG could contain active control louvers to admit the desired amount of heat. Thermal switches could also be used on the viewing side to obtain proper heat. However, the RTG's would have to be located sufficiently close (about 2 feet) to insure good radiation input.

Another method of obtaining thermal energy from the RTG is through heat transfer via heat pipes or in the supporting struts. Heat added at one end vaporizes the fluid, which condenses at the other end and then returns through an internal wick. Because the RTG's are deployable and heat pipes are very susceptible to leaks, the reliability of this system is questionable.

The simplest and most desirable form of thermal energy available is found within the spacecraft itself--its own heat dissipation of electrical components. Except for short periods of time, the power is fairly constant and should be sufficient to maintain proper temperature. Here, again, the two methods of active control of spacecraft temperature are louvers and thermal switches. The louvers would vary the emittance of the bottom panel to control changes in temperature that could develop. The thermal switch causes heat to flow between the heat source and a fixed contact plate through temperature-controlled bimetallic elements or a fluid-expansion-bellows arrangement.

Design Configuration. Project UMPIRE will use internal heat dissipation to maintain proper temperature range through the use of an aluminized Mylar superinsulation and bimetallic, thermally controlled louvers. The instrument placement on the base plate is such that high heat dissipating instruments are alternated around low heat instruments to minimize thermal gradients.

Due to the large variation in external heat during the flyby mission, the temperature sensitive instrument package must be kept isolated from the external environment. To keep heat loss from radiation to a minimum, a superinsulation blanket of numerous alumnized Mylar layers will be used. The effectiveness of this blanket increases with the number of layers, assuming adequate separation between the layers. Separation will be obtained by adding a filler substance in alternate layers. Careful consideration should be made to assure minimal heat loss through structure and sensor openings. Inadequate blanket fabrication around openings could cause a thermal "short". Insulation mounts will be employed to prevent significant heat losses arising from metal-to-metal contact. These mounts will be made of low thermal conductivity fiberglass.

Because the blanket effectiveness is reduced by high temperatures, low α/e outer surface (such as white paint or Kapton) will repel the effects of solar and RTG heat.

A shield of 50 layers of aluminized mylar will allow almost no heat transfer through the spacecraft walls. Forty layers would actually be sufficient, but due to the possible Mylar degradation due to radiation, the extra safety factor was added. This 50 layer shield would be one inch thick and weight 0.25 lbs/ft^2. The affected spacecraft surface area is 56.3 ft^2. Therefore, the weight of this superinsulation jacket would be 14.1 lbs.

Due to unknown reliability, occasional failure at low temperature, and additional weight, thermal switches were eliminated in favor of bimetallic louvers. Bimetallic coils are thermally coupled to the component base plate

and any temperature changes of the plate causes a reaction of the bimetallic element which causes movement of the louvers. Three louvers were chosen in case of failure of one of the louvers. Also, three permit better control of thermal gradients across the plate. Figure 7.2 (Reference 1) shows a bimetallic louver system.

To maintain a 70^{o} F base plate, the total lower area, assuming 70 watt internal heat dissipation, would be 2.5 ft^2. This means that each louver will be circular with a radius of .51 ft. Assuming 15 in^2 of sensor openings and a conducting area of 7 in^2 for structural mounts, the heat losses would be about 7 watts at the beginning of the mission and 25.5 watts at encounter (Reference 1). Using these figures, the effective emittance of the louvers will vary from .7 at earth to .48 at encounter. The area of the louvers was chosen to allow corrections for possible hot or cold spots through mere louver movement. The weight of the louver assembly is 8 lbs. Calculations to support these figures appear in the Appendix E. Diagrams of superinsulation and louver position appear in Figures 7.6 and 7.7.

The reliability of the louver systems have been demonstrated on the Marineers, Nimbus, Pioneers, and other flights. Bimetallic louvers were chosen instead of thermostat louvers because of their greater angle control, and were chosen instead of ground-command control louvers because of the extra weight, power, and communications time required.

7.2.3 Externally Mounted Components and Problem Areas

External Equipment Packages. The design approach for the auxiliary equipment package, including the boom mounted sensors and the forward mounted trajectory motor, is also to insulate and isolate them. These instruments will be jacketed in 50 layer aluminized Mylar insulation blankets with low α/e thermal coatings. A balance between internal heat dissipation and heat leaks can be developed to maintain suitable temperature through the use of insulation mounts. If this is not sufficient, 0.5 watt bimetallic controlled electric heaters could be placed in the package. These wattages have been appropriated in the power budget.

Hydrazine Engines, Lines and Tank. Similar precautions will be taken for the hydrazine system as for the external equipment packages.

TE-364 Rocket Motor. A passive system should provide sufficient protection for the rocket motor because of the ignition early in the flight.

Antenna. The antenna will have a black inner surface to prevent sunlight reflections from overheating the feed or subreflector. To prevent localized heating of the dish from the absorbed solar heat and the heat of the

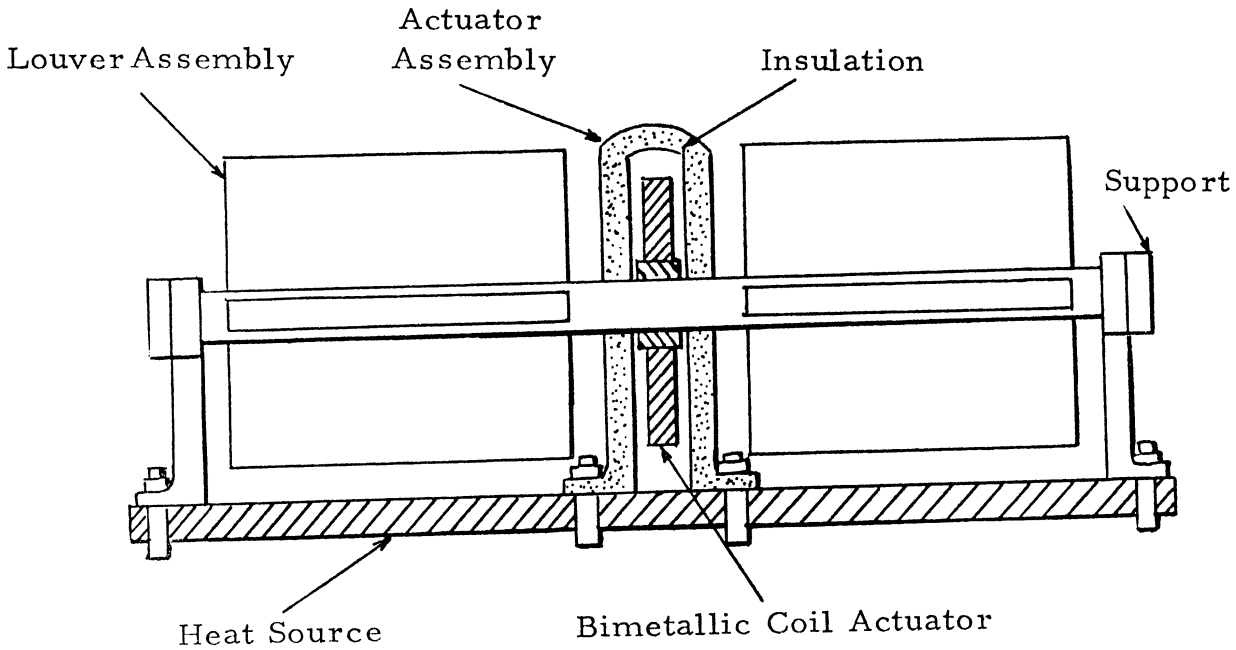

Figure 7.2 Louver System with Bimetallic-Coil Actuator

radiating RTG, the back surface will be left bare. This will emit absorbed heat and reflect RTG heat. Localized heat could warp the antenna causing interruptions in the communication system.

7.2.4 On Pad Cooling and Launch Problems

Due to the compact nature of the spacecraft, the location of RTG's within the shroud during the launch phase, and the excessive RTG heat, danger of overheating the spacecraft exists. On the launch pad, forced-air cooling of the RTG's within the shroud will keep the spacecraft and RTG's at acceptable temperatures. Because the time between launch and payload-shroud separation is small, the heat capacity of the RTG is insufficient to cause a significant temperature rise within the spacecraft or of the RTG itself.

7.3 MICROMETEOROID AND RADIATION PROTECTION

7.3.1 General

Additional environmental constraints with which this first deep space probe must contend are high radiation fields and frequent bombardment of the spacecraft by meteoroids. In analyzing the problem, two factors contribute to its uncertainty. First, the lack of good data on the number, size, and impacts of meteors requires penetration equations to be conservative. Second, the lack of good data of radiation outside the immediate vicinity of the Earth could present problems. Project UMPIRE seeks to answer these uncertainties.

The design approach must decide how far the probability of mission success should be increased at the expense of a weight penalty. Should five pounds of shielding be added to insure another .1% probability of success?

7.3.2 Meteoroid Protection

Meteoroid Environments. The spacecraft, in traveling from the Earth to Jupiter, will encounter many high velocity particles or meteoroids of varying size and flux. This variance is due to the many zones or regions of specific meteoroid types. These regions are Near-Earth, Interplanetary, Asteroid, and Near-Jupiter. Table 7.1 summarizes the uniform findings of References 1, 2, 3, and 4.

Zone	Distance from Sun	Types of Particle	Collision Velocity	Density	Direction
Near-Earth	1 AU	Cometary	5-15 Km/sec	.443 gm/cc	all
Interplanetary	1-5.2 AU	Cometary	40 Km/sec	.443 gm/cc	all
Asteroid Belt	2-4 AU	Meteoritic	10-20 Km/sec	3.0 gm/cc	Posigrade
Near-Jupiter	5.2 AU	Cometary	10-60 Km/sec	.443 gm/cc	all

Table 7.1

Mass of Meteoroids. Meteoroids with masses from 10^{-5} to 10_{5}^{-1} gm are of primary interest in shield design. Those with masses of 10^{-5} gm and less are easily stopped by structure, and ones with masses greater than 0.1 gm have very small projected fluxes.

7.3.2 Penetration

In each region of space, the flux of particles can be related to the average time between impacts as $T = (A\phi)^{-1}$, where A is the appropriate exposed area. The probability of N impacts on an area A in time t to a flux of particles of mass m or greater, assuming a Poisson distribution in defining the frequency of impacts, is

$$P = \frac{(t/T)^N e^{-t/T}}{N}$$

Since the asteroid region represents the worst case of flux and particle size, the spacecraft design will regard it as the upper limit. Using the Marshall flux equation, $(\phi)_m = 10^{-10} M^{-0.77}$, the probability of impact equation, and the Summers and Charters equation of penetration depth (a further conservative step because of environmental uncertainty), then the probability of zero puncture in an aluminum sheet can be related to the spacecraft area, time in the asteroid region, and appropriate skin thickness. The penetration equation can be written as:

$$m = \frac{l^3 p_T^2 C^2}{(4.25)^3 P_m V^2}$$

where

m = maximum meteoroid mass to be stopped, gms
P_T = target density, gram/cc
C = speed of sound in the target, Km/sec
P_m = meteoroid density, gms/cc
V = relative impact velocity, Km/sec
l = effective sheet thickness, cm

assuming 1 = 1.5 penetration depth. JPL has produced penetration charts (Reference 2) and the chart for the asteroid region appears in Figure 7.3 (Reference 2).

Bumper Shields. The effectiveness of a double-wall construction is demonstrated in the Figure 7.4 (Reference 3). With

$$I = \frac{l_1 + l_2}{K}$$

the thickness of and distance between the two bumper sheets can be determined by the appropriate thickness - zero probability ratio desired.

Design Approach. Since the UMPIRE spacecraft will be in the asteroid region for about 200 days and has a surface area of 5.23 m^2, the Area x time (A x t) level will be 1450 m^2 days (Figure 7.3). It is necessary to determine the equivalent thickness of aluminum sheet which will assure a reasonable probability of zero puncture. In making the decision, the additional weight per increase in probability and actual double wall construction must be considered.

Thermal subsystems will employ a bumper shield assembly. The shield will have a two inch filler of polyurethane foam. This foam is light weight (1.2 lb/ft^3) and provides a very effective media for stopping the heavy particles that penetrate the outer bumper sheet. The outer sheet will be .019" thick and the inner will be .079", according to the specifications of a bumper given in the diagram of K factor and distance. This bumper, with a 2" distance, reduces the required thickness of the sheet by a factor of 5. Total weight of the bumper assembly is 44.9 lbs. A bumper shield not only saves weight, but the filler tends to prevent shattering of the wall by absorbing the shock waves produced by the impact of the particles on the outer sheet. Calculations behind these weight figures appear in the Appendix E.

To insure unaffected heat flow from the louvers, the micrometeoroid protection shall consist of 2" honeycomb panel, facings 0.015 inch aluminum alloy, with 2.3 lb/ft^3 trussgrid aluminum core. Douglas tests indicate that this type of core is qualified as an effective filler (Reference 4). Weight of this construction is about one pound.

A curve of the zero puncture probability vs. added spacecraft weight appears in Figure 7.5. A weight of 44.9 lbs and zero probability of puncture of .8 were chosen because of the overall weight problem of the spacecraft and the steepness of the curve beyond this point. However, for any thermal control system, actual testing is the only method to insure any prediction of effectiveness. Unexpected leaks, deviating performances, and calculation errors can be corrected in such testing to provide an efficient, well-defined system. Figure 7.6 shows the relative position of the bumper shield, filler, and superinsulation in the spacecraft wall.

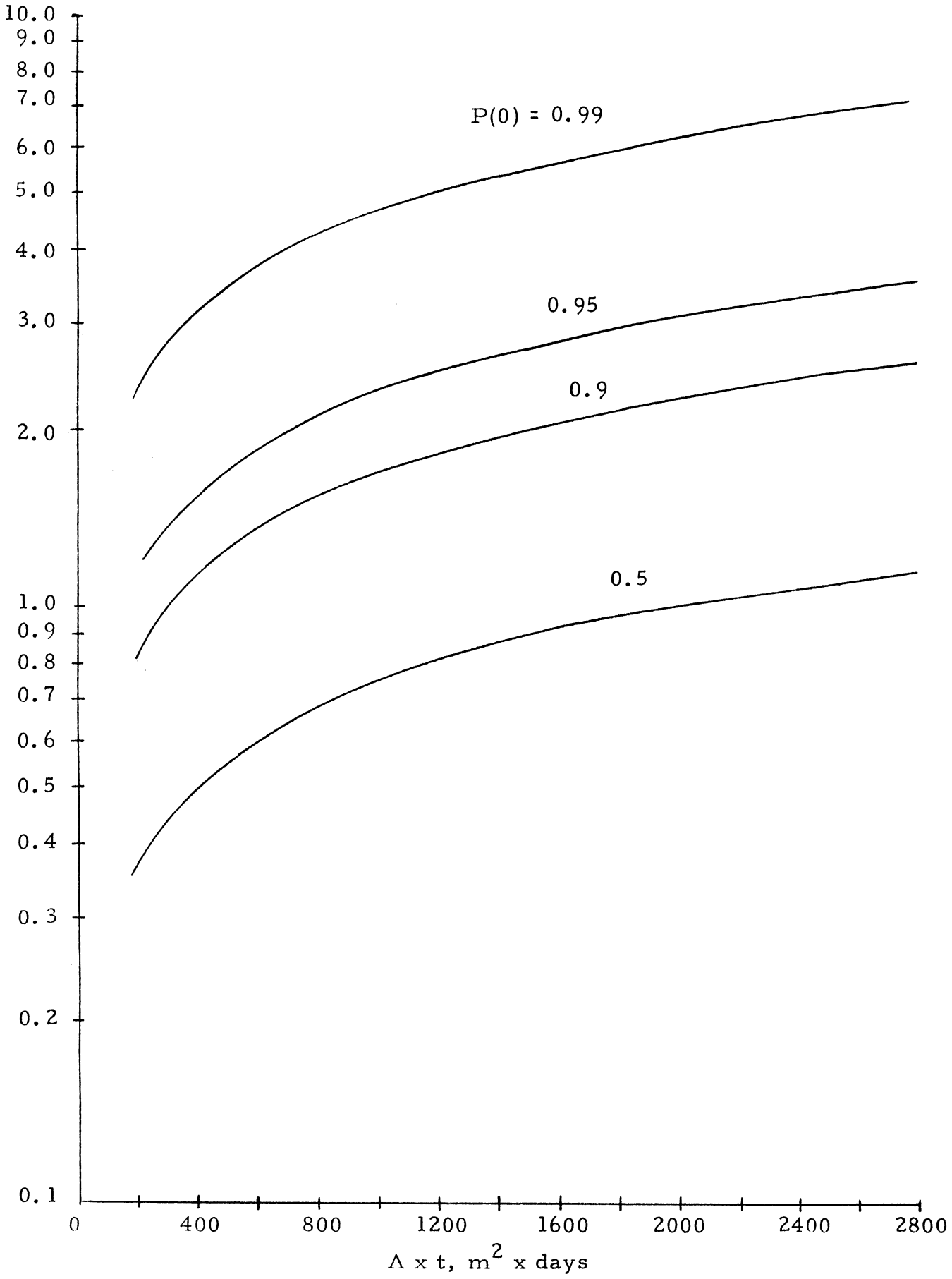

Figure 7.3 Probability of Zero Puncture in Aluminum Sheet From Asteroidal Debris Between Mars and Jupiter (10 km/sec)

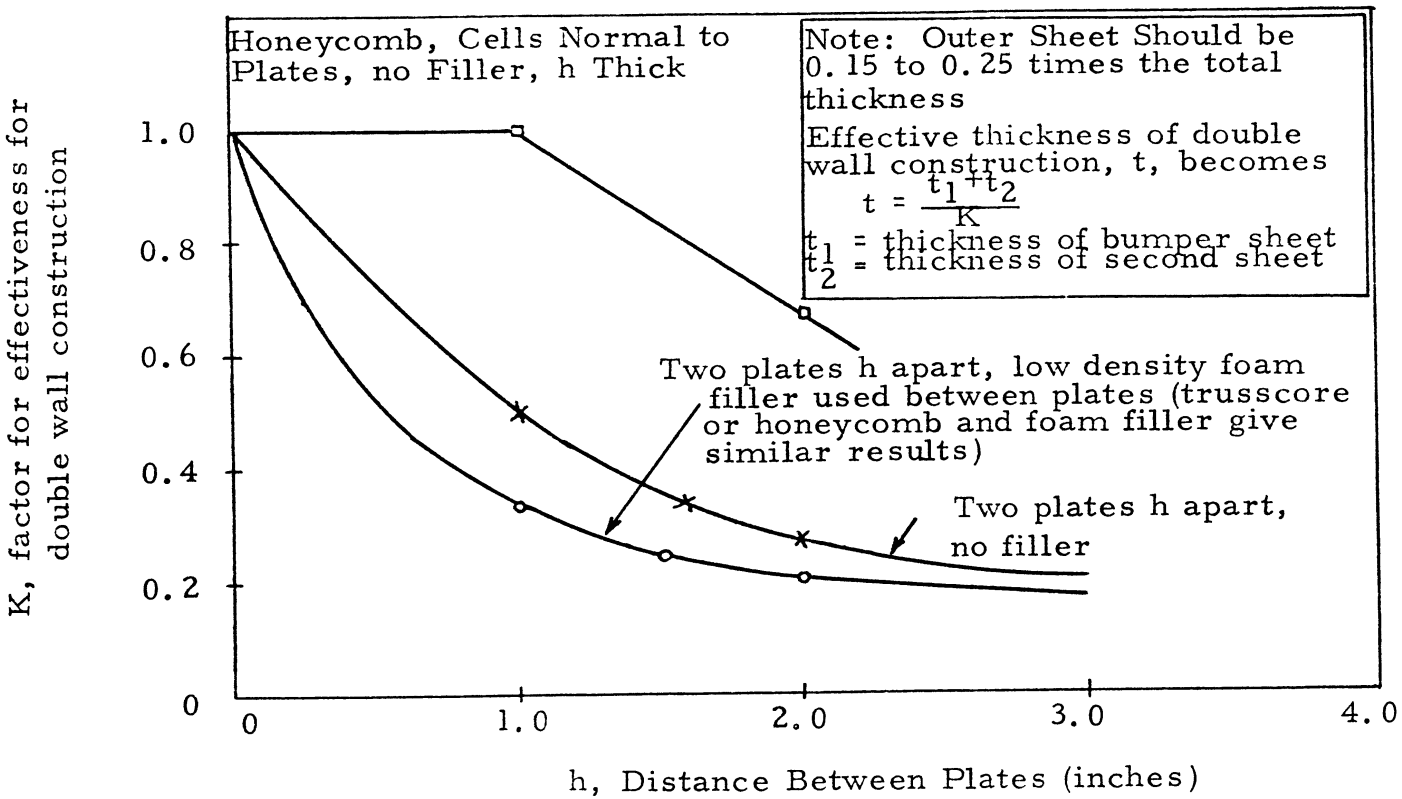

Figure 7.4 Effectiveness of Double Wall Construction

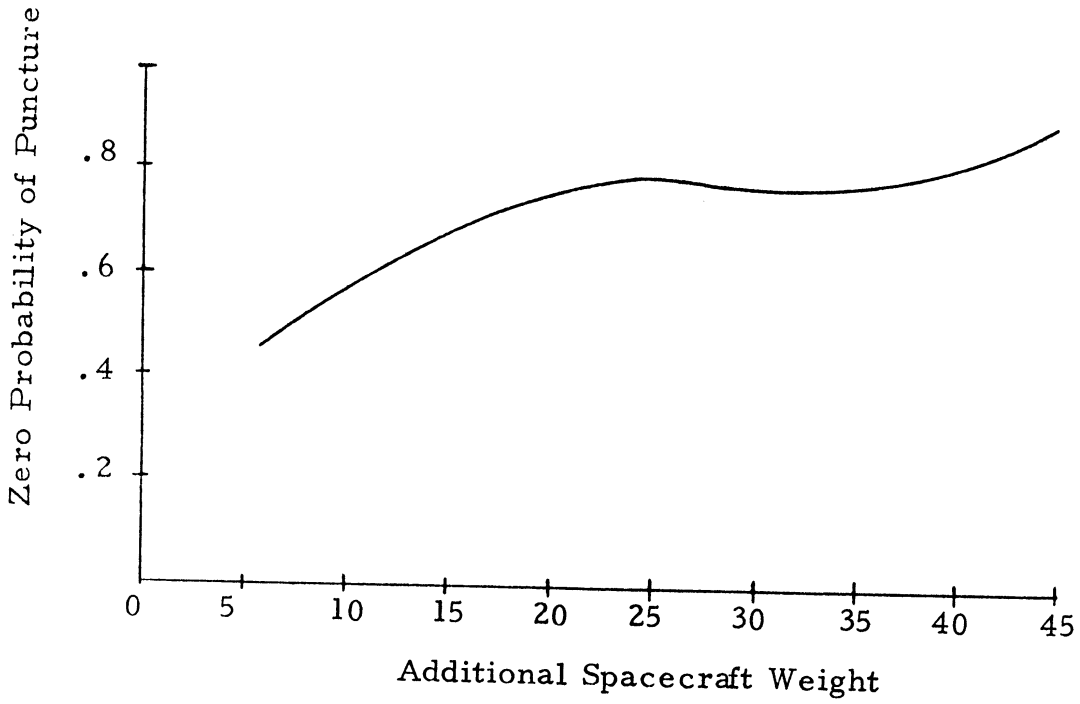

Figure 7.5 Zero Puncture Probability vs. Added Spacecraft Weight

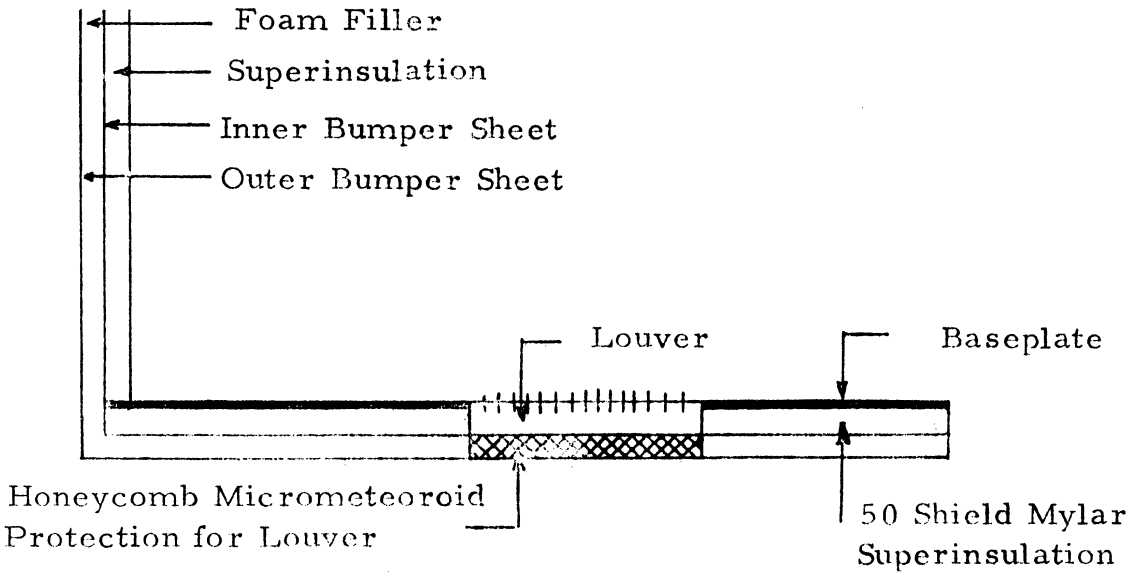

Figure 7.6 Cross Section of Spacecraft Wall at Bottom Corner

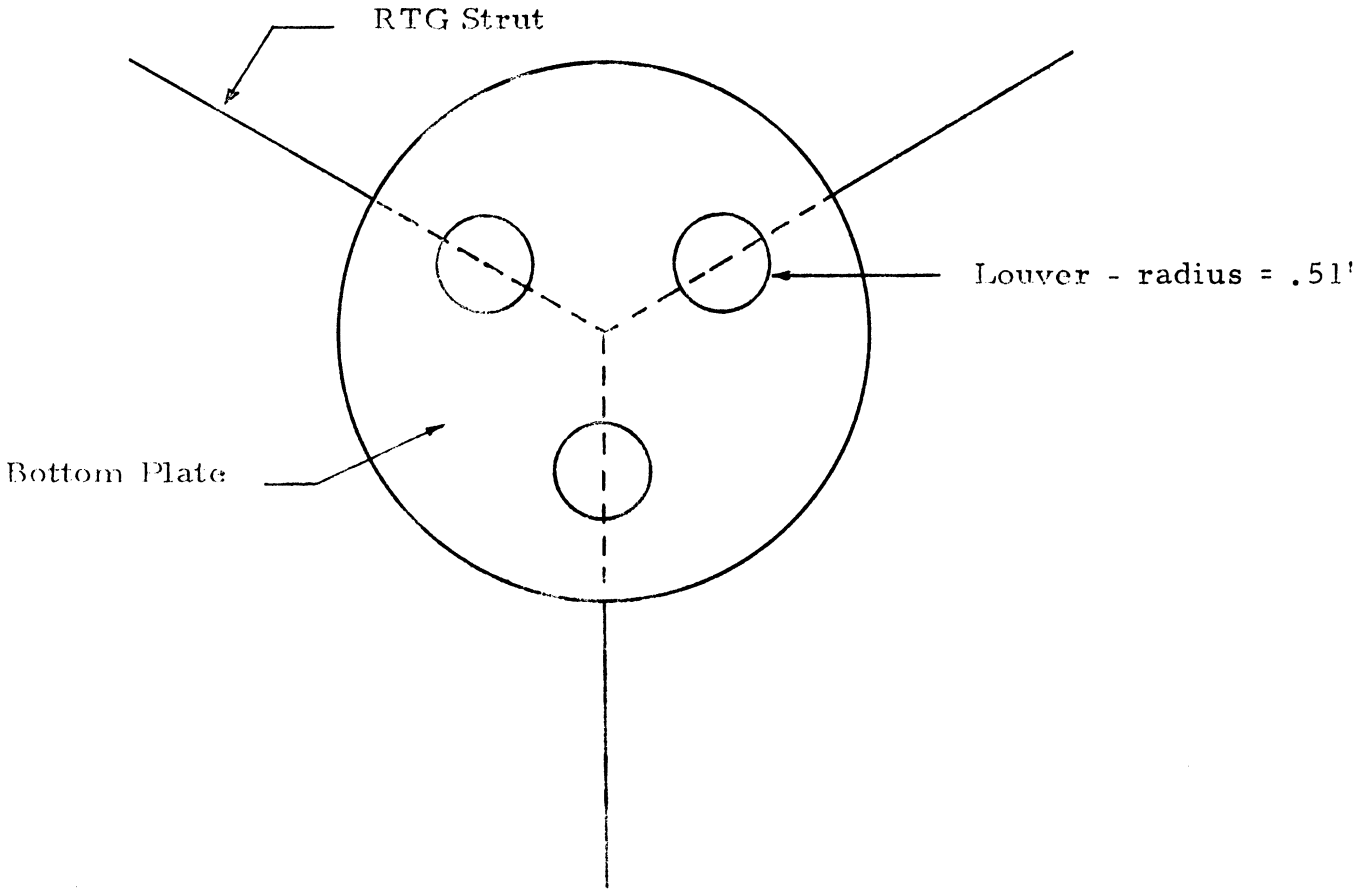

Figure 7.7 Bottom View of Spacecraft

Special Areas of Concern. Several areas present problems of meteoroid and radiation protection that should be resolved in the second phase of this study. The areas include:

a) The outside cabling to the boom package
b) The RTG's
c) Detection openings
d) The boom-mounted package - the glass fiber Mylar superinsulation could possibly be adequate.

7.3.3 Radiation Protection

There exist four types of natural radiation along the spacecraft trajectory. They are galactic cosmic radiation, solar radiation, earth trapped radiation, and Jupiter trapped radiation. A thorough study and review of each type can be found in Reference 4.

The galactic cosmic radiation is not of sufficient intensity to be considered a problem in equipment damage.

The solar radiation is composed of two components, the solar flare and the solar wind particles. The frequency, radiation intensity, and duration of flares are of a magnitude which does not represent a serious hazard to the equipment of the spacecraft, with the possible exception of the low energy component. Damage to thermal coating a minor problem for this design, could result.

The Earth trapped radiation, due to the short duration of time, is also not a problem.

Jupiter's trapped radiation belts are of sufficient magnitudes and energies to cause equipment damage. However, our mission will not pass within 3 Jupiter radii, where the dosage of particles is several thousands rads. This should be no problem since there is a 10^5 rads damage threshold for the electronics system.

The RTG's will be sources of additional radiation emissions. The effects of these emissions and its dependence on RTG location and positioning are discussed in Section 5.6.

7.4 WEIGHT AND POWER SUMMARY

Power - 2.0 watts (possible electric heaters)

Weight -	8.0 lbs	for louvers
	14.1 lbs	for spacecraft superinsulation
	2.0 lbs	for boom-mounted equipment superinsulation
	44.9 lbs	for micrometeoroid bumper shield
	1.0 lb	for micrometeoroid protection of the louvers
	70.0 lbs	TOTAL

7.5 REFERENCES

1. "Phase A Report Galactic Jupiter Probe," Goddard Space Flight Center, Preprint X-701-67-566, November 1967.
2. "Advanced Planetary Probe - Jupiter Flyby Application," Jet Propulsion Laboratory, Technical Report No. EPD-358, 2 May 1966.
3. "Advanced Planetary Probe - Final Technical Report," TRW Systems, Report No. 4547-6004, 27 July 1966.
4. "Final Technical Report of a Study of Jupiter Flyby Mission," General Dynamics, Report No. FZM-4625, 17 May 1966.

Clark, J.F., E.W. Hymowitz, and J.H. Trainor, "Galactic Jupiter Probes," Goddard Space Flight Center, NASA Document No. X-100-67-211, March 1967.

"Final Report - Asteroid Belt and Jupiter Flyby Mission Study," Lockheed Missiles and Space Company, Report No. M-49-65-1, 28 February 1965.

"Handbook of the Physical Properties of the Planet Jupiter," NASA Document No. SP-3031, 1967.

8
ATTITUDE CONTROL AND PROPULSION

8.1 INTRODUCTION

The general purpose of an attitude control system is to insure accurate spacecraft navigation, including orientation, stability, and midcourse correction. The specific objectives of the 450-500 pound deep space probe requires a system that is simple, lightweight, low in power consumption, and above all reliable. The particular use of a narrow beam communication antenna further restricts spacecraft orientation so that continuous, high data rate communication can be maintained throughout the mission.

The choice of spin stabilization was made because of its basic simplicity as compared to a stable attitude system. The spinning spacecraft is inertially stable and will not require gyroscopes, accelerometers, momentum wheels, or more complex attitude sensors that require both more weight and power. The necessity for continuous onboard monitoring of spacecraft orientation could be eliminated using the spin for a conical scan system of tracking. The inertial spin stability would require only periodic correction for drift of the earth line due to the flight path.

A spin rate of 5 rpm was incorporated into this report based on earlier studies (References 1 and 2) which indicate that this is an optimal figure for stability and ease of orientation, and is compatible with the scientific instrumentation.

The propulsion system for the spin stabilized craft must be able to control the spin rate, orientation, and midcourse thrusting. This will be accomplished using a hydrazine blowdown design, with appropriate thrusting controlled by an onboard logic unit.

8.2 MISSION REQUIREMENTS AND DESIGN CRITERIA

The requirements placed on the attitude control system are:

1) Provide for despin and spin rate control after injection, and maintain a stable orientation.
2) Provide earth acquisition and tracking for RF communications.
3) Provide reorientation for midcourse correction(s).
4) Be compatible with scientific measurements.

The basic dynamics of a spinning body are represented by the Euler equations of motion. (A more detailed explanation of the following is found in Appendix F). The body's three principal axes are represented by the indices 1, 2, 3, where 3 is the spin axis. For torque free motion, the angular momentum vector is fixed in inertial space and will point along one

of the body's principal axes. Without loss of generality it is assumed this is the spin axis, and it can then be shown that this is the stable axis. If an impulse torque is applied, the momentum vector will be shifted and the resulting motion will be a "wobble" of the spin axis about the new momentum vector. If the moments of inertia about the 1 and 2 axes, I_1 and I_2, are equal the motion will trace out a circular cone at a fixed apex angle, as schematically shown in Figure 8.1. This is required so that tracking by scanning antennas and sun sensors can be accomplished for any orientation in space. If I_1 is not equal to I_2 the resulting wobble is a complex cone, over which there would be little control for tracking.

In order to make orientation changes, it becomes necessary to eliminate this coning motion so that the spacecraft axis can be finely pointed.. Energy considerations show that if the ratio of I_3 to I_1 (with $I_1 = I_2$) is greater than one and there is some internal energy dissipation, the coning angle will be reduced to zero with time. The size of the initially induced angle can be kept smallest for a ratio of 1.4 to 1.6 (Reference 3). Figure 8.2 shows the variation in wobble for different orientation step sizes versus moment of inertia ratios. If the ratio were less than one, any energy dissipation would increase the wobble, resulting in an uncontrolled tumble; this was observed on an early Pioneer orbital flight where a small flexible antenna provided enough energy dissipation to cause tumbling is less than one orbit. Making the ratio greater than one and providing energy dissipation, in the form of viscous fluid mechanical dampers, the wobble will reduce to zero. Thus the spacecraft can be reoriented and pointed.

8.3 ATTITUDE SENSING AND TRACKING

The primary consideration of the attitude control system is that final earth pointing of the communication dish must be possible from any initial arbitrary orientation. The proposed system is similar to that used on earlier flights for sun pointing of solar panels, but with the addition of RF tracking. A system of sun sensors will give the sun line location, which will be fed to ground through the omni antennas. Once this position is known, command can be sent to the spacecraft, again using the omni antennas, to bring about an open loop precession of the spin axis toward the earth. When the angle has been reduced to less than 20 degrees, the RF uplink signal will be within the cone of the helix scan antenna and the precession will change over to closed loop. Pulsing reference for the jets is switched from the sun sensor to the RF signal. When the main dish is within five degrees of earth, it can be used employing its conical scan capability to bring the antenna axis (spin axis) within one degree of the earth line as required for high gain communication. Orientation is then monitored through the main dish and periodic corrections made due to earth line drift. This will be one degree per day early in flight and decreases to one degree per month as Jupiter is approached (Reference 4). Range and velocity tracking will be done using Doppler shift methods.

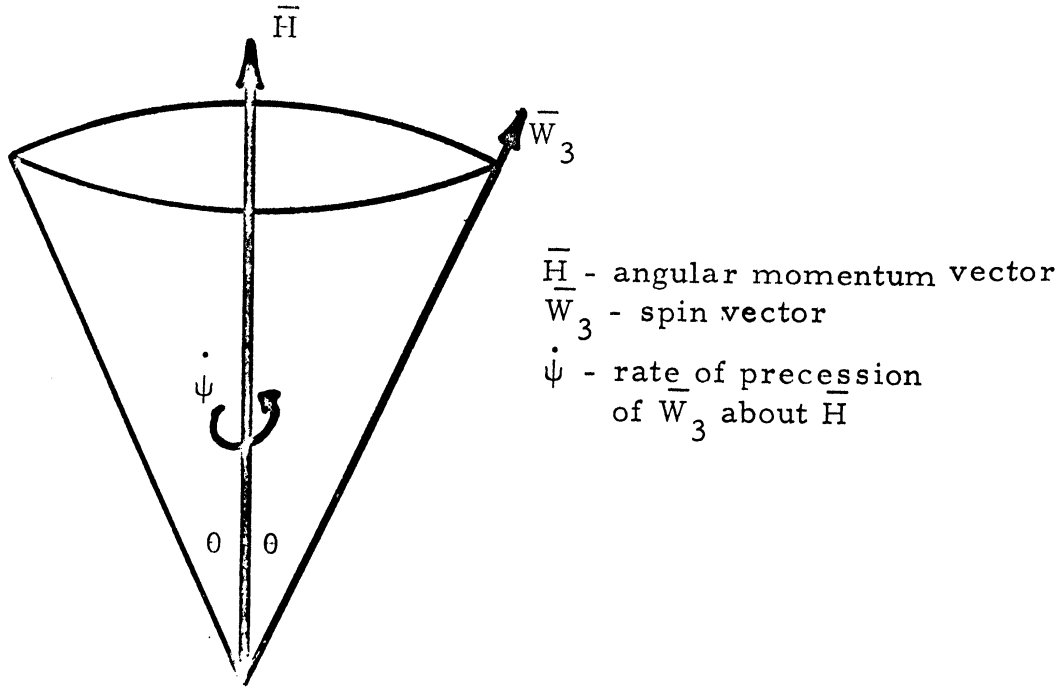

Figure 8.1 Spacecraft Coning Motion

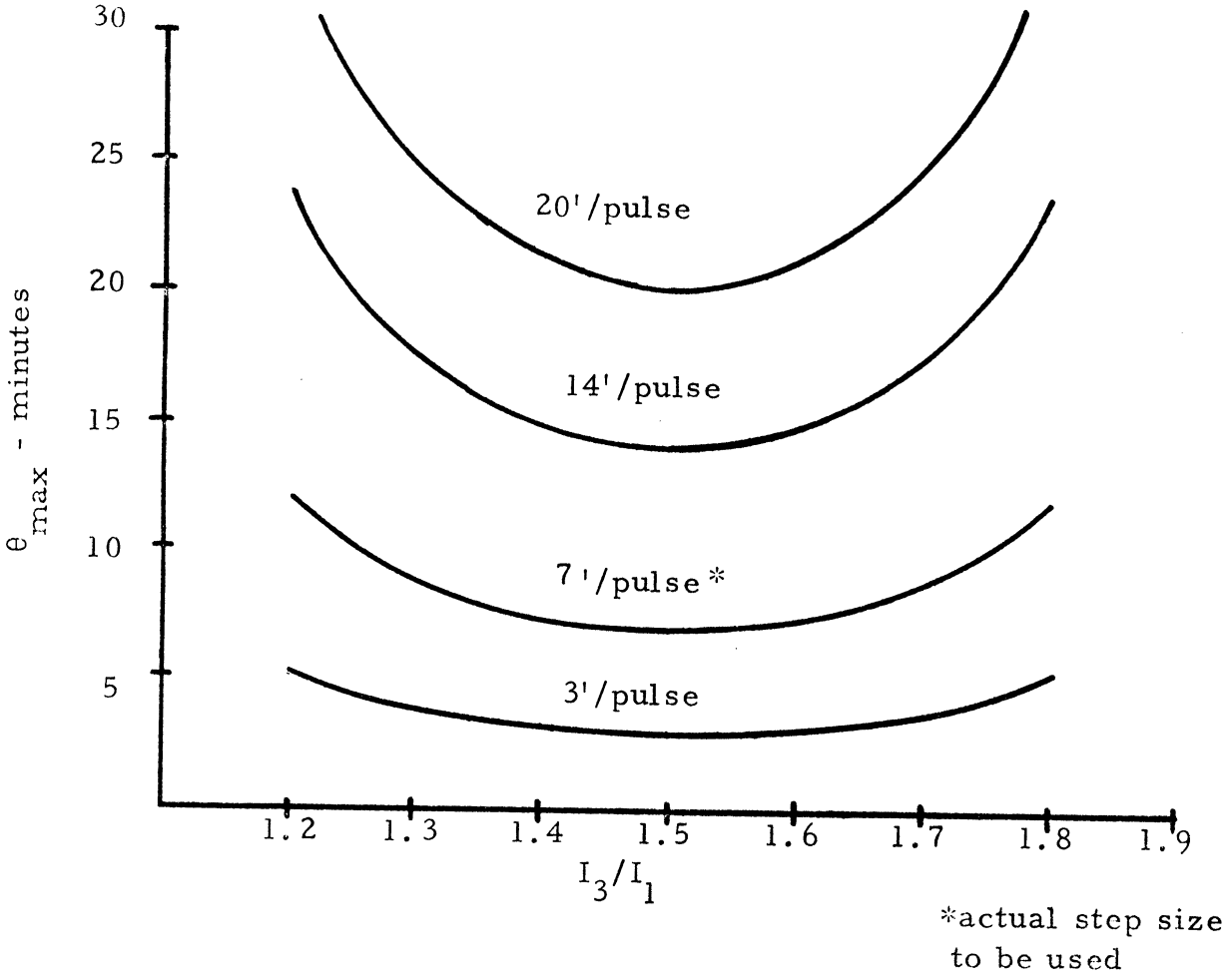

Figure 8.2 Cone Angle vs. I_3/I_1

An additional sensor for sighting of the star Canopus could be used to provide a complete three axis reference system and as a backup to the closed loop RF system. Accuracy of arbitrary orientation late in flight could also be somewhat increased. This sytem was not included because of its basic redundancy to the primary system, and the requirement of arbitrary pointing for midcourse early in flight can be done using the sun sensor-RF system alone. The basic reliability of the primary system, precluding catastrophic failure of the main antenna, and its better accuracy in the closed loop mode only make the open loop Canopus system a less accurate backup method. If it becomes necessary to increase arbitrary pointing accuracy, the Canopus sensor itself can be added with a weight and power penalty of under five pounds and three watts. For a detailed study see Reference 3.

8.4 PROPULSION SYSTEM

The requirements of the propulsion system are to provide attitude control and midcourse correction(s). To provide necessary control this will include 1000 degrees of precession, 10 rpm of spin, and 300 ft/sec change in velocity. It must be capable of firing in a zero gravity, vacuum environment repeatedly with minimum leakage.

Propulsion for both the attitude control and midcourse correction will come from a single hydrazine monopropellant blowdown system.(Figure 8.3). The high specific impulses of hydrazine (230 sec) and ease of storage at low pressures makes this system simpler and more reliable than either a bipropellant or high pressure cold gas system, and has been proven on earlier flights. One hydrazine tank, located on the spacecraft axis and nitrogen pressurized with a bladder blow down, will assure positive fuel flow to the thrusters. Solenoid valves to the precession and spin thrusters are activated by the onboard control unit (Figure 8.4). These thrusters are all 0.5 pound thrust. The two midcourse thrusters of five pounds thrust each are located at each end of the craft to provide thrusting in either direction with minimum reorientation. This will also keep the thermally protected aft portion of the spacecraft from being sun pointed for any appreciable length of time, and will allow corrections along either direction of the earth line while keeping constant communication with the main antenna. This would be especially applicable for a second, earth pointed midcourse correction later in flight. Heating of the forward thruster and lines may become necessary if the thermal insulation does not assure the proper operating temperature.

The entire propulsion system will be controlled by the onboard sequencing unit in response to activation by ground command (Figure 8.4). For a desired precession the required number of pulses, firing time, and total angle will be fed in from the ground. The sequencer will then

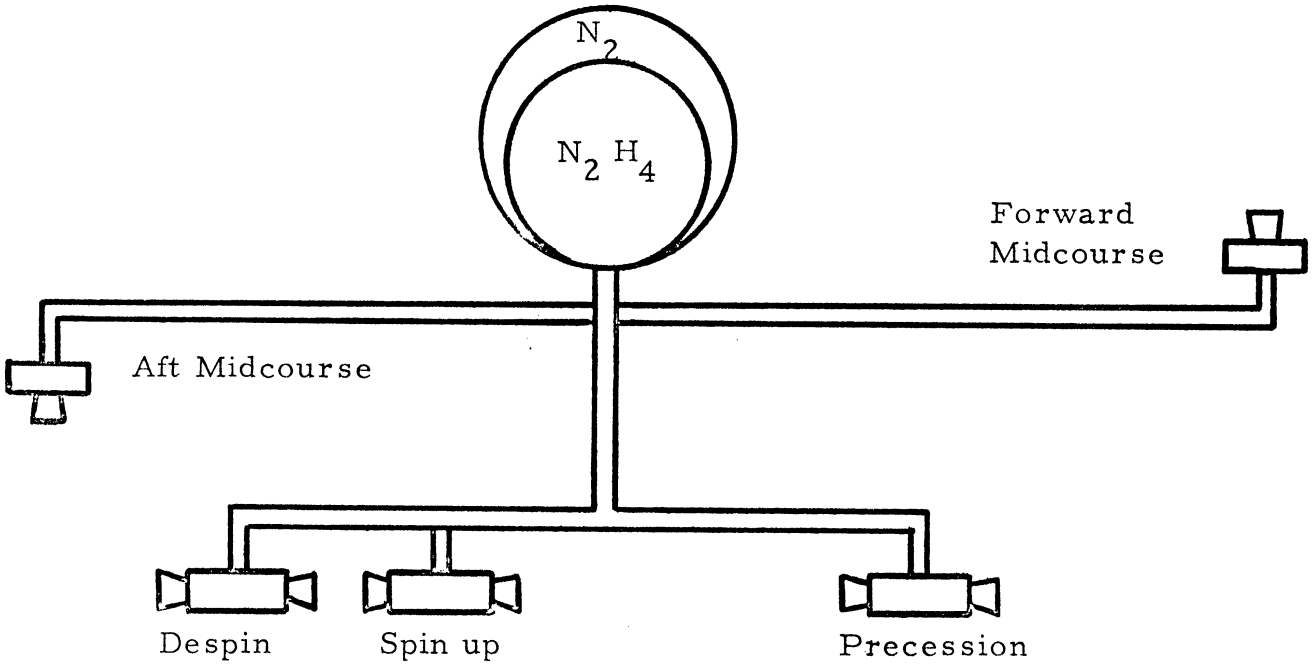

Figure 8.3 Propulsion System

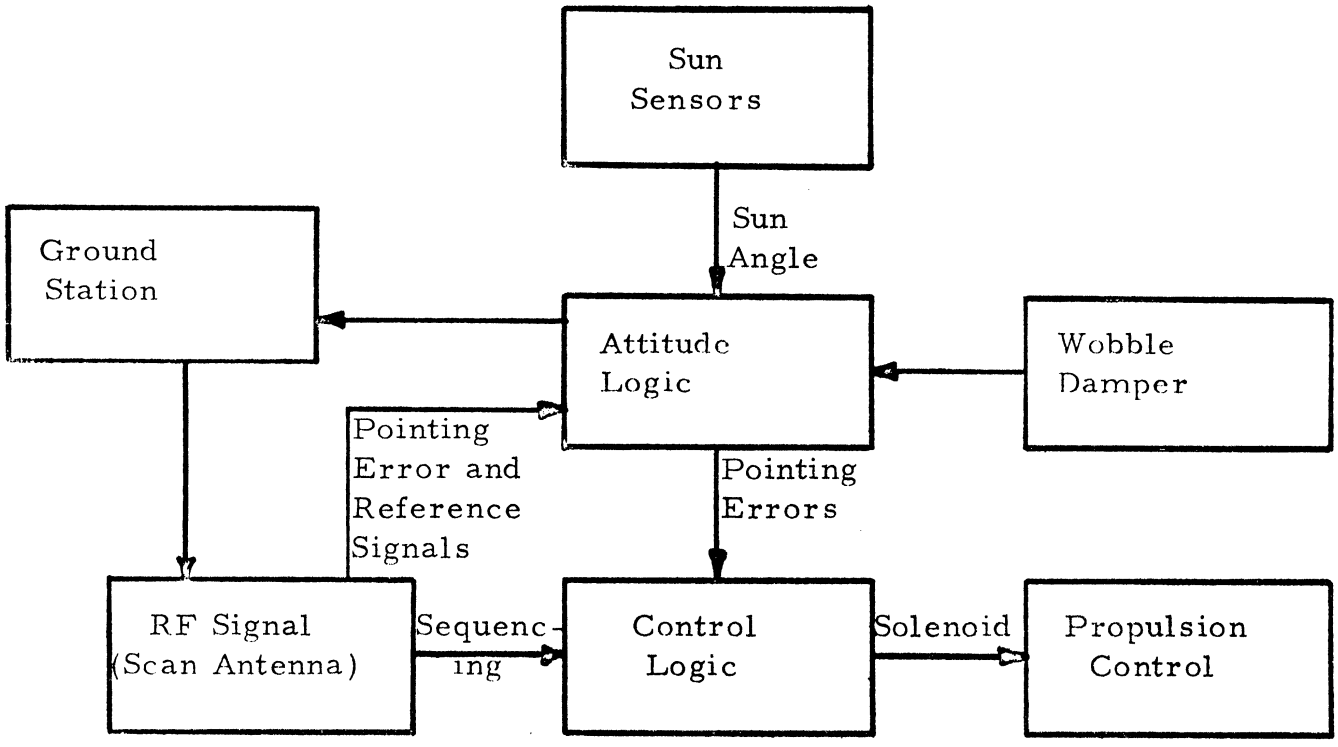

Figure 8.4 Control System

control the spacecraft using the attitude sensors in open loop or the RF signal in closed loop for timing pulses until the command has been completed. Similarly, midcourse firing durations are controlled by the sequencer. In order to minimize fuel usage, there is a dead zone around the nominal pointing direction; only if that limit is exceeded will the control unit detect an error and fire the thrusters.

Table 8.1, the attitude control and propulsion system component breakdown, with weight and power requirements:

Item	No.	Weight (lb)	Power (ω)
Sun sensor	2	2.5	0.0
Spin thruster	4	3.0	6.0*
Precession thruster	2	2.0	6.0*
Midcourse thruster	2	3.0	6.0*
Damper	3	4.0	0.0
Control electronics assembly	1	7.0	6.0
Hardware, regulators, plumbing, pressure and temperature transducers	-	13.5	1.0
Fuel	-	28.0	-
Pressurant system (N_2)	1	1.0	-
Totals		64.0	7.0 (+6.0*)

*Note: for pulse duration only

8.5 INITIAL EARTH ACQUISITION

8.5.1 Despin

The launch sequence calls for spinup of the Burner II prior to firing to a nominal 120 rpm. After burnout, two solid propellant rocket motors of the Burner II will despin the system to 20 rpm, and release the payload. At this time the RTG's will be deployed, increasing the spin moment and decreasing the spin rate to 8 rpm. Following deployment of the sensor booms and the main antenna the final spin rate will be trimmed by the spin thrusters to give a nominal 5 rpm spin. This will all occur within one day of launch. It should be noted that until the sensor booms are deployed the spacecraft will have I_3 less than I_1 so that the wobble dampers must be inactive for this period to prevent tumble.

8.5.2 Earth Pointing

After despin, the attitude sensor information to determine spacecraft orientation will be sent to ground using one of the omni antennas. The onboard sequencer will then be fed the necessary pulse and timing requirements for an open loop precession of the axis toward earth. Once the helix scan antenna begins to pick up the RF uplink signal (about 20 degrees from earth), the control of the precession will switch to closed loop, using the RF signal for pulse timing. This will allow a pointing accuracy of 2-3 degrees so that final pointing to within one degree can be controlled through the main antenna. Throughout the maneuver the spin rate will be refined onboard to keep the desired five rpm, allowing greater accuracy in precession step size. This becomes especially important in the open loop mode.

Orientation will be controlled by two precessional thrusters and four spin rate thrusters. The precessional thrusters will work together to produce a couple providing a discrete change in angular momentum for each impulse firing, while not affecting the spacecraft velocity. The firing of the thrusters is controlled by onboard detection of either the conical scan signal or the crossing of the sun line as detected by the sun sensors. The spin rate thrusters also use these signals as a reference to keep the spin within a specified tolerance. The accuracy for orientation is imposed by the large parabolic antenna's narrow beamwidth (2 degrees), and by orientation for midcourse correction(s).

Requirements of the system throughout the remainder of the flight are to keep the axis earth pointed to within one degree and provide for midcourse orientation and earth reacquisition.

8.6 CRUISE CONTROL

Once the spacecraft is pointed, the orientation is fixed in inertial space. Unlike orbital flight, there are almost no perturbations on orientation. Solar pressure is the only predictable factor and itself is minor. Other factors such as micrometeoroid impact or gravitational effect of large asteroids are more significant, but can only be estimated at this time. One of the purposes of this flight is to make more detailed measurements of these influences. However, the effects are still small compared to orbital missions. The spin rate of five rpm was chosen to keep perturbation effects at a minimum, while also allowing reorientation with minimum use of propellant. Thus five rpm was a compromise figure. It is also compatible with the science package for interplanetary and Jupiter measurements (References 1 and 2).

Corrections for drift of the earth out of the dish's beamwidth will be 1 degree/day early in flight, decreasing to 1 degree/month at Jupiter. One period of communication disruption will occur when the sun is between the Earth and the spacecraft. This will last eight days, 316 days after launch. During that time the earth drift will be less than the main antenna beamwidth so that no major reorientation requirement is expected.

During encounter communications will be required for real time transmission, except during earth occultation. No control problems are anticipated during any phase of the encounter.

The cruise mode will basically be a coasting phase for the attitude control system. Only periodic corrections are required.

8.7 MIDCOURSE COMMAND AND CONTROL

The purpose of the midcourse correction(s) is to provide the proper trajectory change to counteract injection errors. The final aiming point is five radii from Jupiter at encounter. Midcourse orientation can be of three types: earth pointing, pointing in or perpendicular to the plane of the trajectory, and arbitrary pointing. To remove errors with minimum burn time requires arbitrary pointing. As indicated in Section 8.3, this will be possible early in flight using an open loop method with the sun sensors, giving an accuracy of 3 degrees. Late in flight this accuracy is decreased due to decreased accuracy of the sensor output and change in precession steps due to alteration of moments of inertia from fuel losses.

The planned midcourse sequence is for an arbitrary pointing burn five to ten days after launch, as soon as trajectory errors can be determined. Another burn along the earth line later, if needed, will refine the correction and help correct for uncertainties in trajectory perturbation from interplanetary influences. The total change in velocity will be a maximum 300 ft/sec.

Midcourse orientation and reacquisition of earth signal is the same as the initial maneuvers. A combination of open and closed loop precession will provide the necessary pointing. Thrusting times are fed from the ground and controlled by the onboard sequencer. The control of the craft will then be automatic.

8.8 REFERENCES

1. "Pioneer Program," Ames Research Center, NASA Document No. P-200, 1968.
2. "Advanced Planetary Probe, Final Technical Report," TRW Systems, July 1966.
3. Galactic Jupiter Probe," Volume II, Goddard Space Flight Center, November 1967.

4. "Final Technical Report of a Study of Jupiter Flyby Missions," General Dynamics, Report No. F2M-4625, May 1966.
5. Dynamics of Mechanical and Electromechanical Systems, Stephen H. Crandall, editor, McGraw-Hill, New York, 1968.
6. Shames, I.H., Engineering Mechanics Volume II, Dynamics, Prentice-Hall, 1966.
7. Corliss, W.R., Space Probes and Planetary Exploration, NASA, 1965.
8. Guidance and Control of Aerospace Vehicles, Cornelius Leondes, editor, McGraw-Hill, New York, 1963.

"Advanced Planetary Probe - Jupiter Flyby Application," Jet Propulsion Laboratory, Report No. EPD-358, May 1966.

Clark, J.F., E.W. Hymowitz, and J.H. Trainor, "Galactic Jupiter Probes," Goddard Space Flight Center, Report No. X-100-67-211, March 1967.

"Mariner Mars 1964 Project Report," Jet Propulsion Laboratory, Technical Report No. 32-740, 1965.

Park and Newell, "Navigation for Spin Stabilized Deep Space Planetary Spacecraft," TRW Systems.

"Space Programs Summary," Jet Propulsion Laboratory, Report No. SPS37-53, Volume I, 1968.

9
LAUNCH VEHICLE AND SUBSYSTEMS

9.1 INTRODUCTION

Either of two related numbers can describe the capability of a launch vehicle combination. The first is the characteristic velocity V_c which is the velocity at burnout the configuration is capable of attaining, and the second is the C_3 energy which is the square of the hyperbolic excess velocity, (Section 10.2) Payload weight is a function of either of these two numbers for all launch vehicle combinations, and the vehicle can be picked when the desired payload weight and C_3 or V_c are known. Project UMPIRE is designed for a C_3 of 90 km^2/sec^2 (V_c = 47, 714 ft/sec) and a payload weight of 462 pounds. Since no one vehicle can produce the power needed for the mission, it is required that a combination of vehicles be used.

A variety of combinations of vehicles will meet this design; however, power capability is not the only consideration. For this project, the combination should have a high reliability, and should be a standard combination so that the cost will be relatively low. For this reason, an Atlas/Centaur/high energy kick stage was chosen from the combinations capable of providing sufficient power.

The type of kick stage was determined by examining the payload weight versus power capability for Atlas/Centaur/kick stage configurations for various kick stages. The Burner II SS (spin-stabilized) with 1440 pounds of fuel was found to meet the project requirements quite well when mated with the Atlas/Centaur since this combination delivers a C_3 of 90.41 km^2/sec^2 (V_c = 47, 750 ft/sec) for a payload of 462 pounds (Figure 9.1).

The combination Atlas/Centaur/Burner II SS launch vehicle configuration was chosen for UMPIRE because of the power capability, high reliability, and relatively low cost. A table showing weights of the vehicle and a drawing showing dimensions are in Table 9.1 and Figures 9.2 and 9.3.

9.2 ATLAS SLV-3C

The Atlas launch vehicle is made by the Convair Division of General Dynamics and is a standardized vehicle. The vehicle uses a Rocketdyne MA-5 engine burning RP-1 kerosene and liquid oxygen and has a sea level rated thrust of the combination booster, sustainer, and two verniers of 395, 340 lbs. Approximately 1.2 seconds after ignition of the main engine, the vehicle reaches 90 per cent of its full thrust and is released from the launcher (Reference 1). Until booster jettison, the Atlas utilizes an on board flight control system, which contains gyros for attitude reference

Figure 3.1 Power Capability of Atlas/Centaur/Burner II SS (1440) (Reference 3)

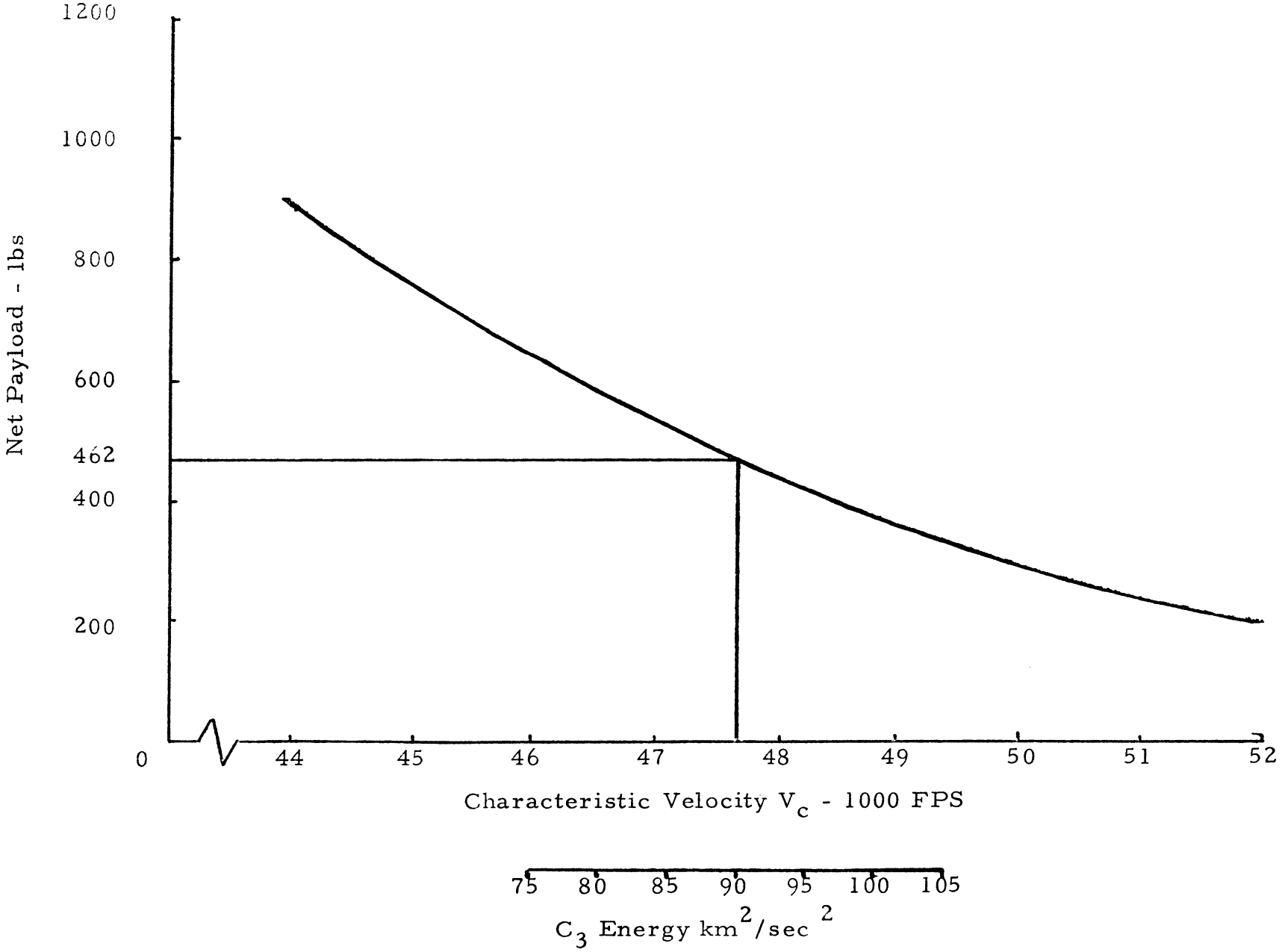

Table 9.1

ATLAS SLV-3C (Reference 2)		
Booster Jetison		7,467
Sustainer Jetison		8,208
Expendables		268,285
Main Impulse Propellant	268,102	
Miscellaneous	183	
Atlas Launch Weight		283,960
CENTAUR (Reference 2)		
Jettison Weight Minus Adapter		4,005
Adapter		196
Destruct	34	
Main Adapter	128	
Spin Table	34	
Expendables		30,402
Main Impulse Prop	29,911	
Hydrogen Peroxide	196	
Miscellaneous	295	
Equipment Jettisoned in launch Phase		3,119
Nose Fairing	1,850	
Insulating Panels	1,219	
Ice	50	
Centaur Launch Weight		37,722
BURNER II SS AND PAYLOAD (Reference 3)		
Structure		53
Motor Case		130
Propellant		1,440
Guidance & Control		0
Expendable Inerts		12
Payload		462
Weight on Centaur		2,097
TOTAL LAUNCH WEIGHT		323,779

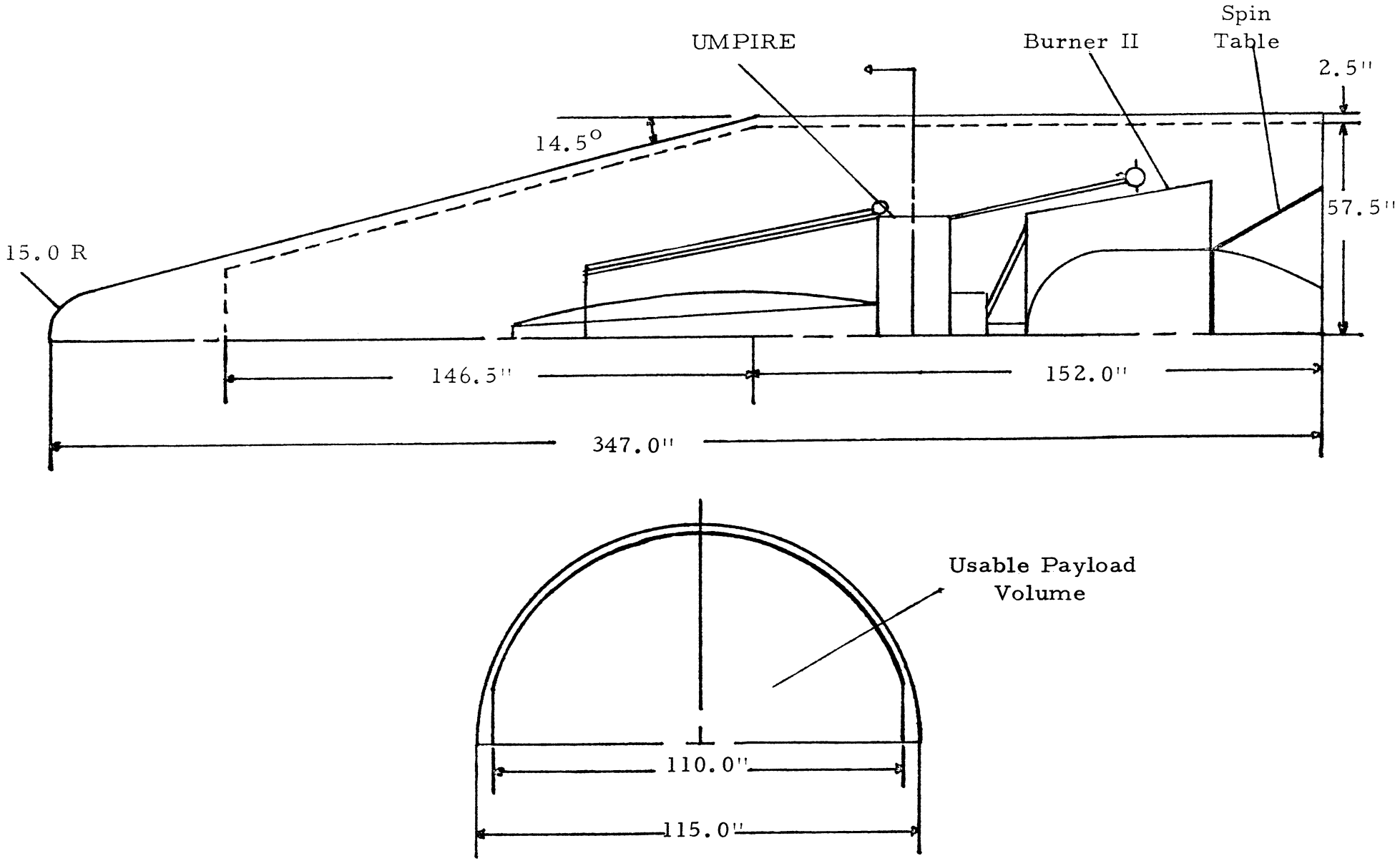

Figure 9.2 OAO Fairing to Accommodate UMPIRE

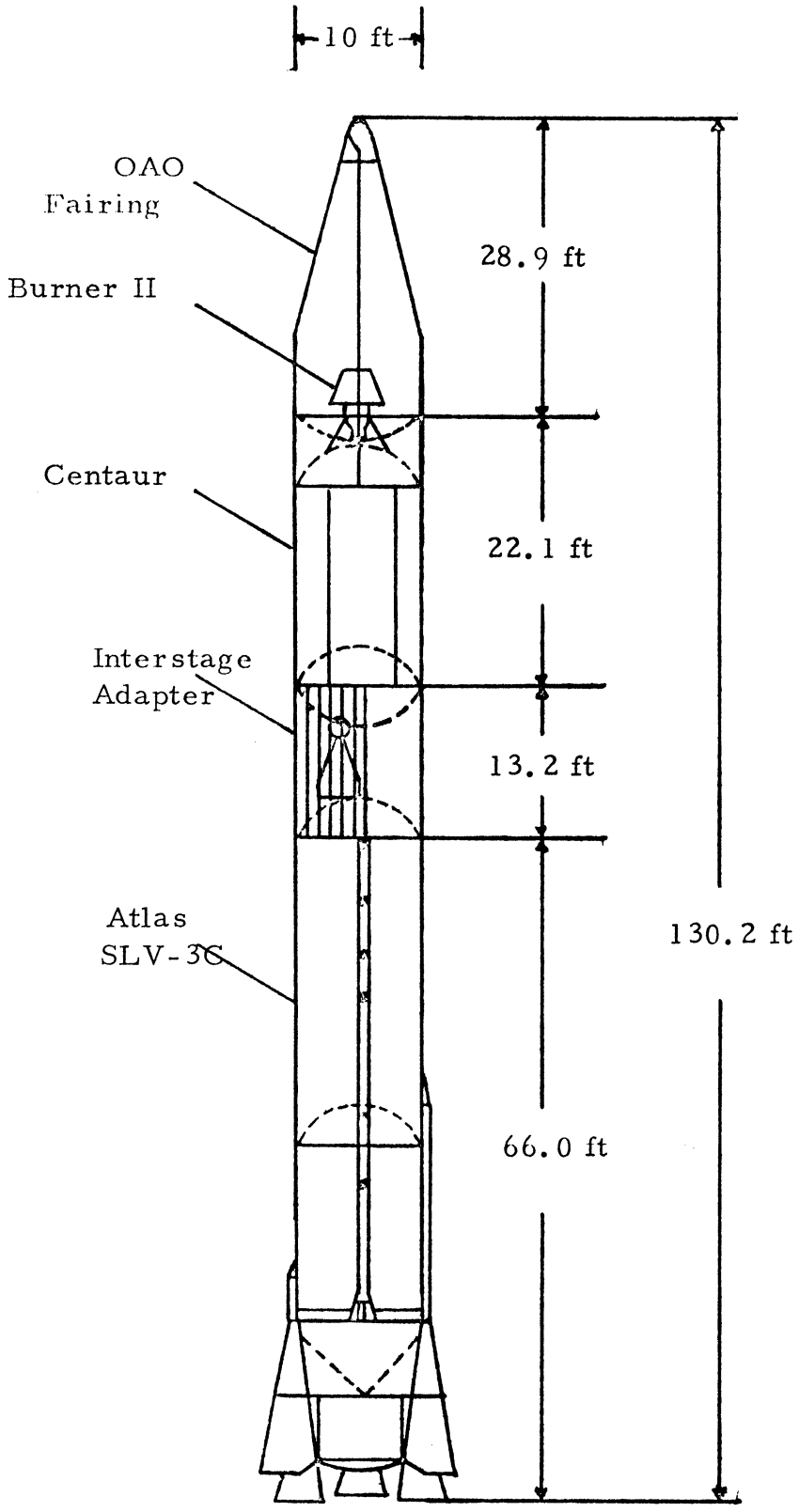

Figure 9.3 Atlas SLV-3C/Centaur/Burner II Launch Vehicle with OAO Shroud

and response damping, and a programmer for flight sequencing. After booster jettison, the Atlas flight control system is supplemented by the guidance and control on the Centaur.

9.3 CENTAUR

The Centaur vehicle is also made by the Convair Division of General Dynamics. The thrust is provided by two Pratt & Whitney RL10A-3-3 engines using liquid hydrogen/liquid oxygen for fuel. The total thrust is 30,000 lbs at a specific impulse of 444 seconds (Reference 2). The guidance and flight control for the Atlas/Centaur vehicle is a four-gimbal, all-attitude, inertial platform system made by Minneapolis-Honeywell that is contained on the Centaur, allowing the vehicle to be oriented in any attitude during the power on and the coast phase. This system makes use of a reprogrammable digital computer on the Centaur. A basic program for guidance is stored in the computer, and the vehicle is made mission particular by changing the temporary-storage constants in the computer. The guidance system makes measurements of accelerations, solves velocity equations, and then gives the autopilot the pitch and yaw steering commands. It has the capability of giving 28 discrete commands (Reference 1). These commands are fed to the Atlas flight control system after booster jettison and until sustainer engine cut off and to the Centaur flight control system after the main engine of the Centaur is ignited. During the powered flight, steering and attitude of the Centaur are attained by directing the thrust vector. This is done by gimbaling the main engine. After shutdown and during coast, the attitude control engines regulate the attitude using on-off commands fed to them by the guidance computer. Power for operation of the guidance computer, flight control system, and propellant systems is provided by an airborne battery. The Centaur can coast in a parking orbit for up to 65 minutes and then restart for a second burn. The Atlas/Centaur combination has a one-day turn around capability for meeting the launch window the next day.

9.4 BURNER II SS AND INTERFACE WITH THE CENTAUR

The Burner II SS vehicle is made by the Boeing Company and uses a Thickol TE-M-364-2 solid propellant engine. The name Burner II implies an elaborate guidance and control system on the engine. For the payload weight and power considerations mentioned in Section 9.1, the vehicle for Project UMPIRE was stripped of this guidance and control and converted into a spin stabilized vehicle by adding a light weight spin guide and spin assembly. This take is a relatively simple manufacturing job. In the spin-stabilized configuration, the accuracy of final injection is reduced from the guided configuration; however, since exact accuracy is not a major constraint, the spin-stabilized configuration is quite capable of accomplishing the accuracy of the project. Propulsion for spin up and despin is provided by solid fuel

rockets on the spin mechanism. The average thrust of the vehicle is 9250 lbs with a specific impulse of 290 second (Reference 2). Ignition, spin up, despin, and separation is actuated by a timer on the Burner II (Reference 4).

The Burner II is mated to the Centaur with a 196 pound adapter. This adapter contains a thermal bulkhead between the Burner II and the Centaur, a spin mechanism, a destruct system, a separation guide, and associated wiring. Separation from the Centaur is accomplished by compression springs. The electrical interface consists of an interface plug that is separated by internal springs when the Burner II separates from the Centaur prior to spin up.

9.5 INTERFACE WITH THE PAYLOAD

The Burner II/spacecraft mechanical interface consists of a payload support structure extending 9.5 inches above the Burner II (Reference 2). On the upper face of this structure are mounting pads spaced at 120-degree intervals (Reference 2) at an 8.25 inch radius (Reference 4) from the center of the upper face. The payload is mounted upon depressed release mechanism springs that are torqued to produce the desired separation force.

9.6 SPIN TABLE AND SEQUENCE

A spin assembly made by the Boeing Company weighing about 34 pounds (Reference 3) is to be used for the mission. The spin-assembly does not carry boost loads and is relatively insensitive to weight of the payload. The primary parts of the assembly are rollers that ride a spin guide ring, spin and despin solid propellant rockets, springs to provide separation energy, and clamps attaching to the main structure of the Burner II.

The sequence for spin and separation consists of an initial separation disengaging the Burner II from the Centaur interface connections and positioning the Burner II for spin up, the firing of the spin up, solid propellant engines, the opening of the clamps holding the Burner II to the spin assembly, and ejection of the Burner II from the Centaur and ejection assembly. After separation from the Centaur, the Burner II burns for about 60 seconds (Reference 5), despins to about 20 rpm, and then is separated from the payload by compression springs.

9.7 FAIRING

The Burner II and payload for the initial phase of ascent are enclosed by a nose fairing. The Centaur OAO fairing made by the Convair Division of General Dynamics was chosen for the project because of its large payload volume. The main cone is of sandwich construction with an inner skin of a laminated epoxy and an outer skin of an insulating resin. The cone is 1.75

inches thick, 347 inches high, 115 inches in internal diameter, and weighs about 1850 pounds (Reference 6). At about 202.8 seconds into the flight (Reference 2), spring loaded actuators are triggered and the fairing is jettisoned by splitting longitudinally (Figure 9.2).

9.8 REFERENCES

1. "Advanced Atlas Launch Vehicle Digest," Convair Division of General Dynamics, Issue No. 2, April 1967.
2. "Atlas Launch Vehicle Family for Spacecraft Contractor Planning," General Dynamics Report No. GDC BGJ 67-002, April 1967.
3. Boeing Document 2-6815-767, August 1968.
4. "Burner II," The Boeing Company, D2 82601-5, April 1968.
5. "Burner II, A Versatile Upper Stage," The Boeing Company, D2-82678-2, November 1966.
6. "Convair Fairing Systems," Convair Division of General Dynamics, October 1966.

"Surveyor VI Mission Report," Jet Propulsion Lab., Technical Report 32-1262, September 1968.

10

TRAJECTORY ANALYSIS

10.1 INTRODUCTION

An Interplanetary Ballistic Trajectory must be designed to be compatible with the mission requirements, payload weight, time of flight, and launch vehicle. In order to establish a feasible science package, a nominal payload weight of 450 lbs. is necessary. Further, only interplanetary flight times of less than 2 years were considered to insure high reliability. The Atlas-Centaur launch combination was specified, both from the point of view of low relative cost and excellent performance record. Various (high energy) kick stages were considered to develop the high energies needed for interplanetary flights.

In addition to the mission requirements, there are certain constraints intrinsic to any interplanetary flight. Launch windows of at least 20 days are considered necessary to provide adequate hold times. In order to make use of the Eastern Test Range, the declination of the geocentric escape asymptote, Φ_S, must be less than -33.5°. No arrivals within 11 days of Earth-Jupiter conjunction are allowed, to make communications feasible at encounter. There is, in general, a soft constraint on the angle between the Jupiter-Sun vector and incoming zeocentric asymptote (ZAP). This angle should be greater than 90° for improved planet viewing during encounter.

Patched conics techniques were utilized in the design of the interplanetary trajectory. The trajectory was considered in three phases: a geocentric escape hyperbola, a heliocentric transfer ellipse, and a zeocentric approach hyperbola. In general, an interplanetary trajectory is a function of n gravitational bodies; but, for the purposes of this report, only one gravitational body in each phase was considered. Near each planet a hypothetical sphere of influence was defined within which gravitational effects of other bodies were neglected. Beyond these spheres the only gravitational effect considered was that due to the sun.

10.2 OVERALL MISSION CONSIDERATIONS

10.2.1 Injection Energy C_3

By their very nature, feasible interplanetary trajectories require injection velocities greater than earth escape velocity. The injection energy C_3 of the escape hyperbola is found by squaring the hyperbolic excess speed (Figure 10.1).

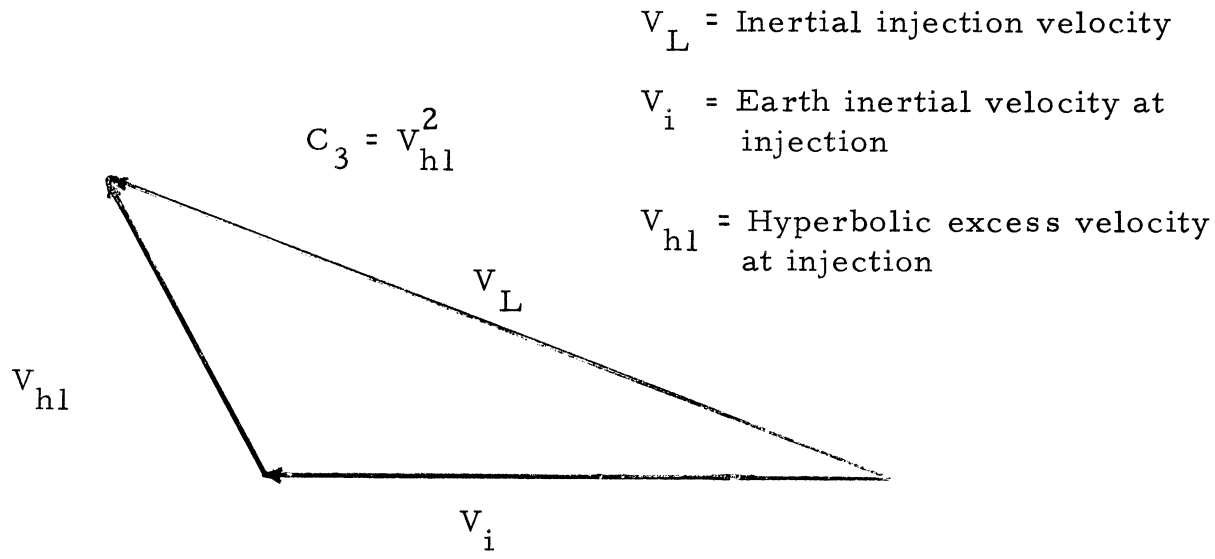

Figure 10.1

Injection energy C_3 may also be related to the characteristic velocity of the booster V_c by the following formula,

$$C_3 = \frac{V_c^2 - (36,164)^2}{(3280.84)^2}$$

where V_c is in units of ft/sec and C_3 is in units of km^2/sec^2.

The customary units of the injection energy C_3 are km^2/sec^2 and will be used throughout this report. The Atlas launch vehicle configuration chosen for the mission has a maximum capability of $C_3 = 90.41$ for a payload weight of 462 lbs. Injection energy of $C_3 = 90$ was chosen in order to provide a contingency for payload weight and also to provide some means of controlling the arrival date within the limits of the launch window.

10.2.2 Trajectory Type and Class

In general, for a given trajectory parameter versus launch date and a fixed injection energy there are two groups of closed contours. These two groups are designated Type I and Type II. Type I trajectories are those having heliocentric transfer angles less than 180 degrees and Type II trajectories are those having transfer angles greater than 180 degrees. Two trajectories usually exist for a given Type, energy, and launch date. Trajectories corresponding to shorter flight times and smaller heliocentric transfer angles are designated as Class I and correspond to the lower portion of the energy contour. Trajectories with longer flight times and longer heliocentric transfer angles are Class II and correspond to the upper portions (Reference 1).

The desirability of shorter flight time in addition with the constraint on the declination of the geocentric escape asymptote forced the selection of a Type I - Class I transfer trajectory for the 1972 launch period (Figure 10.2).

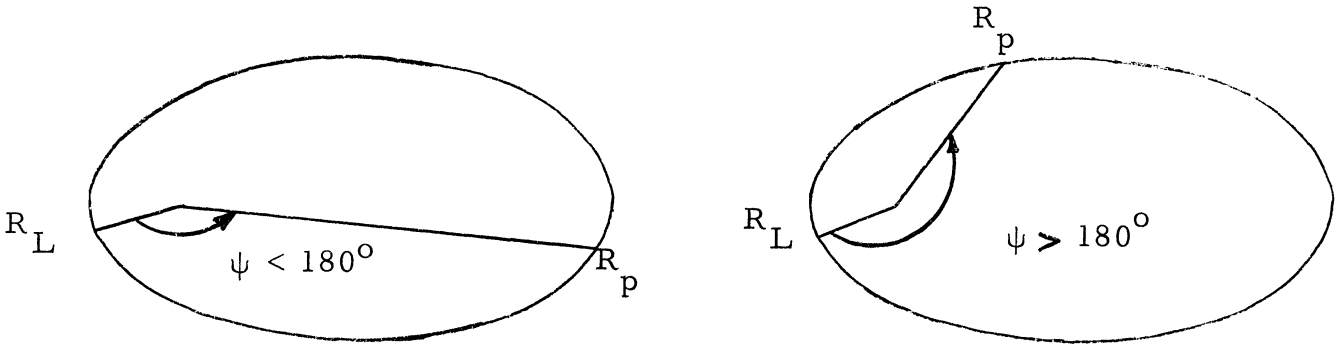

a) Type I b) Type II

Figure 10.2

10.2.3 Encounter Design Considerations

The Jupiter encounter characteristics were established by the science payload group. The desire for better scanning of the planet necessitated a clockwise passage. To decrease chances of radiation degradation, periapsis was chosen at $5R_J$. Further, the desire of earth occultation requires a nominal equatorial pass.

10.3 HELIOCENTRIC PHASE

10.3.1 Launch Date and Window

The orbits of the planets are such that achievable trajectories occur once every synodic period (13 months), i.e., when the relative positions of Earth and Jupiter are such that the energy required for an interplanetary flight are within the capabilities of the prescribed launch vehicle. During 1972, launchings into a Type I - Class I trajectory which require C_3 of 90 or less, occur between February 23 and March 20 (Reference 1). Within this period March 4 is the launch date requiring minimum injection energy. The realizable launch window is shortened to a 21 day period between February 26 to March 19 due to additional constraints discussed below.

10.3.2 Determination of Transfer Ellipse

Obviously, for a successful mission, the transfer ellipse must contain Earth at launch and Jupiter at arrival. Specification of injection energy and launch date immediately fixes the values of all other trajectory parameters.

The inertial velocity of the spacecraft, which ultimately determines time of flight, is the vector sum of two fixed quantities: hyperbolic excess velocity corresponding to C_3 and the velocity of the Earth at launch. Varying the angle α between these two fixed quantities varies both the magnitude and direction of the inertial velocity (Figure 10.3).

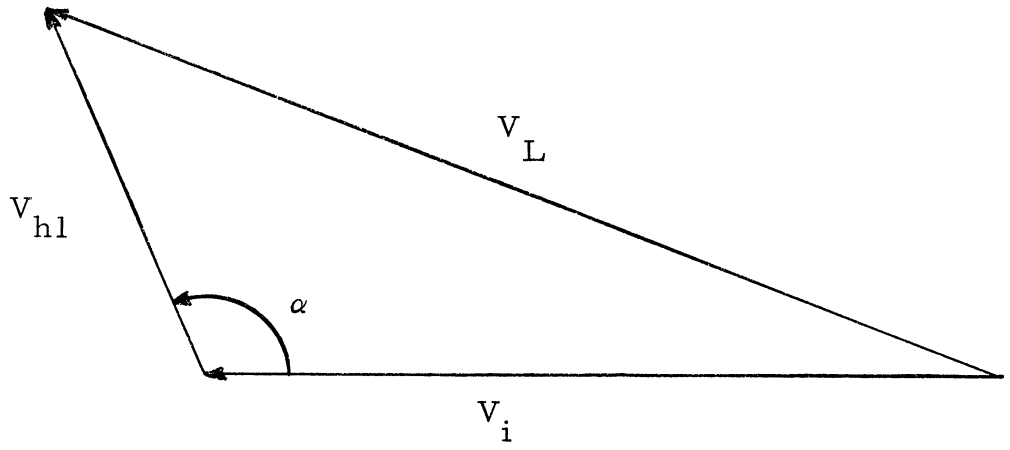

Figure 10.3

Specification of injection energy gives rise to a family of inertial velocity vectors for a specific launch date (as a result of varying α). Each vector determines an inertial ellipse containing Earth at the specified launch date. Traverse time to 5 AU will be uniquely fixed for each of the ellipses. Because Jupiter is also in motion, for a given type and class of trajectory there will be one and only one ellipse that contains both Earth at the time of launch and Jupiter at the time of arrival. (Fig. 10.4) Othe trajectory parameters can now be determined once a unique transfer ellipse is known (Figure 10.5). Standard plots of these parameters as a function of C_3 and launch date are available (Reference 1). For this mission, a C_3 of 90 has been previously established, and launch date will be varied within the launch window. (Variable flight times.)

10.3.3 Discussion of Parameters

For purposes of this report, nominal launch date is defined as the date requiring minimum time of flight for a specified injection energy.

Heliocentric Transfer Ellipse

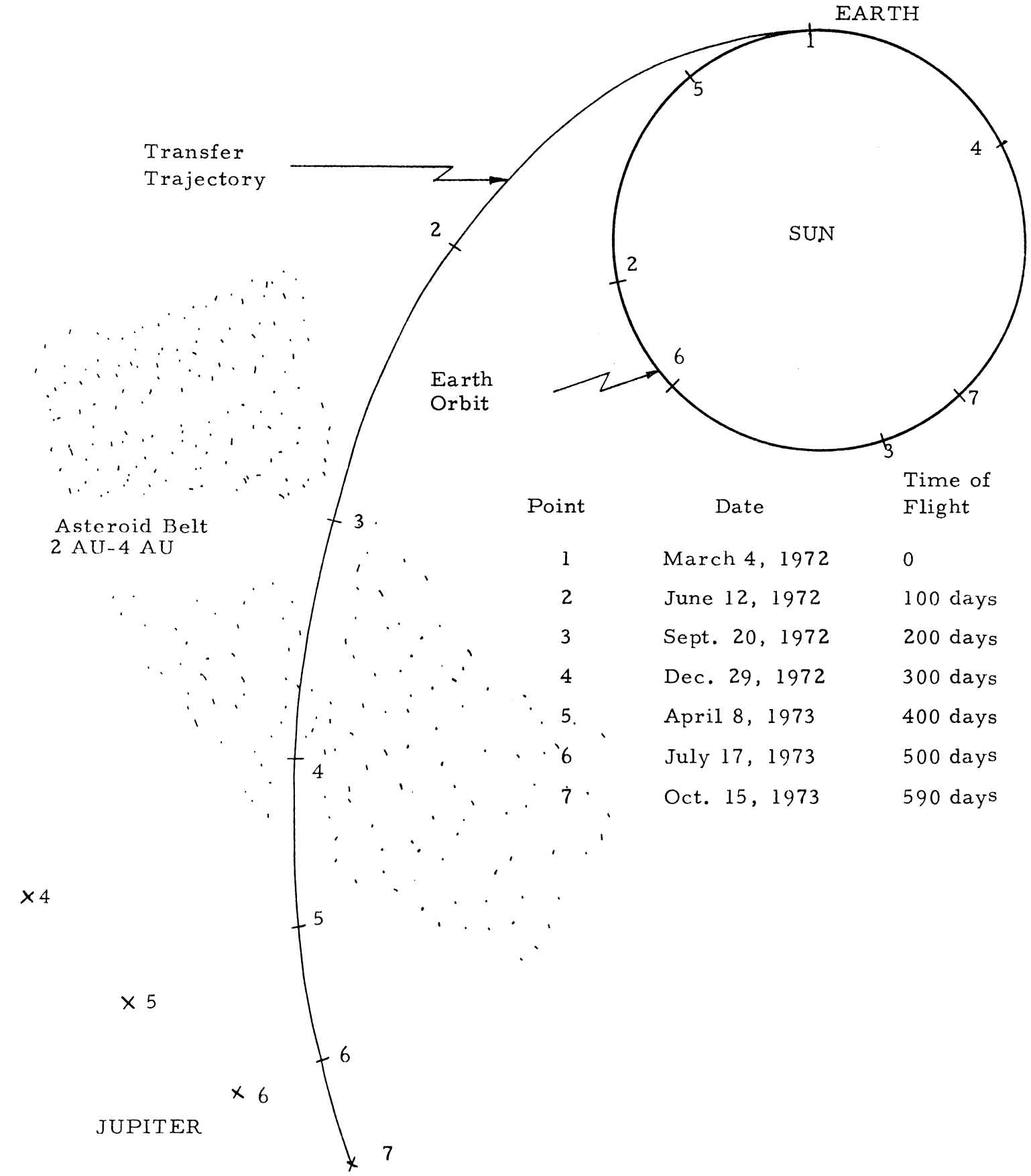

Point	Date	Time of Flight
1	March 4, 1972	0
2	June 12, 1972	100 days
3	Sept. 20, 1972	200 days
4	Dec. 29, 1972	300 days
5	April 8, 1973	400 days
6	July 17, 1973	500 days
7	Oct. 15, 1973	590 days

Figure 10.4

As indicated above, time of flight of the mission is directly reliant on the inertial velocity vector. Therefore, it is advantageous to select as a launch window a period where the magnitude of the inertial velocity is at a relative maximum. Time of flight is relatively constant for a small range (± 5 days) centered about this nominal launch date.

The heliocentric central angle, ψ, the angle between the Sun-Earth vector at launch and the Sun-Jupiter vector at arrival, is a direct function of the geometry of the two planets.

Because of the difference in orbital periods, communication distance at encounter is solely dependent on encounter geometry. In fact, this distance may vary from approximately 4 AU at Earth-Jupiter opposition to 6 AU at Earth-Jupiter conjunction. A further restriction on the mission is that there be no encounter within 11 days of conjunction to avoid sun interference. For feasible 1972 launches this restricted period occurs from February 1 to February 23, 1974.

Since Jupiter's orbital plane is slightly inclined (1.3 degrees) from the ecliptic, the transfer plane is a third plane defined by the Sun, Earth at launch, and Jupiter at arrival; and is itself inclined to the ecliptic by a small angle i.

The following table indicates the major parameters of the heliocentric phase, as derived from the aforementioned graphs (Reference 1).

HELIOCENTRIC PARAMETERS ($C_3 = 90$)

Parameters	Launch Window Acquisition Feb. 26, 1972	Nominal Launch Date Mar. 4, 1972	Launch Window Termination Mar. 19, 1972
time of flight (days)	610	588	800
Heliocentric central angle	158.5°	150.0°	155.8°
Earth-Jupiter Communication dis.	5.0 AU 746×10^6km	4.74 AU 707×10^6km	6.03 AU 900×10^6km
True Anomoly	356.0°	2.5°	17°
i of heliocentric transfer plane	2.1°	1.55°	2.6°

Table 10.1

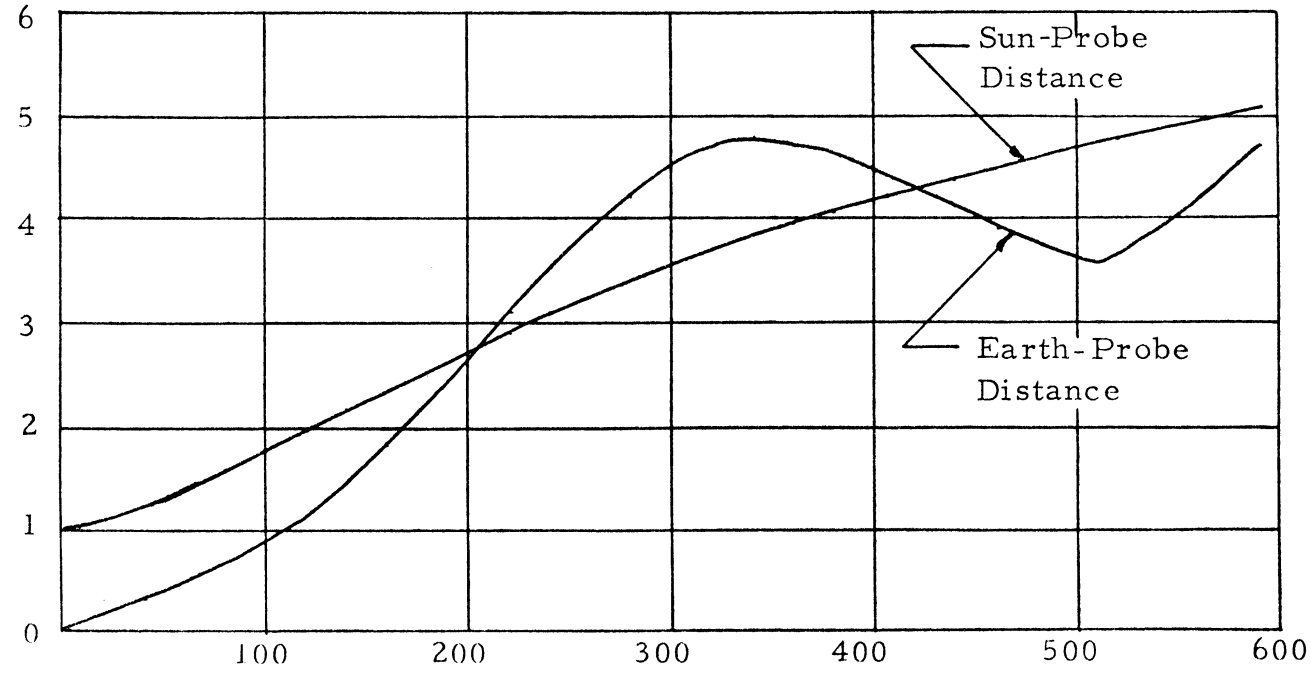
6
5
4
3
2
1
0
100
200
300
400
500
600
Sun-Probe Distance
Earth-Probe Distance
Time of Flight, days

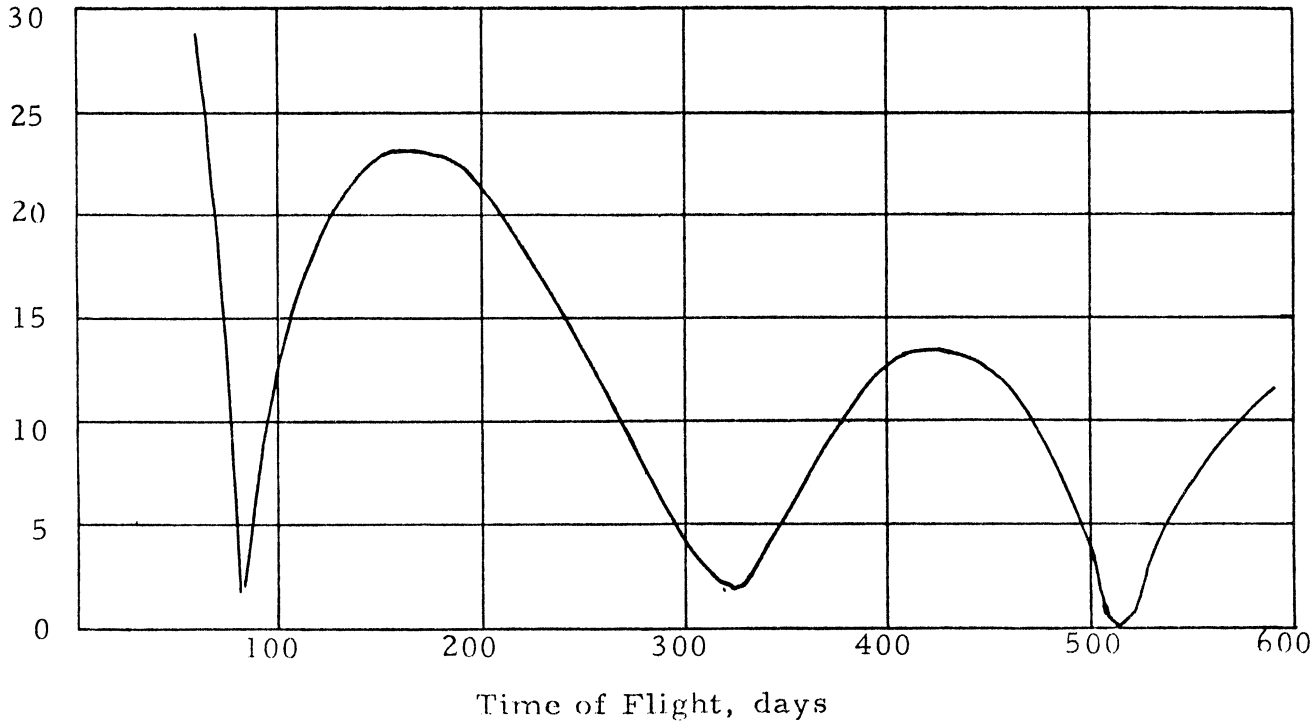
30
25
20
15
10
5
0
100
200
300
400
500
600
Time of Flight, days

Figure 10.5

10.4 GEOCENTRIC PHASE

10.4.1 Ascent Geometry

The chief problem of ascent trajectory design is that of matching the powered portions of flight to the heliocentric coasting portion. There are three primary geometrical properties which strongly influence the ascent trajectory: launch site location, launch azimuth, Σ_L, and the outward radial direction, $\vec{S}$ (Figure 10.6).

Launch will be at the Eastern Test Range.

The geometric constraint which exerts the strongest influence on the ascent path is the outward radial direction. This direction for interplanetary trajectories is defined to be the direction of the outgoing asymptote of the escape hyperbola. The ascent plane must contain this asymptote. The direction of the asymptote is determined by the specification of a declination and right ascension.

It has been shown (Reference 2) that given a launch site and a launch azimuth there are not one, but two space-fixed planes of motion determined. The launch site may pass through each plane twice each day, because it is rotating whereas the planes are fixed in space. This means that there could be two launch times each day for a given launch azimuth, or once for each of the two planes. However, it can be shown (Reference 2) that there are launch azimuths on which it is impossible to fire. This happens when

$$\sin^2 \Sigma_L > \frac{\cos^2 \Phi_S}{\cos^2 \Phi_L}$$

There are, however, limits to the launch azimuth at the ETR for range safety. Thus, using the above inequality, a range of permissible declinations can be solved for. For the ETR: $-33.50^\circ < \Phi_S < +33.5^\circ$. Further inspection of the above inequality indicates that $-29^\circ < \Phi_S < +29^\circ$ in order for launchings to be possible on all launch azimuths. For other values of the declination a range of launch azimuths symmetrical about due east exist from which it is not possible to fire from the ETR. The specified limits of the launch azimuth impose corresponding limits on the time of launch; thus, defining the daily launch window.

GEOCENTRIC ASCENT GEOMETRY

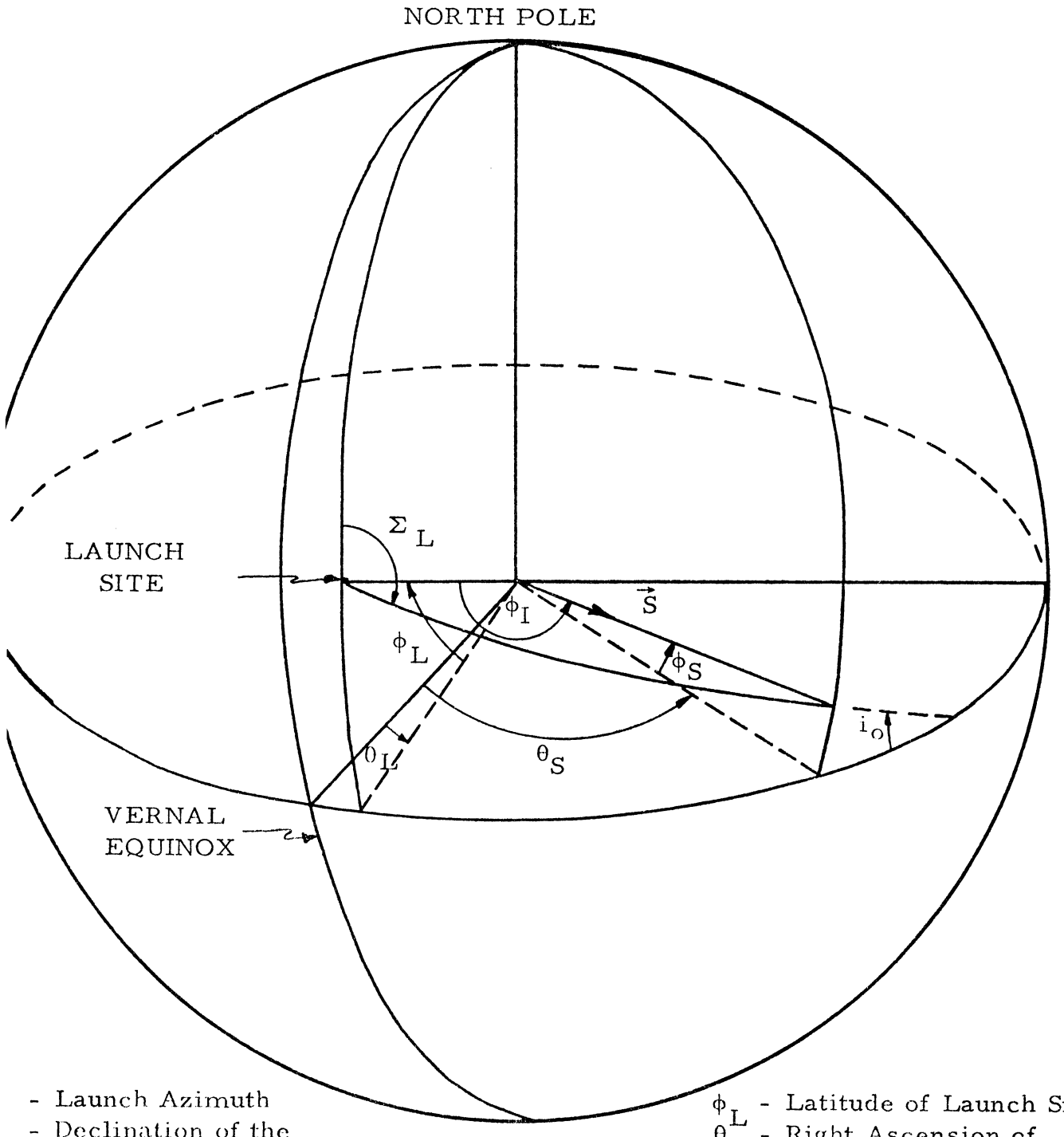

- Σ_L - Launch Azimuth
- i_O - Declination of the Geocentric Asymptote
- θ_S - Right Ascension of the Geocentric Asymptote
- i - Inclination of Heliocentric Transfer Orbit

- ϕ_L - Latitude of Launch Site
- θ_L - Right Ascension of Launch Site
- ϕ_I - Central Angle
- $\vec{S}$ - Outward Radial

Figure 10.6

10.4.2 Parking Orbit Ascent

It is generally desirable to minimize the true anomoly, ν_1, of the escape hyperbola for the most efficient payload injection. True anomoly is a function of the three angles shown in the following diagrams:

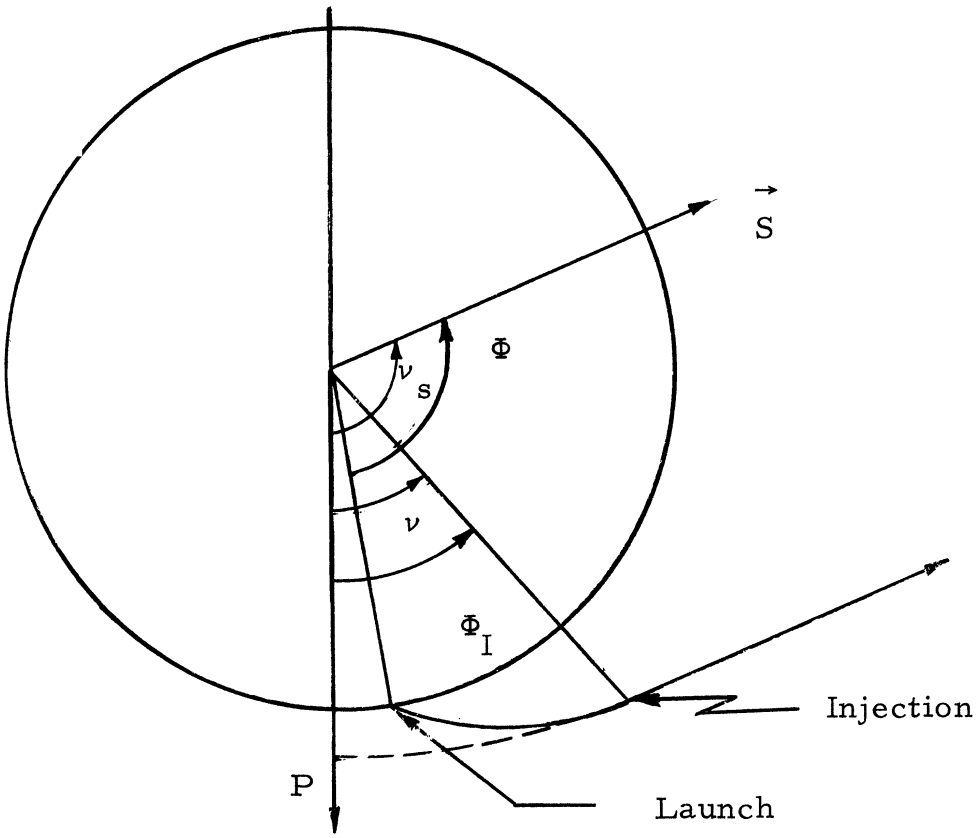

Figure 10.7

From the above diagram, it can be seen that

$$\nu = \nu_s - \Phi + \Phi_I$$

where ν_s and Φ are functions of the mission. By varying Φ_I, ν can be minimized. Using a direct ascent method, there is no capability of varying Φ_I. However, by utilizing a parking orbit technique, the magnitude of Φ_I can be controlled by varying the time of coast (Figures 10.8 and 10.9).

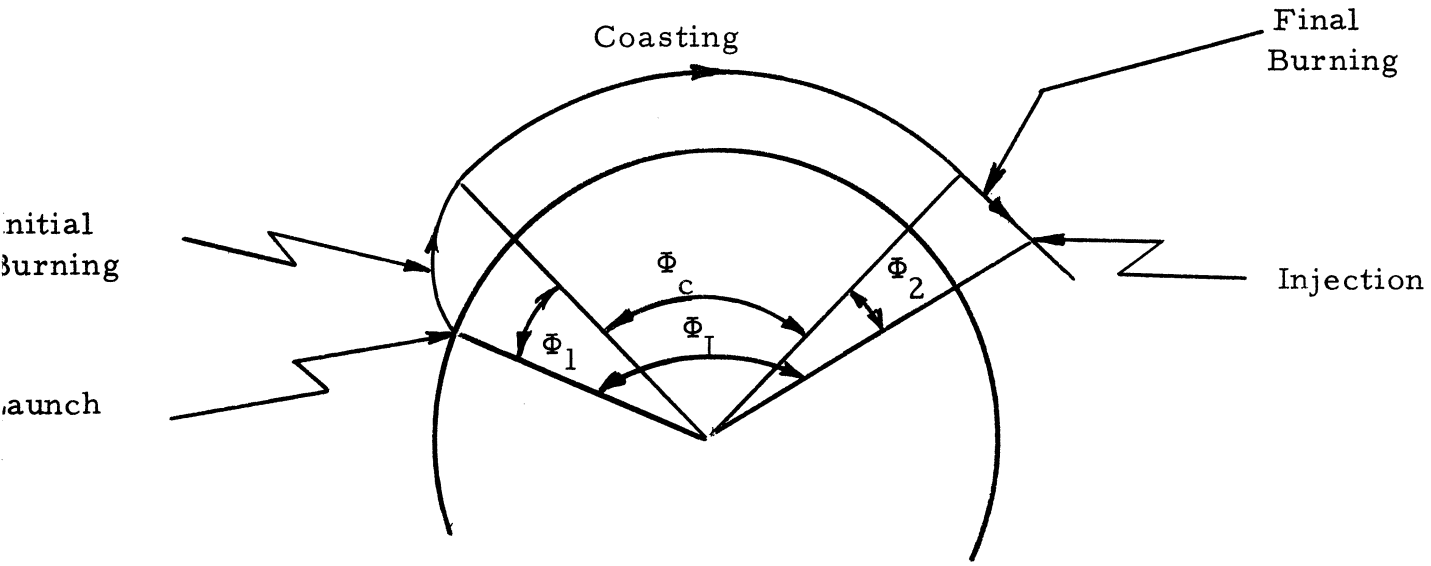

Figure 10.8

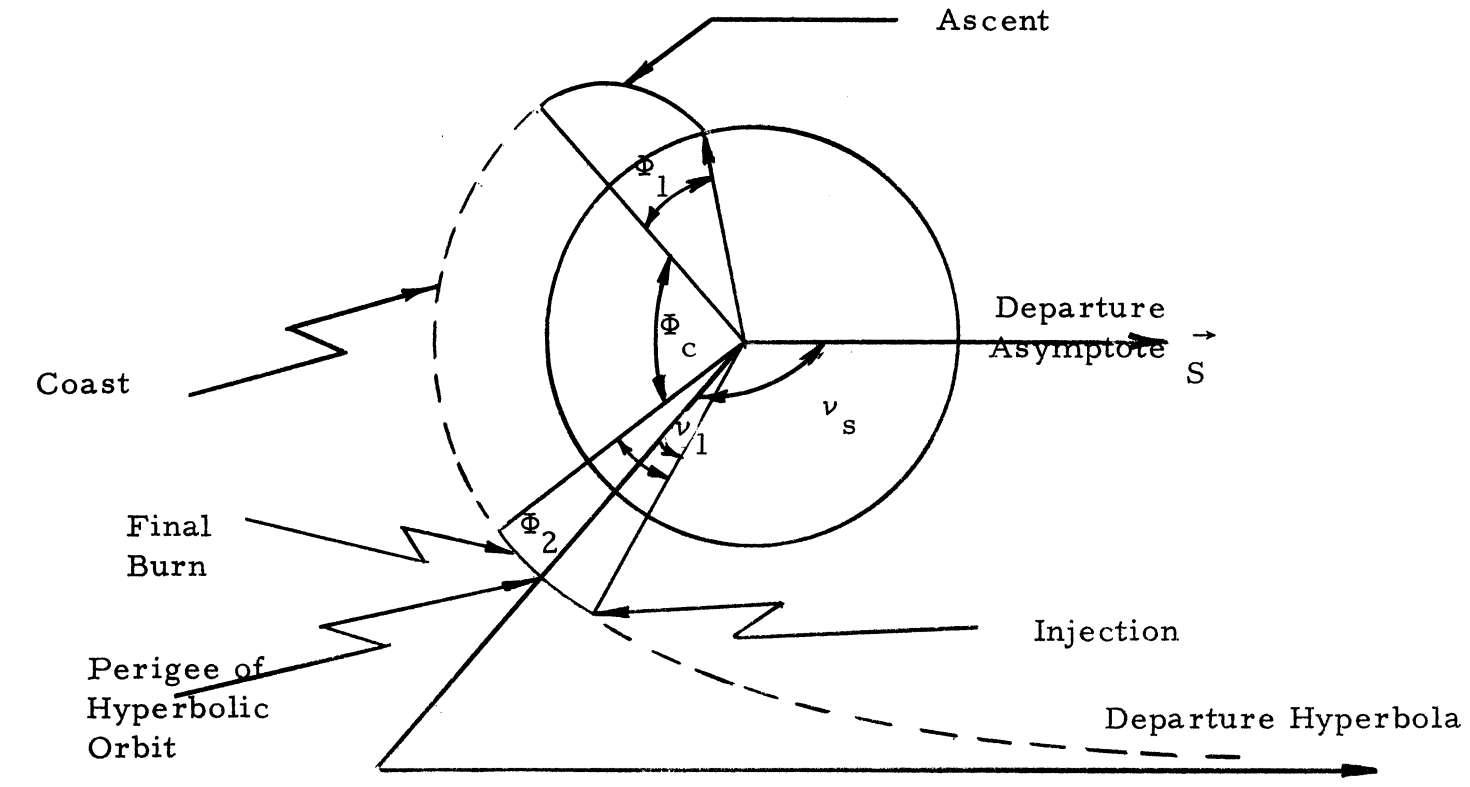

Figure 10.9

The following table indicates the major parameters of the ascent phase (Reference 1).

ASCENT PARAMETERS

Parameter	Launch Window Acquisition Feb. 26, 1972	Nominal Launch Date Mar. 4, 1972	Launch Window Termination Mar. 19, 1972
Declination of Geocentric Asymptote	-33°	-28°	-31°
Right Ascension of Geocentric Asymptote	251.8°	249°	237.5°
ZAL *	99°	89°	64.5°
GAL **	4°	3.2°	3°

Table 10.2

10.5 ZEOCENTRIC PHASE

10.5.1 Encounter Trajectory

Upon entering Jupiter's sphere of influence, the spacecraft assumes a hyperbolic path (Figure 10.11 and 10.12). A unique hyperbola is defined by the hyperbolic excess velocity with respect to Jupiter and the impact parameter $\vec{B}$, where $\vec{B}$ is the vector from the center of the planet to the incoming asymptote (Figure 10.10).

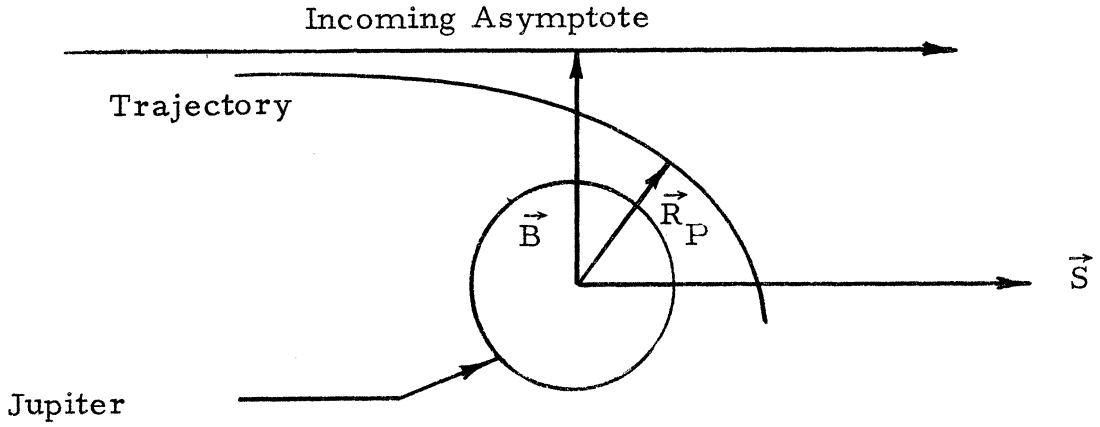

Figure 10.10

* Angle between sun-earth vector and outgoing geocentric asymptote

** Angle between outgoing geocentric asymptote and the ecliptic

ENCOUNTER GEOMETRY AT JUPITER

$R_p = 5\ R_J$

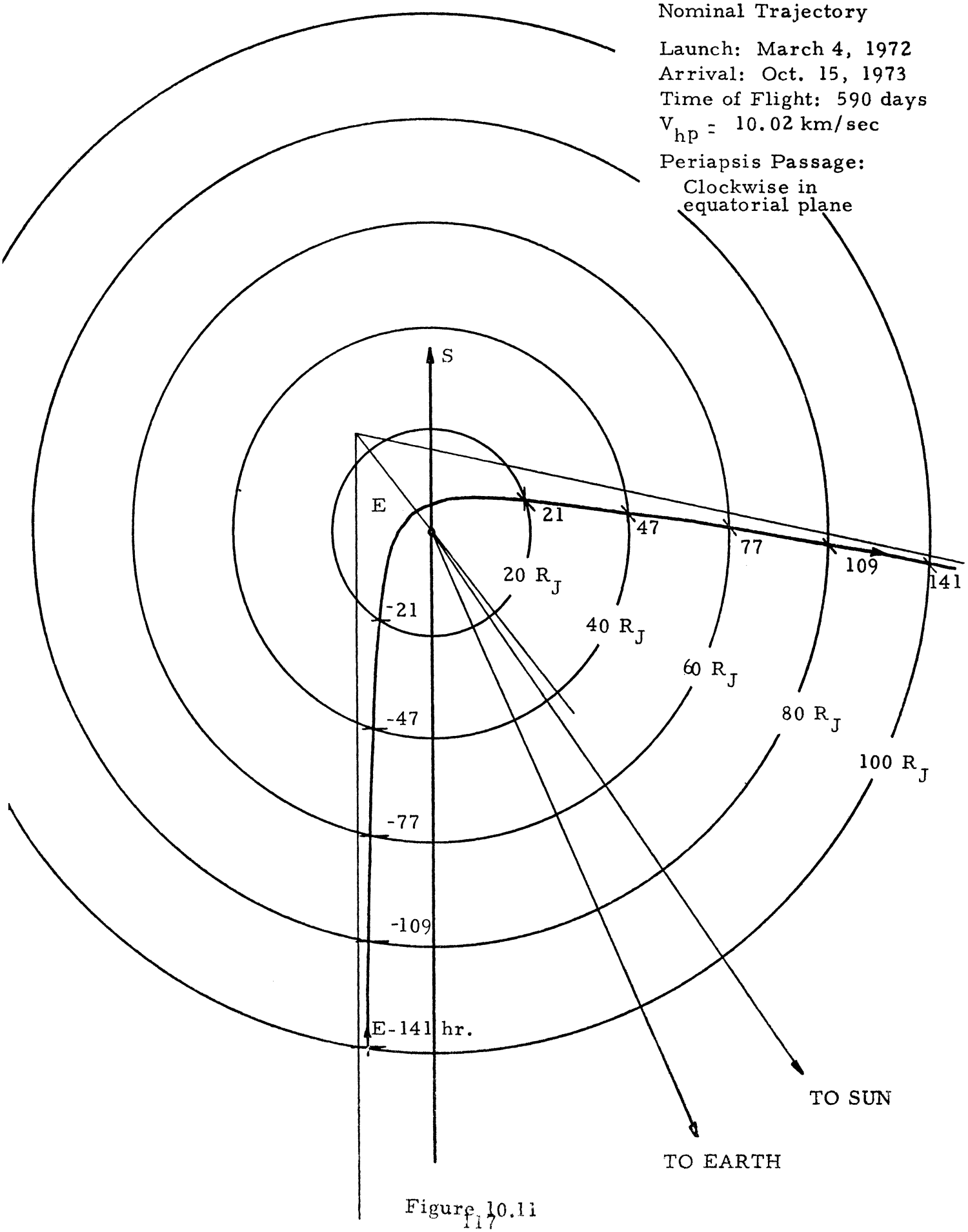

Figure 10.11

ENCOUNTER GEOMETRY AT JUPITER

$R_p = 5\ R_J$

Nominal Trajectory
Launch: March 4, 1972
Arrival: Oct. 15, 1973
Time of Flight: 590 days
$V_{hp} = 10.02$ km/sec
Periapsis Passage:
Clockwise in the
equatorial plane

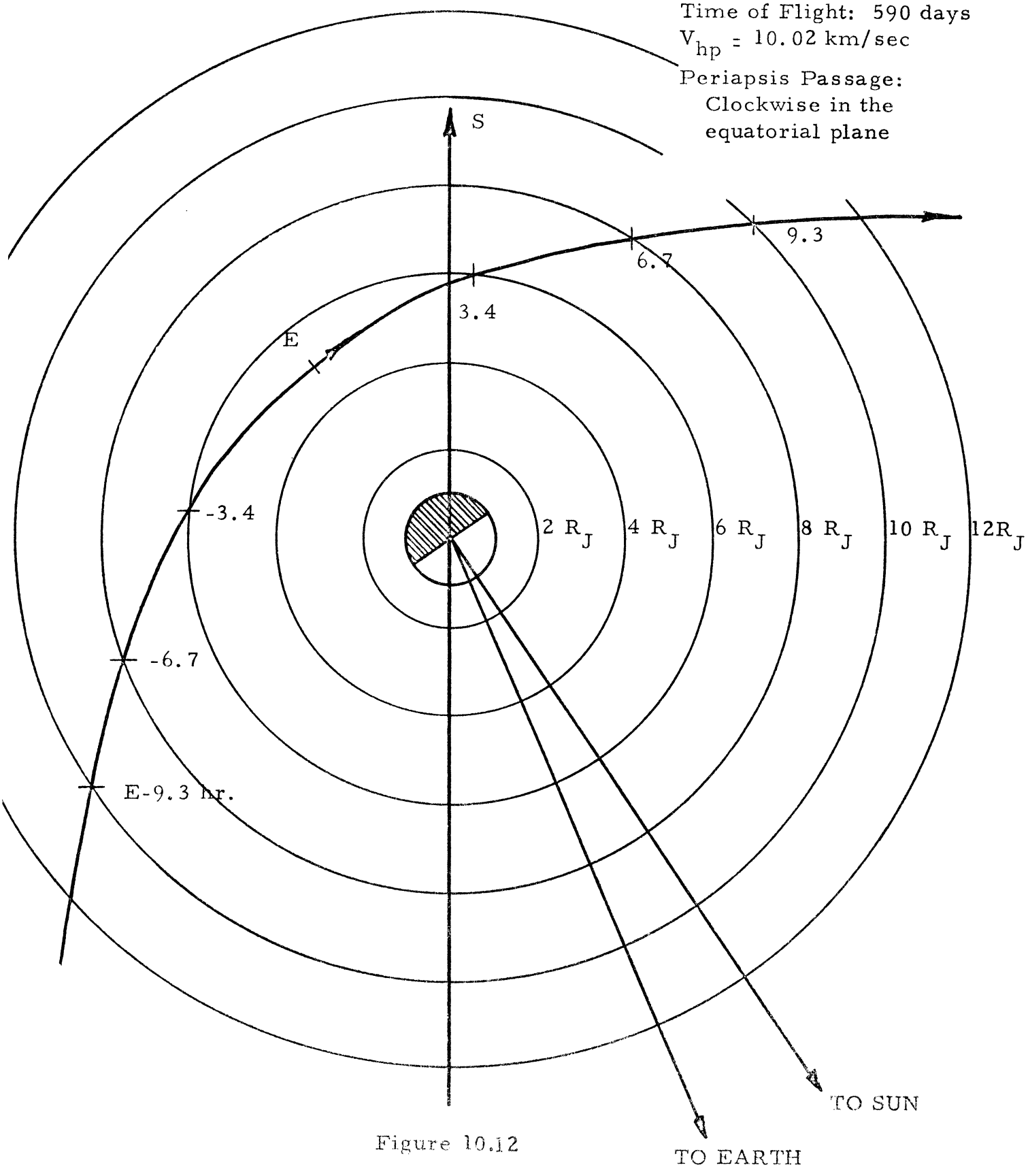

Figure 10.12

For this mission the hyperbolic excess velocity is fixed, and $\vec{B}$ is determined by science requirements as stated in Section 10.2.3.

10.5.2 Trajectory Characteristics

The ZAP angle is defined as the angle between the Jupiter-Sun vector and the incoming hyperbolic asymptote. The primary importance of this angle is to determine the degree of illumination of the planet during the approach as seen from the spacecraft. For a 1972 launch, the magnitude of ZAP indicates that the spacecraft will approach Jupiter from the sun-lit side and view an almost full planet.

The ZAE angle is defined as the angle between the incoming asymptote and the Jupiter-Earth direction. For a spin stabilized, Earth pointing spacecraft the ZAE angle is equivalent to the cone angle of an instrument mounted on the spacecraft which can view Jupiter as the spacecraft approaches the planet (Figure 10.[13]). For high values of ZAE, occultation begins soon after periapsis and is of relatively short duration.

The planes of Jupiter's equator, Jupiter's orbit, the ecliptic, and the transfer plane are all within a few degrees of being coincident. Thus, passage in any of these four planes can loosely be referred to as equatorial. The GAP angle is defined as being the angle between Jupiter's equatorial plane and the ecliptic. The following table indicates the major parameters of the zeocentric phase (Reference 1).

ZEOCENTRIC PARAMETERS

Parameter	Launch Window Acquisition Feb. 26, 1972	Nominal Launch Date Mar. 4, 1972	Launch Window Termination Mar. 19, 1972
V_{hp}(km/sec)	9.55	10.02	6.4
GAP	2.5^{o}	2.2^{o}	3.55^{o}
ZAP	142.4^{o}	145.0^{o}	111.0^{o}
ZAE	154^{o}	156^{o}	100^{o}

Table 10.3

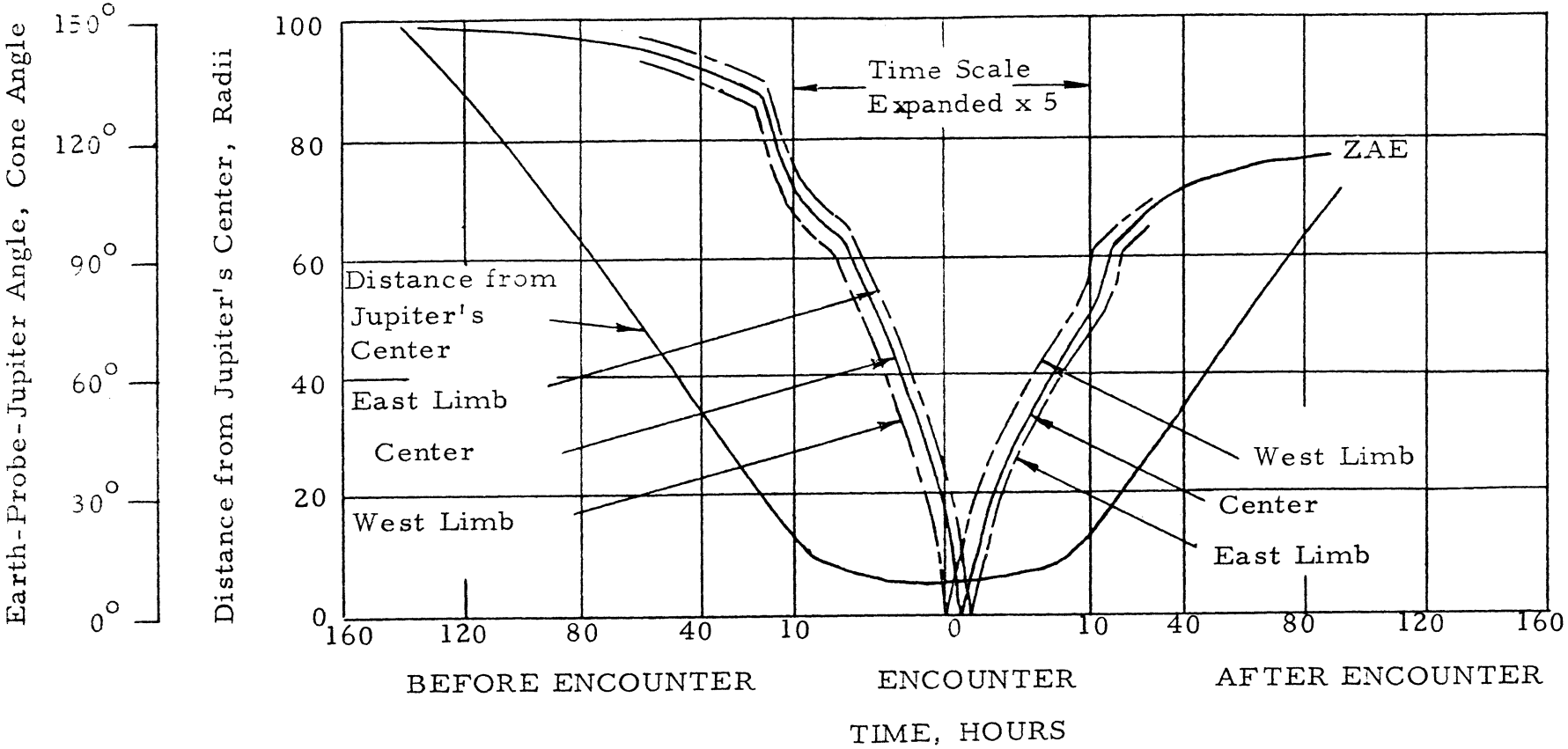

ZEOCENTRIC CHARACTERISTICS

Nominal Trajectory

Figure 10.13

10.6 MIDCOURSE

10.6.1 Miss Ellipse

Inherent in any launch vehicle guidance system, there are unavoidable random errors at injection. These random errors can be statistically represented by probability curves. For a particular launch vehicle, an injection covariance matrix can be generated to describe the accuracy of the launch vehicle. When suitable 3-sigma error sources are inserted, and the matrix is transformed into the proper coordinate system, the covariance matrix will generate a miss ellipse in the Jupiter impact parameter plane. This ellipse is known as a 99% miss ellipse, i.e., 99% of all launchings will impact within the area contained by the ellipse (Figure 10.14, Reference 3).

$a = 31.8 \times 10^5$ km

$b = 1.8 \times 10^5$ km

$\theta = 7.28^\circ$

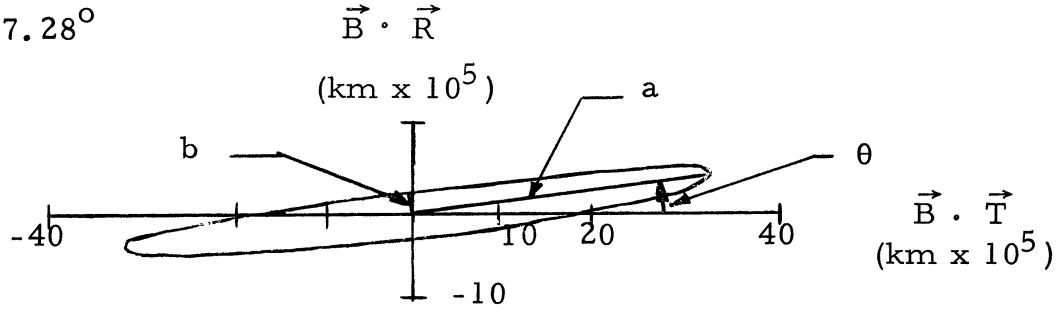

Figure 10.14

For convenience, a Jupiter centered orthogonal coordinate system is defined in the following manner. $\vec{R}$, $\vec{S}$, and $\vec{T}$ are a right hand set of mutually orthogonal unit vectors aligned as follows: $\vec{S}$ is parallel to the zeocentric approach asymptote, and centered at the planet; $\vec{T}$ is parallel to the plane of the ecliptic and positive eastward; and $\vec{R}$ completes the set and has a positive southerly direction. The impact point in this plane can be described by values of $\vec{B} \cdot \vec{T}$ and $\vec{B} \cdot \vec{R}$, and are contained by the miss ellipse. The purpose of the mid-course maneuver is to remove enough of the random injection errors to reduce the resultant error to an acceptable distance from the nominal impact point.

10.6.2 Types and Characteristics of Midcourse Maneuvers

In this report, two types of midcourse maneuvers were considered: Earth pointing and Arbitrary pointing. To remove the injection errors in the $\vec{B} \cdot \vec{T}$ and the $\vec{B} \cdot \vec{R}$ plane requires a ΔV uniquely oriented in space.

To achieve this ΔV while maintaining an Earth pointing spin axis requires at least 2 separate ΔV's, the vector sum of which is the desired ΔV. If the spacecraft has the capability to be arbitrarily pointed in space, the desired ΔV can be accomplished in a single firing. Since, fuel wise, it is more economical to achieve the desired ΔV in one firing, the arbitrary pointing technique will be utilized by this mission. The desired mission accuracy of $\pm$ 1/2 R_J is within the capability of this technique. Further, no attempt will be made to correct time of flight; rather, the midcourse maneuver will be carried out in the critical plane only. There is, however, a restriction that the spin axis of the spacecraft cannot be pointed within 20 degrees of the sun line early in the flight for accurate orientation of the spacecraft. (Fig. 10.5) For a specified mission, the midcourse maneuver must be designed to provide an adequate ΔV capability for the worst case. On the basis of available information, a ΔV capability of 90 m/sec was determined to be adequate for this mission.

10.7 ADDITIONAL CONSIDERATIONS

10.7.1 Communication Disruption

Due to a new characteristic of this mission, namely the extended time of flight, the geometry of the solar system introduces signficiant noise interference from the sun at various times throughout the flight. Specifically, at the time when the spacecraft-sun-earth line is established, the level of noise interference from the sun may necessitate communication cut-off. Also, during the two periods when the earth passes between the sun and the spacecraft the interference from the sun may cause a disruption of communication.

10.7.2 Asteroidal Perturbations

Since the spacecraft will spend considerable time in the asteroid belts, there exists a definite possibility of trajectory perturbations due to interactions with the larger asteroids. For a detailed analysis of this possibility, refer to Reference 4.

10.7.3 Galilean Moons

An additional aspect of this mission, which has not been considered in this report, is the possibility of the effect of the Galilean moons on the post encounter phase of the mission. The possibility of significant perturbations indicates a more detailed study of this problem. A detailed analysis of this possibility is presented in Reference 5.

10.7.4 Post Encounter

The post encounter trajectory is a direct result of the choice of encounter trajectory impact point in the $\vec{B}\cdot\vec{T}$, $\vec{B}\cdot\vec{R}$ plane. For this study, the post encounter trajectory was considered to be of secondary importance. As a result of the specified mission encounter trajectory, the post encounter trajectory will be a heliocentric ellipse, and the spacecraft will be moving toward perihelion.

10.8 REFERENCES

1. Clarke, V.C., W. E. Bollman, P.H. Feitis, and R.V. Roth, "Design Parameters for Ballistic Interplanetary Trajectories, Part II: One-Way Transfers to Mercury and Jupiter," Jet Propulsion Lab. Technical Report No. 32-77, 15 January 1966.
2. Clarke, V.C., Jr., "Design of Lunar and Interplanetary Ascent Trajectories," Jet Propulsion Laboratory, Technical Report No. 32-30, 15 March 1962.
3. "Study of Pioneer Missions to Jupiter," TRW Systems Group, Report No. 11339-6001-R0-00, 8 August 1968.
4. Rosen, A., "On the Possibility of Asteroidal Perturbations of a Jupiter Flyby Trajectory," Goddard Space Flight Center, NASA Document No. X-641-67-623, December 1967.
5. Kaufman, B., "The Effects of the Galilean Moons on Jupiter Flyby Trajectories," Goddard Space Flight Center, Report No. X-551-67-497.

"Advanced Atlas Launch Vehicle Digest," General Dynamics, Convair Division, Issue 2, April 1967.

"Advanced Planetary Probe," TRW Systems, Final Technical Report, 27 July 1966.

Bollman, W. E., "An Ambiguity in the Orbit Determination of Planetary Flyby Trajectories," Jet Propulsion Laboratory, Technical Report No. 32-1331, 1 November 1968.

Coady, R.E., "Trajectory Analysis - Near Earth and Jupiter Approach Phases of the 1972 Galactic Jupiter Probe Mission," Goddard Space Flight Center, 28 April 1967.

"Galactic/Jupiter Probe Study," Lockheed Missiles and Space Company, Preliminary Progress Report, 30 June 1967.

"Jupiter Flyby Missions," General Dynamics, Final Technical Report, 17 May 1966.

Lang, J. E., "Advanced Planetary Probe, Jupiter Flyby Application," Jet Propulsion Laboratory, 12 August 1966.

Larren, H.A. and R. A. Park, "Symposium on Unmanned Exploration of the Solar System," Presented by the American Astronautical Society, TRW Space Technology Laboratories, 8 February 1965.

Norton, A. R. M., E. Cutting and F. L. Barnes, "Analysis of Radio-Command Mid-Course Guidance," Jet Propulsion Laboratory, Technical Report No. 32-38, 8 September 1960.

"Pioneer Program," Ames Research Center, NASA Document No. P-200, 18 October 1968.

Soong, T. T., C. G. Pfeiffer and R. Hamburg, "Unified Guidance Analysis in Design of Space Trajectories," Jet Propulsion Laboratory, Technical Report No. 32-577, 31 January 1964.

"Trajectories to Jupiter, Ceres, and Vesta," Space Flight Handbooks, Volume III, Part 5, NASA Document No. SP-35, 1966.

11
SCHEDULING, COST AND PROBABILITY OF MISSION SUCCESS

11.1 INTRODUCTION

The purpose of this section, in conjunction with the preliminary design concept, is to present some type of plan by which the program may be guided through development phases, to present a plausible and consistent cost estimate and to evaluate the possibility of the mission being successfully carried out.

Project UMPIRE will cost approximately one hundred eighteen million dollars and it will take thirty-three months from the time the project is contracted, through the development phases, to the time of launch in March of 1972. Efficient use of current redundancy techniques indicates that the mission has an acceptable probability of being successful.

11.2 COST

The cost of Project UMPIRE was estimated from cost relationships developed in the Air Force Systems Command Space Planners Guide (Reference 1). The spacecraft subsystems costs are based on cost as a function of weight while various other costs are determined as a function of mission time.

UMPIRE will be a nonrecurring launch and thus the cost will be limited to one booster system, one set of qualification units, one prototype and one flight model.

Only two sets of Radioisotope Thermoelectric Generators (RTG's) will be necessary, one for the flight model and one for the prototype. Qualification tests for radiation, safety, temperature control, etc., will be conducted on these units and then the RTG's will be integrated into the flight model and prototype.

The spacecraft cost is separated into the nonrecurring costs for development; design, test, and evaluation (Table 11.1) and the recurring cost per unit spacecraft (Table 11.2).

The data handling subsystem cost is computed as a part of the communication subsystem, and the spacecraft structure subsystem also includes the subsystem costs of the deployables, mechanical devices, thermal control and meteoroid shielding since these are closely related to the structure.

Table 11.1
Design, Test and Evaluation Cost in Millions of Dollars ($\overline{M}$)

Subsystem	Cost ($\overline{M}$)
Sensors	10.4
Communication	8.7
Power	10.5
Structure	5.0
Attitude Control and Propulsion	3.4
TOTAL	38.0

Table 11.2
Per Unit Cost in Millions of Dollars

Subsystem	Cost ($\overline{M}$)	No. of Units	Total Cost ($\overline{M}$)
Sensors	1.40	2	2.80
Communication	.61	2	1.22
Power	.61	6	3.66
Structure	.35	2	.70
Attitude Control and Propulsion	.63	2	1.26
TOTAL			9.64

The total cost for development of UMPIRE is 38.0 $\overline{M}$ and the total cost for the units built is 9.64 $\overline{M}$.

In addition to the subsystem costs, there are other major cost items for which cost estimating relationships were developed. Among these are costs incurred during the development program for operational support equipment, tooling and special equipment, system integration and ground test subsystems (Table 11.3). These costs come to 16.0 $\overline{M}$.

Table 11.3 Other Development Costs in Millions of Dollars

Item	Cost ($\overline{M}$)
Operational Support Equipment	9.5
Tooling and Special Equipment	4.0
System Integration	2.1
Spacecraft Assembly and Checkout	.4
TOTAL	16.0

For the booster system, the Atlas SLV-3C costs 3.5 $\bar{M}$ and the Centaur costs 6.32 $\bar{M}$. The Burner II, including the adapter and shroud, costs .75 $\bar{M}$. The total cost of the booster system is then 10.57 $\bar{M}$ (Reference 1).

The final major cost items are those incurred during the actual flight and include Deep Space Network (DSN) support and spacecraft operations cost. On the basis of cost data related to Mariner IV (Reference 1), cost was found to be directly proportional to mission duration. Spacecraft operations costs include activities such as spaceflight operations, system analysis, spacecraft support analysis, technical documentation and computing. Based on an operational time of 650 days to allow a sufficient period for data recovery after encounter, these costs amount to 44.5 $\bar{M}$ (Table 11.4). DSN support will cost 41.5 $\bar{M}$ and spacecraft operations will cost 3.0 $\bar{M}$.

Table 11.4 Total Project Cost in Millions of Dollars

Item	Cost ($\bar{M}$)
Spacecraft	47.64
Booster	10.57
Test and Support Equipment	16.00
DSN and Operations Support	44.50
TOTAL	118.71

The cost for the entire project will be 118.71 $\bar{M}$.

11.3 PROBABILITY OF MISSION SUCCESS

A mission of the duration of UMPIRE, which must remain operational for three years and traverse the asteroid belt, requires the incorporation of redundant subsystems, where needed, to assure a high probability of mission success.

Since the communications subsystem is of relatively great importance, redundancy has been incorporated wherever component failure would result in loss of transmission. Similar steps have been taken in other subsystems where failure of vital components would seriously compromise the mission; these steps are indicated within the respective sections.

The outlook for UMPIRE, making use of present redundancy techniques, indicates that no major technical barriers exist and that the probability of mission success is high.

11.4 SCHEDULING

Figure 11.1 shows a program development plan with all steps numbered in sequence except for major steps which are numbered out of sequence. The abbreviations used are given in Table 11.5.

From events 1 to 2 the preliminary design of the whole Jupiter fly-by system is completed. This includes preparation of launch vehicle specifications and interface designs, launch facility needs and interface specifications, DSN facilities, etc. When this system design phase is completed, procurement of long lead items such as the launch vehicle and RTG fuel can be initiated.

Also, after event 2, a preliminary spacecraft design can be prepared and the science payload defined to some extent. Procurement and buildup of the instruments can then proceed as indicated by event 7. In parallel with the initial science procurement, the spacecraft detail configuration design can be completed, and the subsystem specification finalized.

Event 24 signifies the start of the integrated system tests. At this point, the Systems Test Model (STM) structure, data management, communications, and the control subsystems are assembled for what is called the astrionics compatibility test. These tests have the external interfaces mocked up for a more realistic simulation.

The entire spacecraft is functionally qualified at event 35.

A Temperature Control Model (TCM) is fabricated and tested at the same time as the STM. At event 59, a series of structural tests begins in order to qualify the structural and mechanical designs; this is accomplished at event 31.

The fabrication of the Launch Environmental Test Model (LETM) begins after event 31 and should incorporate all the changes from the preliminary structure testing, the STM tests and the TCM tests. Once it is functionally qualified and the changes have been incorporated, the design is frozen at event 46. Subsequently, at event 47, the manufacture of the Primary Mission Vehicle (PMV), and the Proof Test Model (PTM) can then be completed.

After complete checkout at the manufacturing sites, at events 47 and 48, the PMV is shipped to the launch site. About this same time, the launch vehicle component parts should also be available at the launch site and the launch operations will commence at event 51.

Table 11.5 (Reference 1)
Abbreviations Used in Figure 11.1

ACTVT	Activated
APPR	Approved
ASSY	Assembly
AVAIL	Available
BGN	Begin
COFG	Configuration
COMM	Communication
COMPAT	Compatibility
COMPL	Complete
CONT	Control
C/	Complete
DEL	Delivery/-ed/
DSGN	Design
DWG	Drawing
ETR	Eastern Test Range
FAC	Facilities
FLT	Flight
IMPLMTN	Implementation
INFRCE	Interface
INC	Incorporates
LETM	Launch Environmental Test Model
MCKUP	Mockup
MECH	Mechanical
MFGR	Manufacture
OPER	Operation/-al/
PMV	Primary Mission Vehicle
PREL	Preliminary
PRI	Primary
PROC	Procurement
PRPLN	Propulsion Subsystem
PTM	Proof Test Model
PYLD	Payload
QLFD	Qualified
R/	Release
RE/	Received
REV	Revised
RTG	Radioisotope Thermo-electric Generator
S/	Start
SCNCE	Scientific Payload
SPEC	Specification/-s/
SPCRFT	Spacecraft
STE	Site
STM	System Test Model
STR	Structure/-al/
VEH	Vehicle
SUBSYS	Subsystem/-s/
SYS	System
TC	Temperature Control
TCM	Temperature Control Model

FIGURE 11.2

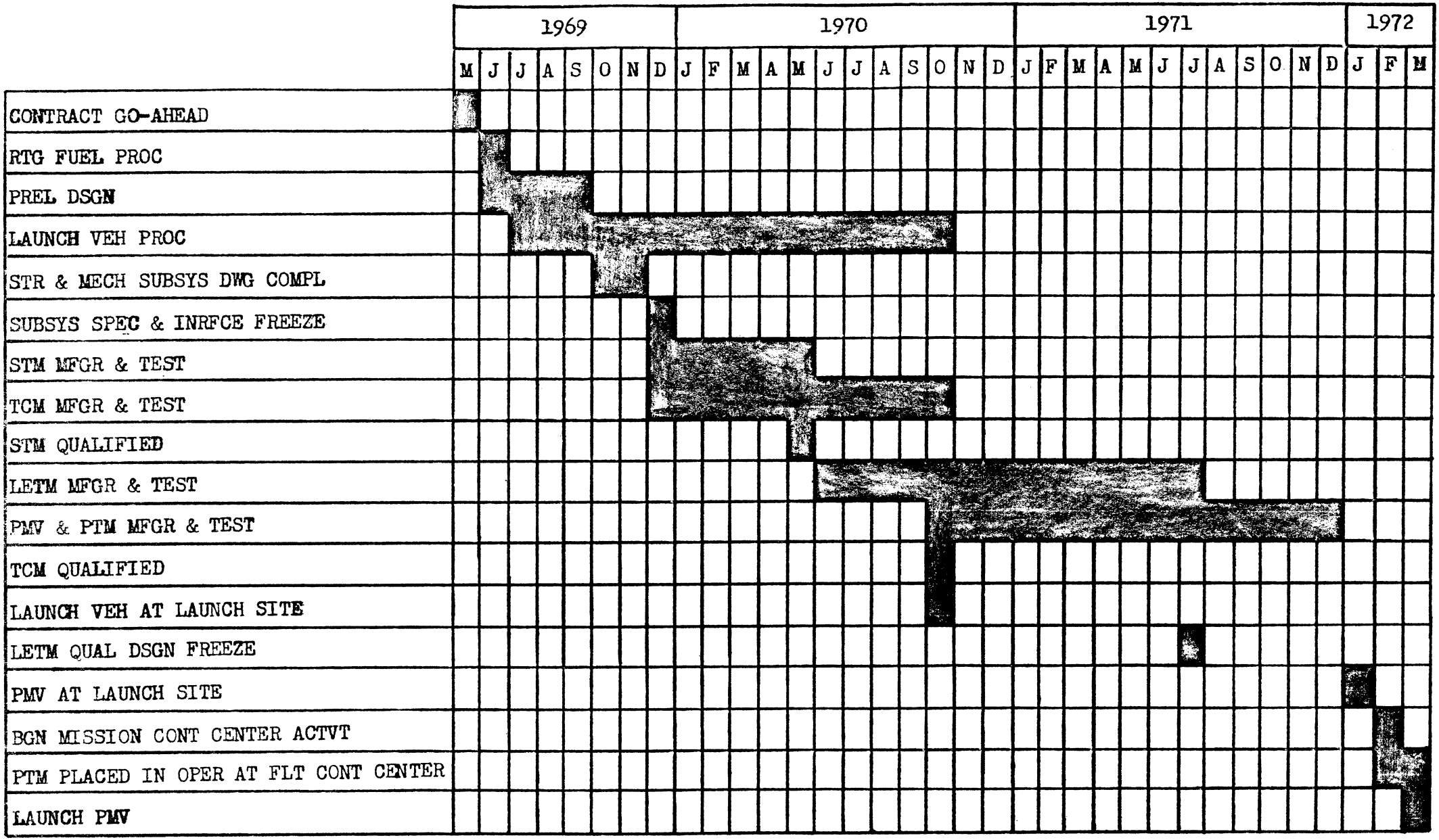

PROJECT TIME SCHEDULE

During launch site preparation, the PTM which is to be used as a diagnostic aid during the mission is shipped to the mission control center, placed into operation, and the inflight mission ground support operations begin at event 56.

The PMV is launched at event 54.

Once the implementation plan is arrived at, the program time development schedule can be formed for the March 1972 launch date to allow for development, fabrication, testing and integration. Figure 11.2 gives the proposed project time schedule.

A thirty-three month schedule is considered nominal since it lessens the overlap of prototype and flight spacecraft integration. The program could be shortened to twenty-nine months if the testing period were shortened but this would compromise the program.

11.5 REFERENCES

1. "Jupiter Flyby Missions," General Dynamics, Final Technical Report, 17 May 1966.

"Advanced Planetary Probe," TRW Systems, Final Technical Report, 27 July 1966.

"Galactic/Jupiter Probe Study," Lockheed Missile and Space Company, Preliminary Progress Report, 12 August 1967.

"Michigan Instructional Satellite for South American Countries," The University of Michigan, April 1968.

"Phase A Report, Galactic Jupiter Probe," Volume II, Goddard Space Flight Center, November 1967.

"Project Observer," The University of Michigan, December 1968.

"Solar Probe Experiment Created for Technological Research by the University of Michigan," The University of Michigan, April 1967.

APPENDIX A
COMMUNICATIONS

A.1 LINK PARAMETER BREAKDOWN

Since ground facility capabilities can be increased somewhat if necessary (up to 100 kw with the 210' dish), the downlink parameters are much more critical. The following figures were taken from Reference 4, Section 6: Downlink; nos. 2, 4, 6, 8, 9, 14, 16, 18, 20, 22, 23. Uplink; nos. 2, 6, 8, 9, the 10 db noise figure in 11, 14, 16, 18, 21-24.

A.1.1 Downlink Parameters (from spacecraft to E_{arth})

1) For transmitter power, P_t, the 12 watt TWT has a gain relative to one watt of 10 log 12 = 10.79 db
2) Coupling loss, L_{cs}, refers to losses incurred in the system due to the cabling and various connections necessary. -1.7 db
3) The spacecraft antenna is a 16' parabolic dish which has a gain $G = n\pi^2 d^2/\lambda^2$ where n = efficiency, d = dia. = 16' = 4.69m

$$\lambda = \frac{c}{f} = \frac{3 \times 10^8 \text{ meters/sec}}{2300 \text{ megahertz}} = .1305 \text{ meters}$$

$$G_s = \frac{(.55)(\pi^2)(4.69)^2}{(.1305)^2} = 7000 \quad 10 \log 7000 = 38.45 \text{ db}$$

4) The pointing loss, L_{ps}, of the spacecraft antenna is due to the inherent difficulty of keeping the most intense part of the RF beam directed toward the ground station. Off-center losses are taken as -.5 db
5) Space loss, S.L., is the degradation in signal strength due to the distances and particular frequencies involved.

$$\text{S.L.} = \frac{(4\pi)^2 R^2}{\lambda^2} = \frac{(4\pi)^2 (5 \times 9.3 \times 10^7 \text{ miles})^2}{(8 \times 10^{-5} \text{ miles/sec})^2} = -277.13 \text{ db}$$

6) Polarization losses, L_{p_l}, are due to the slight difference in polarization of the spacecraft transmitter and the ground receiver antennas, which also depends somewhat on the spinning of the spacecraft. -.5 db
7) The gain, G_g, of the 210' dish at Goldstone is given but could also be calculated with the previous formula. 61.6 db

8)	Pointing losses, L_{pg}, for the receiving antenna are zero because the ground antennas may be oriented in the best position.	0
9)	The coupling loss, L_{cg}, on the ground for the 210' dish for cables, connections etc., is small due to the improvements possible in the ground system.	-.2 db
10)	Hence power received = $P_t + L_{cs} + G_s + L_{ps} + S.L. + L_{pl} + C_g + L_{pg} + L_{cg}$ =	-169.9 db
11)	Since the Goldstone antenna is cooled with liquid nitrogen its temperature for noise density is only 30^{o} K. So noise density = 10 log kT = 10 log ($1.38 \times 10^{23} \times 30$) =	-213.8 dbw
12)	Hence S/N = Power received minus noise density =	44.61 db
13)	Due to unknown and unaccounted for losses, a margin of . and the remaining signal to noise ratio available is	4.6 db 40.01 db
14)	The carrier modulation loss is associated with carrier power lost when the signal is modulated onto it. β is a modulation system parameter related to message and transmitted bandwidths and losses related to imperfect filter rolloff and sampling.	-5.34 db
15)	Accounting for the above loss the carrier to noise ratio =	34.67 db
16)	The lowest carrier to noise ratio possible to still maintain phase lock loop is with a signal to noise ratio of zero db with the noise bandwidth of the phase lock loop at 3 hz or	4.77 db
17)	The relative carrier power above threshold is 34.67-4.77 =	29.90 db
18-19)	Associated with the above is a loop bandwidth of 26.3 hz or 14.20 db-hz and a SNR of C/N - 10 log $2B_L$ = 34.67-14.20 =	20.37 db-hz
20)	Similarly the loss in data power due to modulation is	-1.5 db
21)	Associated with data processing, command decoding, and other precise programming parameters is a synchronization loss of	2.49 db
22)	The stated required SNR or data to noise ratio for this system is only	3.8 db
23)	Subtracting synchronization losses and the SNR required from the data to noise leaves a noise bandwidth of	32.22 db
24)	Assuming 1 bit/sec = 1 cycle/sec, the bit rate transmissible at 5 AU = antilog 32.22/10 =	1664 bps
25)	Since each data bit requires a parity bit, using an 8 bit code requires 16 transmission bits/data bit. Hence data rate capability at 5 AU = 104 bps and at 4.74 AU =	116 bps

A.1.2 Uplink Parameters (from Earth to spacecraft)

To find the available uplink signal to noise ratio involves essentially the same process as the downlink. Hence parameters 1-10 are similar or equal to downlink, any differences being obvious.

11) Using a noise figure of 10 db and a system temperature of 350° K yields noise density = 10 log kTF = 10 log $(1.38 \times 10^{-23})(350^{\circ}\text{ K})(10)$ = -193.14 dbw/hz

12) Resulting S/N available then = -146.53 -(-193.14) = 46.61 db-hz
where -146.53 is total received power. As in the downlink relations the SNR level must be found which can handle a command rate of 9.16 bits/sec, which is higher than would normally be needed but would be necessary for complicated sequences of command.

13) From a graph of error probabilities versus SNR in the Aero 485 Communications Course Notes, it is found that for an error probability of 10^{-5} (1 error in 10^{5} bits), the SNR required for differential coherent phase reversal keying (a type of pulse code modulation) = 13.4 db

14) The synchronization loss is associated with coding, phase locking, signal comparisons and such precise relations, and the limiter degradation is that due to the limiter filtering out the abnormally high pulses. The loss allowed for this is 8.0 db

15) Adding quantities 13 and 14 above yields SNR required = 21.4 db

16) A command bit rate of 9.16 bits/sec means noise bandwidth = 9.62 db

17) Adding quantities 15 and 16 yields the required data to noise = 31.02 db

18) As before a loss is associated with modulating data on the carrier which when using $\beta = 1.2$ corrects for such things as imperfect filter rolloff and sampling losses. The figure is 3.01 db

19) Adding the data modulation loss to D/N yields S/N required = 34.03 db-hz

20) Subtracting this required S/N form the available S/N yields a power margin of 12.18 db

To find carrier performance at the S/N ratio of 34.03 db-hz with phase lock loop operation, we proceed as follows:

21) The loss associated with getting the carrier into phase lock operation and modulating the data onto it = -3.47 db

22) This leaves a carrier to noise ratio of 34.03-3.47 = 30.56 db-hz

23) The threshold carrier to noise ratio or the lowest conditions for which phase lock loop can be maintained is for a 6 db $(S/N)_{in}$ into the system with a noise loop bandwidth of 20 hz which yields $(S/N)_{out}$ = 19.03 db-hz

24) Therefore the carrier power above threshold is 30.56 - 19.03 = 11.53 db

A.2 COMMUNICATIONS SYSTEM WEIGHT, POWER, AND VOLUME BREAKDOWN

Item	No.	Total Wt. (lb)	Volume/Item(in.)	Total Pwr. (w)
Traveling Wave Tube and Integral Power Supply	2	6.5	10x4.5x3.5	29.3
Transmitter	2	2.8	6.4x4.1x1.75	1.5
PLL Receiver	2	6.2	10.6x5.8x8	1.3
Diplexers	3	1.5	4.3x2.2x1.3	-
Omni-coupler	1	.2	3x2x.5	-
Coax Switches	6	1.0	1.5x1.5x.5	-
TWT Control Selector	1	.5	4x5x1	.3
Receiver Control Selector	1	.5	4x5x2	.4
Cabling	-	1.5	-	-
Total (internal)	18	20.7	780	32.8
16' parabolic dish, feed support, and feed positioner	1	50.0	-	2.6/50ms
Omni Antenna	2	5.0	-	-
Conical Scan Antenna	1	2.8	-	-
Total (external	4	57.8	-	-
TOTAL SYSTEM	22	78.5	-	32.8

APPENDIX B
DATA HANDLING

B.1 QUANTIZING ERROR (Reference 1)

Quantizing is a technique whereby discrete values are assigned to the amplitude of the analog pulse from the commutation process. The amplitude is divided into intervals and each interval is assigned a unique element of a code. An uncertainty is introduced as to just precisely where within the interval the true amplitude is located. This uncertainty is called quantizing error. If the interval is Δ, then it can be shown that the mean square quantizing error is

$$\overline{e^2}_{qtz} = \frac{\Delta^2}{12}$$

and the Root Mean Square Error (RMS) is

$$e_{qtz} = \sqrt{\frac{\Delta^2}{12}} = \frac{\Delta}{\sqrt{12}}$$

Since we are using an 8 bit code, an incoming analog signal, if the maximum amplitude is normalized to unity, falls into one of 255 intervals. This is the result of an 8 bit word expressing 2^8 or 256 decimal numbers or levels), which implies there are 2^8 -1 intervals, which is 255 intervals. For our system therefore, the RMS error due to quantizing is

$$e = \frac{\Delta}{\sqrt{12}} = \frac{1}{\sqrt{12}} \quad \frac{1}{255} = .11\%$$

B.2 DIGITAL ERROR (Reference 1)

The process of digitizing provides a code whose elements are assigned to the quantized data. The data will be digitzed by using the binary number system.

Because of additive noise, digital errors are introduced. With the assumptions that:

a) any bit in a word is equally likely to be in error, and
b) only a single bit is in error in a word, then the mean square digital error is

$$\overline{e^2}_{dig} = \frac{4 P_b (\eta^2 - 1)}{3 \eta^2}$$

The RMS digital error is

$$e_{dig} = \sqrt{4/3}\ \frac{P_b^{1/2}\,(\eta^2 - 1)^{1/2}}{\eta}$$

where

P_b = binary error probability
η = number of quantizing levels

Choosing a binary error probability of $P_b = 10^{-5}$, the RMS digital error will be

$$e_{dig} = \sqrt{4/3}\ \frac{(10^{-5})^{1/2}\,(255^2 - 1)^{1/2}}{255} = .36\%$$

The value for P_b was chosen on the basis that this is an error probability for present systems.

B.3 DATA STORAGE ELEMENT CAPACITY AND DUMP TIME

The bit rate from the sensors is 413 bits per second at encounter. Assuming encounter lasts for 154 hours, the following capacity is needed in the DSE:

$$\left(\frac{413 \text{ bits}}{\text{sec}}\right)\ (154 \text{ hrs})\ \left(\frac{3600 \text{ sec}}{\text{hr}}\right)\ (16 \text{ bits encoding}) = 3.7\text{x } 10^9 \text{ bits}$$

The communications bit rate at 5 AU is 1664 bits per second. Time to transmit $3.7\text{x}10^9$ bits at this rate would be:

$$\left(\frac{3.7\text{x}10^9 \text{ bits}}{1664 \text{ bits/sec}}\right)\left(\frac{1 \text{ hr}}{3600 \text{ sec}}\right) = 618 \text{ hrs}$$

Assuming the DSIF is available only 16 hours a day it would take

$$\frac{618 \text{ hrs}}{16 \text{ hr/day}} = 38.7 \text{ days}$$

Using data compression of 4.2:1 it would take

$$\frac{618 \text{ hrs}}{4.2} = 147 \text{ hrs}$$

which is 9.2 days, assuming 16 hours per day transmission.

B.4 REFERENCES

1. Bauer, Louis, "Aerospace Communications, Aerospace Engineering 485", University of Michigan, 1969.

APPENDIX C
POWER

C.1 AUXILIARY POWER

If the new thermoelectrics, TAGS-2N, are not developed in time to be used for this mission, the main power supply will be the currently existing SNAP-19 with 2N-3P thermoelectrics. Figure C-1 shows the power supply and power demand curves for this situation. The three SNAP-19's will provide 81.4 watts of conditioned power at launch and 71.4 watts of conditioned power at Jupiter encounter. As this does not allow a contingency for emergencies and does not supply enough power for the post-encounter phase, an auxiliary power subsystem is required.

Consideration was given to three types of batteries: silver cadmium, nickel-cadmium, and silver-zinc. Nickel-cadmium has the greatest number of cycles per lifetime followed by silver-cadmium and then silver-zinc; however, the silver-cadmium value is sufficient for UMPIRE requirements. Silver-cadmium and nickel-cadmium batteries give the best range of operating temperatures; silver-zinc the worst. For a given power to be supplied, a silver-cadmium battery is the lightest, and a nickel-cadmium is the heaviest. Since silver-cadmium and nickel-cadmium both satisfy cycles per lifetime and temperature consideration requirements, silver-cadmium was chosen because it is the lightest battery system.

The type of battery selected has a normal capacity of 10 ampere-hours. It is designed for a 40% discharge and approximately 25% deterioration after a period of two years. This subsystem consists of 22 cells connected in series with the total battery weight of 15.5 pounds. In addition an on-board battery charge-discharge regulator, a load circuit current sensor will be required. The total power system weight will then be approximately 120 pounds.

C.2 RADIATION AND MAGNETIC FIELD CALCULATIONS (Reference 1)

The neutron production rate of a fueled RTG is proportional to the thermal energy of the fuel. Thus, since each SNAP-19 in the UMPIRE power system produces 625 watts of thermal energy, the neutron production rate of one RTG is 0.625×10^8 n/sec. Similarly, the gamma flux of an RTG is also proportional to the thermal energy of the fuel. Thus associated with each RTG is a gamma dose rate of 4.167 mrad/hr measured at a distance of one meter (3.28 feet) from the RTG.

Under normal operating conditions, each SNAP-19 produces a magnetic field of 12.5γ measured at a distance of one meter from the RTG.

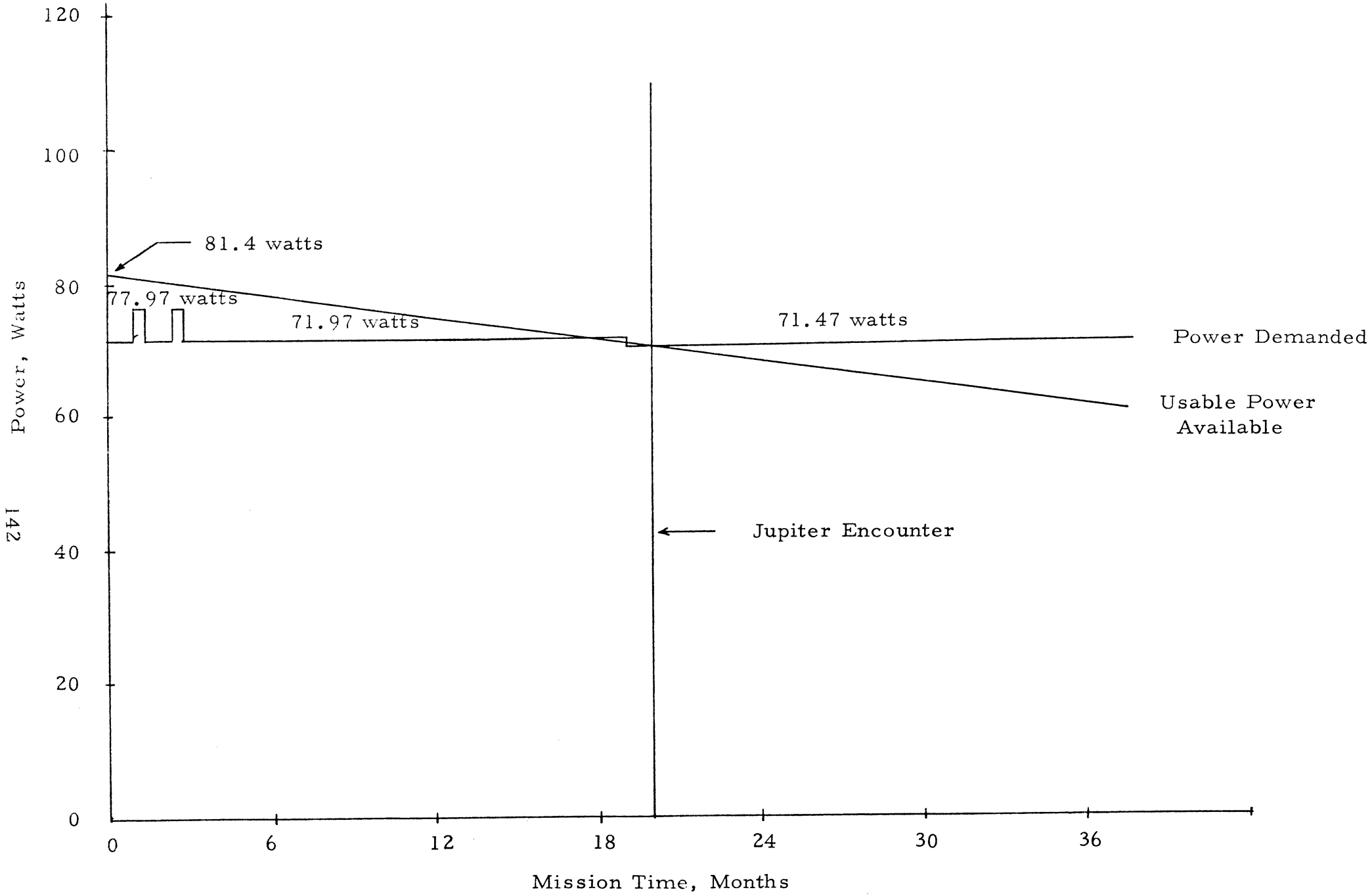

Figure C-1 Power Supply/Demand Profile

Each RTG is equidistant from the center of the baseplate of the instrument package. Specifically, each RTG is 2.60 feet from the center point horizontally, and 5.71 feet vertically. The straight-line distance between each RTG and the center point of the baseplate is thus 6.26 feet.

The neutron flux at the center point can be determined by evaluating the expression:

$$\frac{3 \times 0.625 \times 10^{8}}{4\pi d^{2}} \qquad \frac{n}{cm^{2}\text{-sec}}$$

where d is the separation distance expressed in centimeters. The neutron flux at the center point is found to be 409 n/cm^{2}-sec.

The gamma flux at this point can be determined by applying the principle that the flux is inversely proporational to the separation distance. Thus the following expression can be written:

$$\frac{3 \times 4.167}{d^{2}} = \frac{G}{1}$$

where G is the gamma flux in mrad/hr; and d is the separation distance expressed in meters. Thus the gamma flux at the center point is 3.425 mrad/hr.

Because of the symmetry of the spacecraft, the magnetometer and the radiation experiments packages mounted on the 14-foot booms are interchangeable so far as the separation distances are concerned. There are two RTG-experiment separation distances involved: the distance between the experiment and the two near RTG's, and the distance between the experiment and the RTG on the opposite side of the spacecraft, the far RTG.

The far RTG is 22.07 feet from the experiment package horizontally, and 3.82 feet vertically. Thus the straight-line distance between each experiment package and the far RTG is 22.40 feet. Each experiment package is 14.53 feet from each of the near RTG's horizontally, 3.82 feet vertically, so that each package is 15.03 feet from each of the two near RTG's.

Employing the previous formulae

$$\text{Total neutron flux} = \frac{0.625 \times 10^{8}}{4\pi d_{1}^{2}} + \frac{2 \times 0.625 \times 10^{8}}{4\pi d_{2}^{2}} \qquad \frac{n}{cm^{2}\text{-sec}}$$

where d_1 is the separation distance between the experiments package and the far RTG, and d_2 is the separation distance to one of the near RTG's; both distances expressed in centimeters.

Thus, the neutron flux at each boom mounted sensor is $57.87 \frac{n}{cm^2\text{-sec.}}$

The gamma flux is given by:

$$\frac{4.167}{d_1^2} + \frac{2 \times 4.167}{d_2^2} = G \frac{mrad}{hr}$$

where d_1 and d_2 are the separation distances to the far and near RTG's, respectively, expressed in meters. The gamma flux at each boom mounted sensor is 0.485 mrad/hr.

The magnetic field strength measured at the experiments package is given by:

$$\frac{12.5}{d_1^3} + \frac{2 \times 12.5}{d_2^3}$$

where d_1 and d_2 are separation distances to the far and near RTG's respectively, expressed in meters. The magnetic field strength due to the three RTG's in normal operation is 0.30 at the boom mounted sensor.

Because some instruments are damaged by integrated radiation fluxes, the neutron and gamma fluxes were integrated from launch to 20 months, the time of Jupiter encounter, and from launch to 36 months, the rated lifetime of the mission. Assuming a uniform 30 days per month:

$$20 \text{ months} = 1.44 \times 10^4 \text{ hours} = 5.18 \times 10^7 \text{ seconds.}$$

Thus for the boom mounted sensors, the integrated gamma flux for 20 months is:

$0.485 \text{ mrad/hr} \times 1.44 \times 10^4 \text{ hours} = 6.9810 \times 10^3$ mrad, and the integrated neutron flux for 20 months is:

$$57.87 \frac{n}{cm^2\text{-sec}} \times 5.18 \times 10^7 \text{ seconds} = 3.00 \times 10^9 \text{ n/cm}^2.$$

Similarly:

$$36 \text{ months} = 2.59 \times 10^4 \text{ hours} = 9.34 \times 10^7 \text{ seconds.}$$

Thus, for the boom mounted sensors, the integrated gamma flux for 36 months is:

$$0.485 \text{ mrad/hr} \times 2.59 \times 10^{4} \text{ hours} = 1.256 \times 10^{4} \text{ mrad},$$

and the integrated neutron flux for 36 months is:

$$57.87 \frac{n}{cm^{2}\text{-sec}} \times 9.34 \times 10^{7} \text{ seconds} = 5.40 \times 10^{9} \frac{n}{cm^{2}}$$

At the baseplate center point, the integrated gamma flux for 20 months is:

$$3.425 \text{ mrad/hr} \times 2.59 \times 10^{4} \text{ hours} = 8.87 \times 10^{4} \text{ mrad}.$$

Similarly, at the baseplate center point, the integrated neutron flux for 20 months is:

$$409 \frac{n}{cm^{2}\text{-sec}} \times 5.18 \times 10^{7} \text{ seconds} = 2.12 \times 10^{10} \frac{n}{cm^{2}}$$

and for 36 months is:

$$409 \frac{n}{cm^{2}\text{-sec}} \times 9.34 \times 10^{7} \text{ seconds} = 3.82 \times 10^{10} \frac{n}{cm^{2}}$$

C. 3 REFERENCES

1. Schulz, R. B., "Radioisotope Thermoelectric Generator (RTG) for Improved ALSEP," Aerospace Systems Division, Bendix Corporation Report No. ETM-087, 18 June 1968.

"Power System Design for a Jupiter Solar Electric Propulsion Spacecraft," Jet Propulsion Laboratory Technical Report No. 32-1347, 15 Oct. 1968.

Francis, H. T., "Space Batteries Handbook," NASA Report No. SP-5004, 1964.

"Batteries Handbook," Yardney Silcade Co., 1968.

APPENDIX D
STRUCTURES

The standard adapter used to attach the craft to the TE-364 supports the craft at three points. To obtain a reasonable estimate of the forces transmitted to the cross-struts, it is necessary to assume that the load is distributed evenly among the four joints where the cross-struts meet the base plate. Assuming a loading of 20 G's (Reference 1) and a spacecraft weight of 462 lbs, the total load becomes:

$$20 \times 462 = 9240 \text{ lbs.}$$

Dividing the load among the four joints gives

$$\frac{9240}{4} = 2310 \text{ lb/joint}$$

The compressive force in the joint is found by considering the vertical components.

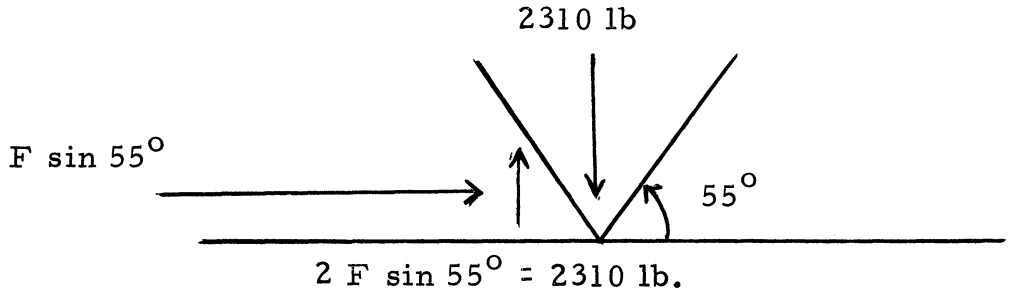

$$2 F \sin 55^\circ = 2310 \text{ lb.}$$

$$F = 1410 \text{ lb.}$$

Assuming that the elastic limit of 2024-T4 aluminum is 37,000 lb/in^2, then the minimum area of the cross-strut is

$$A_{min} = \frac{1410}{37,000} = 0.0381 \text{ in}^2.$$

The area of the actual strut is 0.075 in^2 giving a safety factor of 1.97 or 197%.

The critical modes of the craft in the dynamic sense are those where the spin rate is either 120 or 5 rpm. The speed of 5 rpm corresponds to the cruise mode. Therefore the forces due to this speed will be constant for most of the flight. The speed of 120 rpm corresponds to the spin-up mode for stabilization of the craft. The large accelerations incurred here may be damaging to the main structure. Those structural elements most

susceptable to damage from the radial accelerations are the booms and the dish. The large rpm occurs when the dish is in the stowed position, so the accelerations will not be large. The dish was therefore neglected. Considering the booms first in the deployed position;

RTG Booms

$a = rw^2$

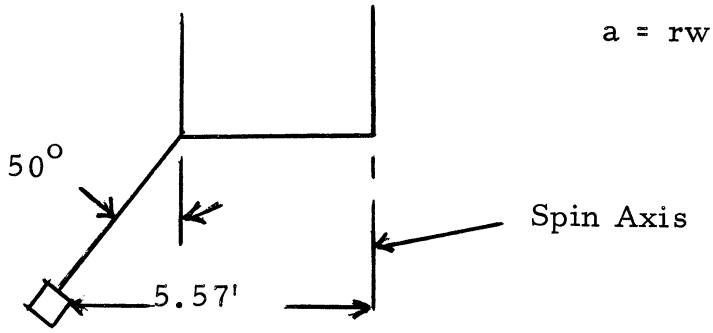

$a = (5.57)(0.273)/32.2 = 0.0471$ G's

Science Booms

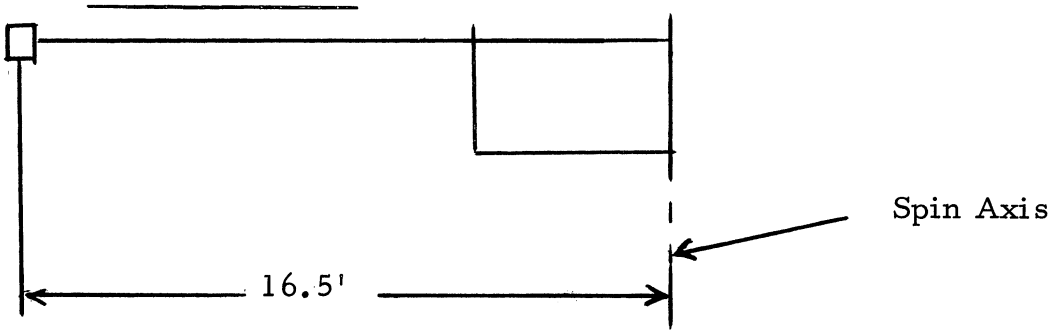

$a = (16.5)(0.273)/32.2 = 0.135$ G's

These small accelerations will cause extremely small forces and they may be neglected.

When the booms are in the stowed position, the speed is a maximum of 120 rpm. Following the same procedure as in the previous case;

RTG Booms

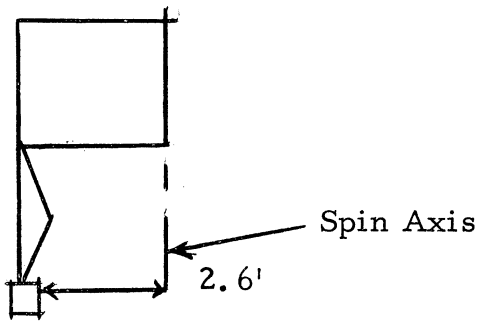

$a = (2.6)(159)/32.2 = 12.7$ G's

Science Booms

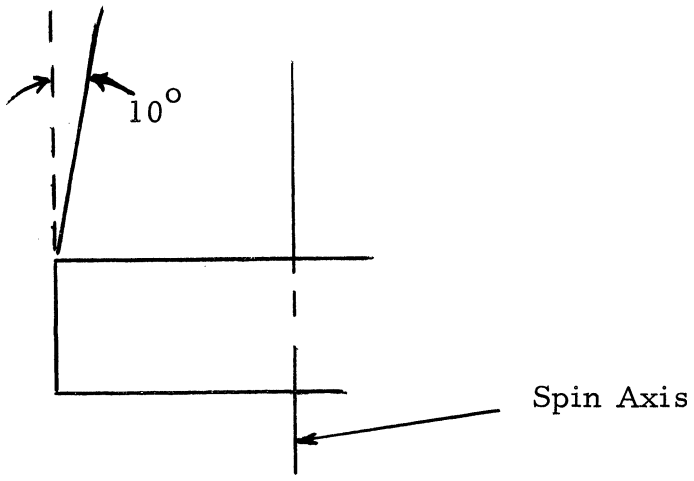

a = 12.7 G's

The acceleration on the science boom is the same because its angle from the vertical is very small (10 degrees). The forces here become significant. The force is, for the RTG's,

$$F = ma = 12.7 \times 30.5 = 388 \text{ lb.}$$

Thus the explosive mechanism restraining the RTG boom must withstand a tensile force of 388 lbs. The case for the science booms is similar. Existing mechanisms will withstand such forces and no problem is anticipated in this area.

REFERENCES

1. "Atlas Launch Vehicle Family for Spacecraft Contractor Planning," General Dynamics Report No. GDC BGJ 67-002, April 1967.

APPENDIX E
THERMAL CONTROL

E.1 NUMERICAL ANALYSIS OF THERMAL BALANCE EQUATION

$$Q_{in} = Q_{out}$$

with $Q_{in} = Q_{environ.} + Q_{internal} + Q_{conduction/RTG's} + Q_{radiation/RTG's}$

and $Q_{out} = Q_{radiation/spacecraft} + Q_{heat\ loss}$

With the use of superinsulation and insulation mounts, $Q_{environ.}$ and $Q_{conduction/RTG}$ may be neglected. Furthermore, $Q_{radiation/spacecraft}$ and $Q_{radiation/RTG}$ are reduced to include only that heat passing through the louvers.

$$Q_{internal} = 70 \text{ watts}$$

$$Q_{radiation/RTG} = Q_{RTG} \frac{1}{4\pi r^2} A_{p_{louver}} \alpha_L$$

where

Q_{RTG} = heat radiated from RTG's (watts)

r = distance from RTG to louver

A_{p_L} = projected area of louver as seen by RTG

α_L = effective admittance of RTG

Using three louvers located at the mid-radius of that corresponding to the RTG, this value becomes

$$Q_{radiation/RTG} = 3.3\ A_L\ \alpha_L \text{ watts}$$

$Q_{heat\ loss}$ = 5 watts at beginning of mission
25.5 watts at encounter (Reference 1)

$$Q_{radiation/spacecraft} = F \sigma T^4 A_L e_L$$

where

F = view factor of louvers (assumed equal to 1)

σ = Stefan-Boltzman Constant

T^4 = spacecraft design temperature

A_L = area of louvers

e_L = effective emittance of louvers

$$Q_{\text{radiation/spacecraft}} = 39.6\, A_L e_L \text{ watts}$$

Therefore, the thermal balance equation at beginning of mission becomes

$$70 - 5 = A_L(39.6\, e_L - 3.3\, \alpha_L)$$

or

$$A_L = \frac{65}{39.6\, e_L - 3.3\, \alpha_L}$$

Fully open, the louver e_L and α_L are 0.8. To allow a safety factor, the design was set for e and α = 0.7 at the beginning of the mission. Therefore,

$$A_L = 2.50 \text{ ft}^2$$

At encounter, $A_L = 2.50 \text{ ft}^2$ and the heat loss of 25.5 watts produces an α_L and e_L = .49. This also allows a great safety factor at encounter. For three louvers, totally 2.50 ft^2, each circular louver must have a radius of .51 feet.

E.2 CALCULATIONS BEHIND WEIGHT BUDGET

E.2.1 Temperature - Control Weight

a. Weight of louvers = 8 lbs.

b. Weight of superinsulation for main equipment compartment =

$$(\text{Surface Area})_{s/c}\ (\text{weight/ft}^2)_{50 \text{ shield Mylar}}$$

$$= 56.3\ (0.25)$$

$$= 14.1 \text{ lbs.}$$

$$\text{Surface Area} = \text{Area}_{\text{sides}} + \text{Area}_{\text{top}} + (A_{\text{bottom}} - A_{\text{louvers}})$$

$$= 2\pi rh + \pi r^2 + (\pi r^2 - 2.5)$$

$$= 2(3.14)(2.5)(1.25) + 3.14(2.5)^2 + 3.14(2.5)^2 - 2.5$$

$$= 56.3 \text{ ft}^2$$

or

$$5.23 \text{ m}^2$$

c. Weight of superinsulation for boom-mounted = 2 lbs (approx.)

d. Total weight of temperature control =

8.0 lbs for louvers
14.1 lbs for main compartment superinsulation
2.0 lbs for boom-mounted superinsulation
24.1 lbs

E.2.2 Micrometeoroid Protection Weight

a. Protection weight for louvers = 1 lb.

b. Foam for filler of bumper shied =

density of filler (surface area)$_{s/c}$ (width of filler)

= 1.2(56.3)(1.6)

= 11.3 lbs.

c. Weight of aluminum added

for .80 probability of zero puncture -

need $\bar{l}$ = 1.25 cm (Figure 7.3)

= .492 inches

Therefore,

$$.492 = \frac{l_1 + l_2}{K}$$

K = 0.2 for 2" bumper

$l_1 + l_2 = .0984$ inches of aluminum sheet needed

Weight of this sheet would be 33.6 lbs.

In finding the probability of zero puncture vs. additional spacecraft weight, various probabilities were chosen and the weights needed were calculated in a similar manner.

d. Total weight of meteoroid protection system

33.6 lbs for aluminum sheet
1.0 lb for louver protection
11.3 lbs for foam filler (Polyurethane)

45.9 lbs.

APPENDIX F
ATTITUDE CONTROL AND PROPULSION

F.1 SPACECRAFT DYNAMICS

The general discussion of Section 8.2 is here expanded for the proposed design. Orientation is controlled by two precessional thrusters of .5 pound thrust each. Depending on the point of firing in the rotation of the craft, as controlled by the sun sensor or RF signal, any desired change in the angular momentum vector (i.e., spin axis) can be made. The spin rate is maintained by the spin rate thrusters.

The body's principal axes are indicated by the indices 1, 2, 3, where 3 is the spin axis. The basic general relation of dynamics states that the total external torque equals the time rate of change of moment of momentum of the body; that is, $\bar{M} = \dot{\bar{H}}$. However, for torque free motion $\bar{M} = 0$, so that $\bar{H}$ must be constant, equal to $\bar{H}_o$. The body's center of gravity is the reference point for determination of $\bar{H}_o$.

If the body rotates about a principal axis, then the angular velocity and angular momentum are parallel and remain constant as long as there is no external moment. Consider an inertially symmetric body (i.e., $I_1 = I_2$). The basic Euler Equations apply to give

$$M_1 = I_1 \dot{\omega}_1 + (I_3 - I_2)\, \omega_2\, \omega_3$$

$$M_2 = I_2 \dot{\omega}_2 + (I_1 - I_3)\, \omega_3\, \omega_1$$

$$M_3 = I_3 \dot{\omega}_3 + (I_2 - I_1)\, \omega_1\, \omega_2$$

where M_i are the external torques in each principal direction. For torque free motion ($M_i = 0$) these reduce to

$$I_1 \dot{\omega}_1 = (I_1 - I_3)\, \omega_3\, \omega_2$$

$$I_2 \dot{\omega}_2 = -(I_1 - I_3)\, \omega_3\, \omega_1$$

$$I_3 \dot{\omega}_3 = 0$$

From the third, ω_3 = constant (i.e., spin rate is unchanged). Also the constant quantity

$$S = \frac{I_3 - I_1}{I_1}\, \omega_3 \text{ is introduced to give}$$

$$\dot{\omega}_1 = S\, \omega_2$$

$$\dot{\omega}_2 = -S\, \omega_1$$

from the Euler Equations. The general solution can be then given

$$\omega_1 = \omega_o \cos(\gamma - st)$$

$$\omega_2 = \omega_o \sin(\gamma - st)$$

where ω_o and γ are determined by initial conditions. This is represented in the body axis by Figure F.1. The resultant vector $\bar{\omega}$ traces out a circular cone as viewed from the body, and gives the instantaneous axis of rotation of the body coordinate system and magnitude of the rotation with respect to an inertial system.

In the inertial reference frame $\bar{H}_o$ lies in a plane through the 3 axis, which also contains $\bar{\omega}$. Thus, $\bar{H}_o$ also traces out a circular cone, centered on the 3 axis as viewed from the body. However, in the inertial frame $\bar{H}_o$ is fixed, so that the relation between the reference frames is now determined. In the inertial frame the 3 axis appears to trace out a circular cone about $\bar{H}_o$, as in Figure 8.2 of Section 8.2. The coning motion is called precession, with a precession rate of $\psi = |\bar{H}|/I_1$. To determine the change in orientation for each firing of the thrusters (so-called "precession step") first solve for $\bar{H}_o$, for the case where $\bar{H}$ lies along ω_3. Then $\bar{H}_o = I_3 \bar{\omega}_3$. Substituting the values ω_3 = 5 rpm = .523 rad/sec and I_3 = 256 slug-ft^2, get H_o = 134 slug-ft^2/sec.

The change in $\bar{H}$, $\overline{\Delta H}$, resulting from the precession thrusters is produced by an effective .1 sec pulse, fired so as to center the moment vector along the desired direction of orientation. The two .5 pound thrusters produce a moment $\bar{M} = 2(\bar{r} \times \bar{F})$ = (2)(2.5)(.5) ft-lb, so that M = 2.5 ft-lb perpendicular to $\bar{H}_o$. Now $\overline{\Delta H} = \bar{M}\,\Delta t$ (Figure F.2). Until the next pulse the motion is torque free so that $\bar{H} = \bar{H}_o + \overline{\Delta H}$ and the subsequent motion is a wobble of the 3 axis about the new $\bar{H}$ direction fixed at an inclination θ. The size of the precession step is $\tan^{-1} \Delta H/H_o = 0^o\ 7'$. The precession rate $\dot{\psi}$ = .735 rad/sec.

Energy consideration shows that θ can be reduced with time. Writing the angular momentum and kinetic energy

$$H^2 = I_1^2 \omega_1^2 + I_2^2 \omega_2^2 + I_3^2 \omega_3^2$$

$$T = \frac{1}{2}\left(I_1 \omega_1^2 + I_2 \omega_2^2 + I_3 \omega_3^2\right)$$

Combining and imposing $I_1 = I_2$, $H^2 - 2TI_1 = I_3(I_3 - I_1)\,\omega_3^2$ but $I_3 \omega_3 = H\cos\theta$ from Figure 8.1 of Section 8.2. Substituting, $H^2 - 2TI_1 = H^2/I_3(I_3 - I_1)\cos^2\theta$ and solving for $\dot{T}$, $\dot{T} = H^2/I_3\,(I_3/I_1 - 1)\,\dot{\theta} \sin\theta \cos\theta$.

It now becomes apparent that if $\dot{T} = 0$ (no energy dissipation) and $\dot{H} = 0$ (no external moment), then θ = constant. However, if I_3/I_1 were less than zero and $\dot{T}$ were less than zero, then $\dot{\theta} < 0$ and θ is reduced with time.

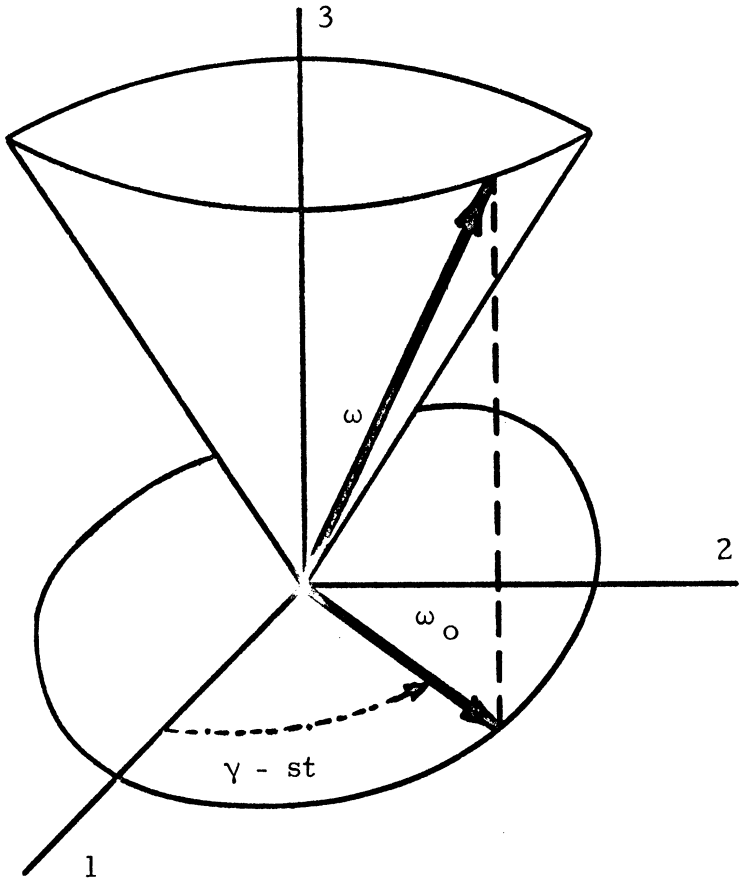

Figure F.1 Body Reference Coning Motion

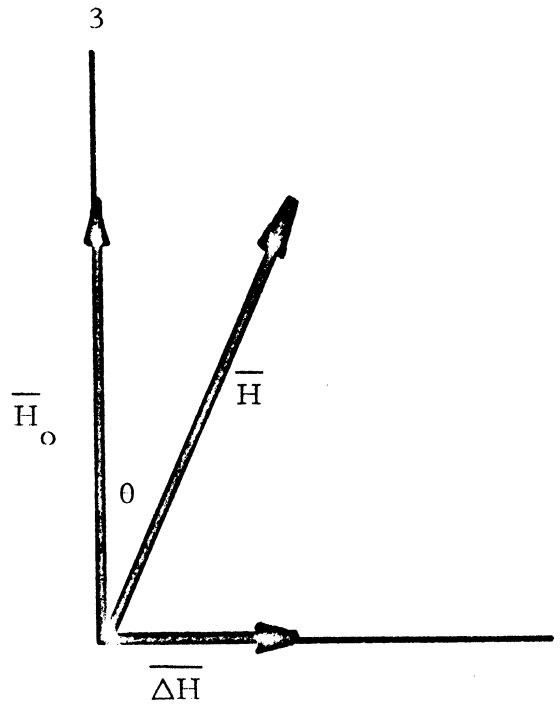

Figure F.2 Precession Angle

The influence of I_3/I_1 is also important in determining the maximum value of the wobble angle (Reference 3, Section 8).

$$\theta_{max} = \frac{1}{\sin\left(\frac{I_3}{I_1} - 1\right)\pi} \quad \frac{\Delta H}{H}$$

For $1.4 < I_3/I_1 < 1.6$ this gives θ_{max} minimum values as shown in Figure 8.2.

Energy dissipation is produced by three mechanical viscous fluid dampers located on the RTG booms. Though small in size (one pound each) they act to reduce the residual wobble to zero so that final pointing can be accomplished.

(References 3, 5, 6, 7, 8 in Section 8)

F.2 SPACECRAFT WEIGHT AND MOMENTS OF INERTIA

The following weight breakdown by system and location was used to determine gross weight and moments of inertia:

SUBSYSTEM	ITEM	WEIGHT(lb)	LOCATION
Science	Boom sensors	10.0	End of sensor booms
	Sensor	3.0	Antenna feed structure
	Instrumentation	38.5	Instrument package
	subtotal	51.5	
Communication	Main antenna	21.0	Antenna structure
	Antenna feed	29.0	Antenna feed structure
	Omni and helix anten.	5.3	Antenna feed structure
	Instrumentation	23.2	Instrument package
	subtotal	78.5	
Data Handling	Instrumentation	30.0	Instrument package
	subtotal	30.0	
Power	RTG	91.5	End of RTG booms
	Instrumentation	8.5	Instrument package
	subtotal	100.0	

Structures	Sensor booms	14.6	Sensor booms
	RTG booms	8.0	RTG booms
	Structure	45.4	Instrument package
	subtotal	68.0	
Thermal control and meteoroid protect.	Bumper shield	44.9	Instrument package
	Insulation	14.1	Instrument package
	Louvers	8.0	Instrument package
	Louver protection	1.0	Instrument package
	Insulation	2.0	Boom sensors
	subtotal	70.0	
Attitude control and propulsion	Fuel and Instrumentation	58.5	Instrument package
	Midcourse thruster	1.5	Antenna feed structure
	Dampers	4.0	RTG booms
	subtotal	64.0	
	TOTAL	462.0	

Spin moment of inertia I_3 = 256 slug-ft^2

Transverse moment of inertia I_1 = 182 slug-ft^2

Moment of inertia ratio I_3/I_1 = 1.41

Precession step size - 0^o 7' per pulse

APPENDIX G
TRAJECTORY ANALYSIS

Before meaningful calculations of the heliocentric parameters can proceed, it is necessary to accurately determine the semi-major axis of the transfer ellipse. The value of the semi-major axis, a, can be determined by graphical means or as the result of a numerical iterative process (Reference 1). In this report, a was determined from the standard plots of aphelion and perihelion vs C_3 and launch date, and was also verified graphically.

The method used for calculating the heliocentric position of the spacecraft was as follows:

$$a = \frac{R_p + R_A}{2}$$

$$R_p = 148.3 \times 10^6 \text{ km}$$

$$R_A = 1120 \times 10^6 \text{ km}$$

$$a = \frac{1268.3 \times 10^6}{2} = 634.15 \times 10^6 \text{ km}$$

$$\hat{R}_a = \hat{a}(1 + e)$$

$$\frac{\hat{R}_a}{\hat{a}} - 1 = e$$

$$\frac{1120 \times 10^6 \text{ km}}{634.15 \times 10^6 \text{ km}} - 1 = e$$

$$1.767 - 1 = e$$

$$.767 = e$$

This value of e is then used in the following formula

$$\frac{\hat{t}}{\hat{\tau}} = \frac{1}{2\pi} \left[\eta - e \sin \eta\right]$$

where $\hat{t}$ represents the nondimensional time of flight from the perigee to an arbitrary point, and η and θ are related by the following formulas

$$\eta = 2 \tan^{-1}\left\{\sqrt{\frac{1 - e}{1 + e}} \tan \frac{\theta}{2}\right\}$$

$$\sin \eta = \frac{\sqrt{1 - e^2}\ \sin \theta}{1 + e \cos \theta}$$

where

η = eccentric anomaly

θ = true anomaly

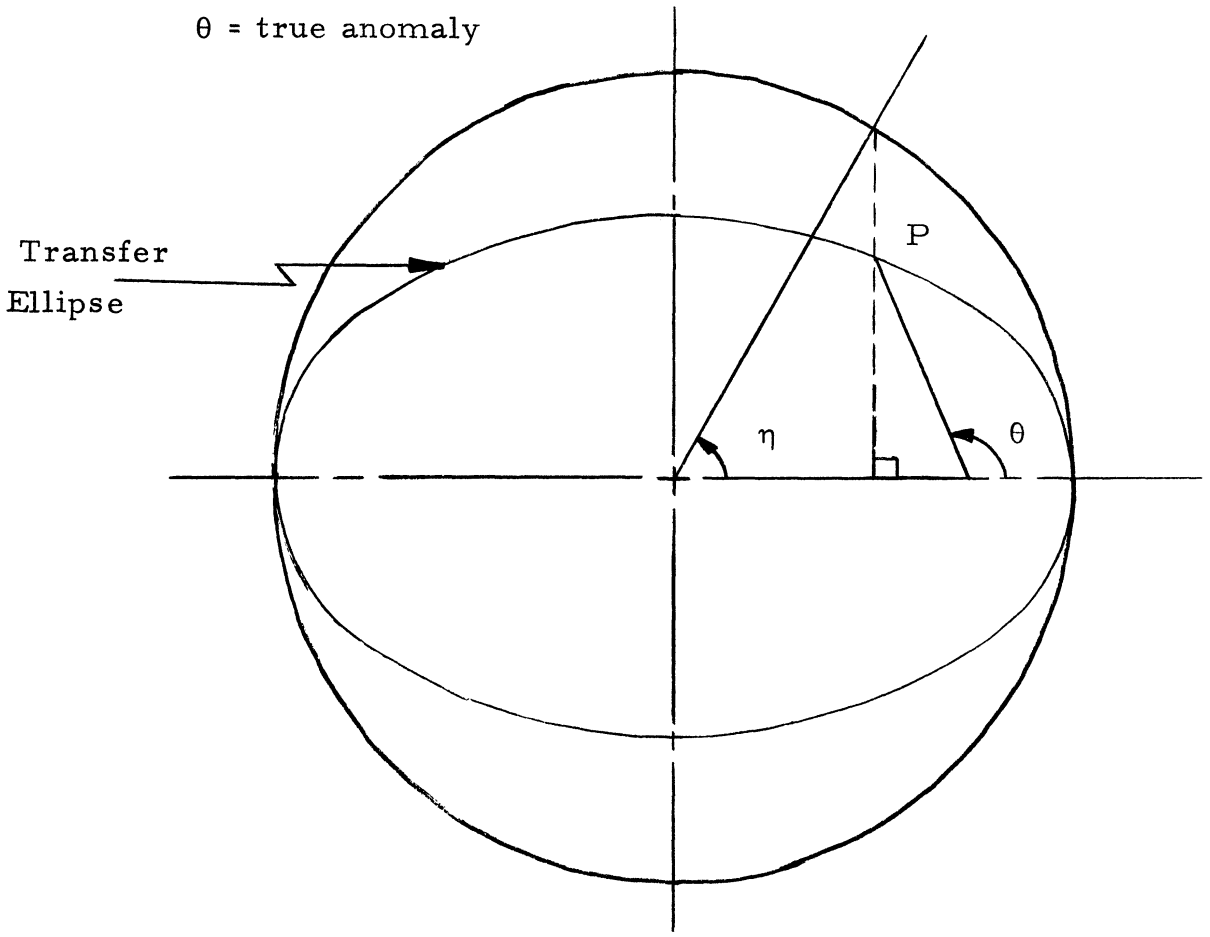

Spacecraft positions were determined from the graph of $\frac{e}{2\pi} \sin \eta$ vs $\frac{\eta}{2\pi}$, with $\frac{\hat{t}}{\hat{\tau}}$ as the variable.

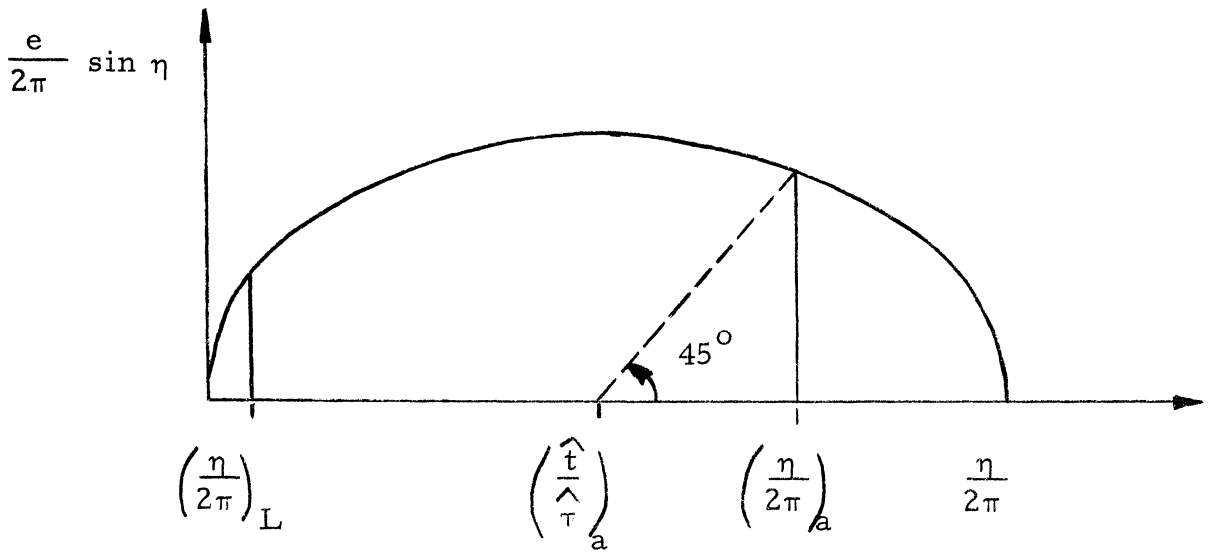

$\left(\frac{\eta}{2\pi}\right)_L$ = value of η at launch

$\left(\frac{\eta}{2\pi}\right)_a$ = value of η at arrival

$\left(\frac{\hat{t}}{\hat{\tau}}\right)_a$ = time of flight from perigee to arrival point

The zeocentric phase is considered to be the time that the spacecraft is within Jupiters sphere of influence so that the flight path is a hyperbola. The radius of Jupiter's sphere of influence, defined as the distance from Jupiter at which the force on the spacecraft due to Jupiter is equal to the force due to the sun, was calculated to be 324 Jupiter radii. Calculations used in this report were, however, performed within 100 Jupiter radii.

The following process utilizing nondimensional equations was used:

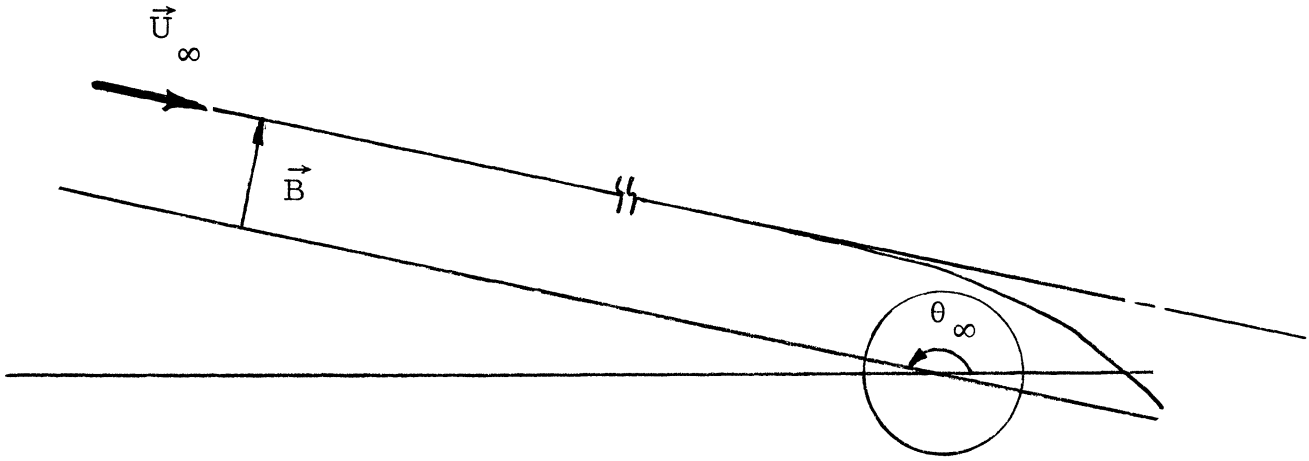

$$\hat{E} = \hat{U}^2 - \frac{2}{\hat{r}}$$

At ∞

$$\hat{E} = \hat{U}^2$$

$U_\infty = U_{hp} = 10.02$ km/sec

U_c = characteristic nondimensional quantity

= 42.1 km/sec

$$\hat{U} = \frac{10.02}{42.1} = .2371$$

$$\hat{U}^2 = \hat{E} = (.2371)^2 = .0562$$

Then for RCA = 5 R_J

Non-dimensionalized with respect to R_J

$$\hat{r}_p = 5$$

$$\hat{E} = \hat{U}_p^2 - \frac{2}{\hat{r}_p}$$

$$\hat{U}_p = \left[\hat{E} + \frac{2}{\hat{r}_p} \right]^{1/2}$$

$$\hat{U}_p = \left[.0562 + .4 \right]^{1/2}$$

$$\hat{U}_p = \left[.4562 \right]^{1/2}$$

$$\hat{U}_p = .6763$$

$$U_p = (.6763)(42.1 \text{ km/sec})$$

$$U_p = 28.42 \text{ km/se}$$

Next the impact parameter B is determined by

$$\hat{H} = \hat{U}_\infty \hat{B} = \hat{U} \hat{r} \cos \gamma$$

At perigee $\cos \gamma = 1$. So:

$$\hat{U}_\infty \hat{B} = \hat{U}_p \hat{r}_p$$

$$\hat{B} = \frac{\hat{U}_p \hat{r}_p}{U_\infty}$$

$$\hat{B} = \frac{(.6763)(5)}{.2371}$$

$$\hat{B} = 14.3$$

$$B = 14.3\ R_J$$

Knowing the impact parameter $\bar{B}$, the RCA, and the focus, the approach hyperbola is graphically constructed.

Using the energy formula, the velocity at various points on the hyperbola were calculated. Sufficiently small regions were chosen in order that a linear representation of the velocity within the region is an acceptable approximation. For the purpose of calculation the time of flight within a region, the velocity was considered to be constant at the linear average.

Within the geocentric phase, acceptable launch azimuths determined for various values of the declination of the geocentric asymptote were calculated from:

$$\sin^2 \Sigma_L \geq \frac{\cos^2 \phi_S}{\cos^2 \phi_L}$$

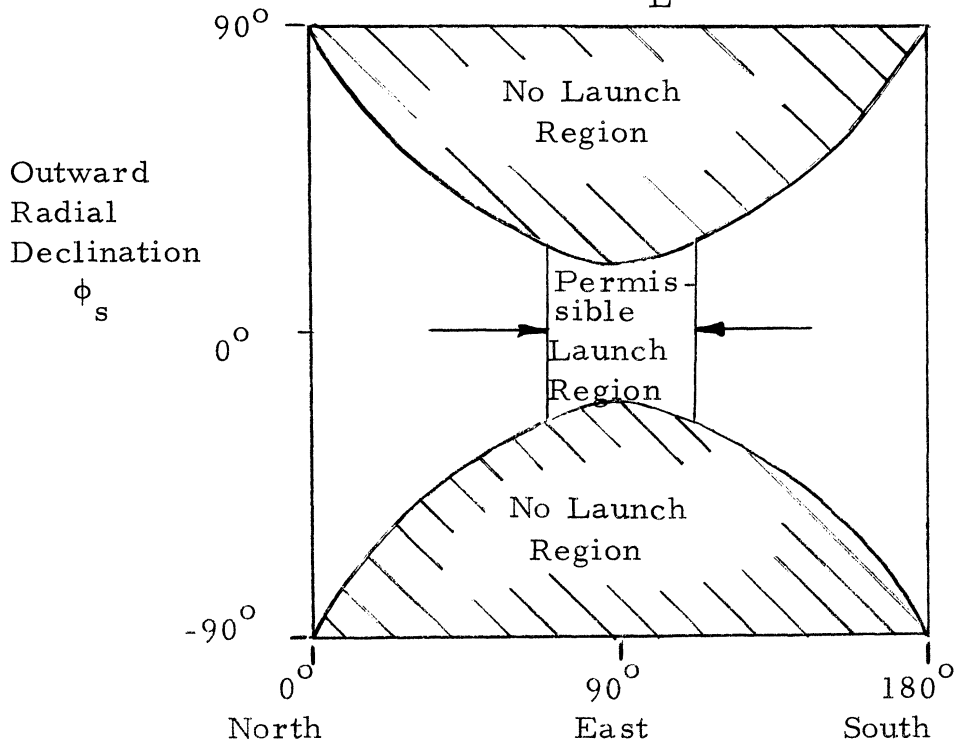

ACKNOWLEDGEMENTS

We would like to thank our lecturers for the expert advise and invaluable guidance which we received through them; in order of name, affiliation and lecture topic

Prof. Wilbur C. Nelson
The University of Michigan
"Introduction to Systems Design"

Mr. Donald Bianco
Bendix Aerospace Systems Division
"Approach to Systems Design"

Mr. Robert Peltzer
The University of Michigan
"U of M Experimental Proposal for a Jupiter Mission"

Mr. Jack Braithwaite
The University of Michigan
"Optical Scanning"

Prof. Harm Buning
The University of Michigan
"Trajectory Analysis"

Mr. R. B. Schulz
NAR, Atomics International
"Radioisotope Thermoelectric Generator"

Mr. L. Bauer
The University of Michigan
"Communication Systems Design"

Mr. R. J. Simms
Bendix Aerospace Systems Division
"Thermal Control"

Prof. George Haddad
The University of Michigan
"Travelling Wave Tubes"

Mr. John Niehoff
IITRI
"Resume of Galactic Probe Studies"

Mr. R. Gibson
Bendix Aerospace Systems Division
"Space Power Systems"

Mr. James Owens
Bendix Aerospace Systems Division
"Structural Systems Design"

Mr. William Haggerty
General Electric
"Radioisotope Thermoelectric Generators"

Mr. Emil Hymowitz
Goddard Space Flight Center
"Galactic Jupiter Probe Studies"

Prof. W. E. Britton
The University of Michigan
"Written Reports"

Prof. T. Sawyer
The University of Michigan
"Oral Reports"

We would also like to thank those who have allotted their time to us, individually, for detailed critique and recommendation. Data Handling would like to thank Mr. L. Bauer (The University of Michigan), Mr. R. Fatka (Bendix Aerospace), Mr. E. Hymowitz (Goddard Space Flight Center), and Mr. R. J. Treadwell (RCA, Astro-Electronics Division); Power thanks Mr. R. B. Schulz and Mr. R. Gibson (both from Bendix Aerospace); Trajectories would like to thank Prof. Buning (The University of Michigan); Thermal Control thanks Mr. R. J. Simms (Bendix Aerospace); and Communications would like to thank Prof. Rauch (The University of Michigan).

We would especially like to thank Prof. Wilbur C. Nelson for his interest, devotion, and guidance throughout Project UMPIRE. We are grateful for the excellent job done by Caroline Rehberg in typing the UMPIRE report.

The cover of UMPIRE was designed by Jose Canadas.

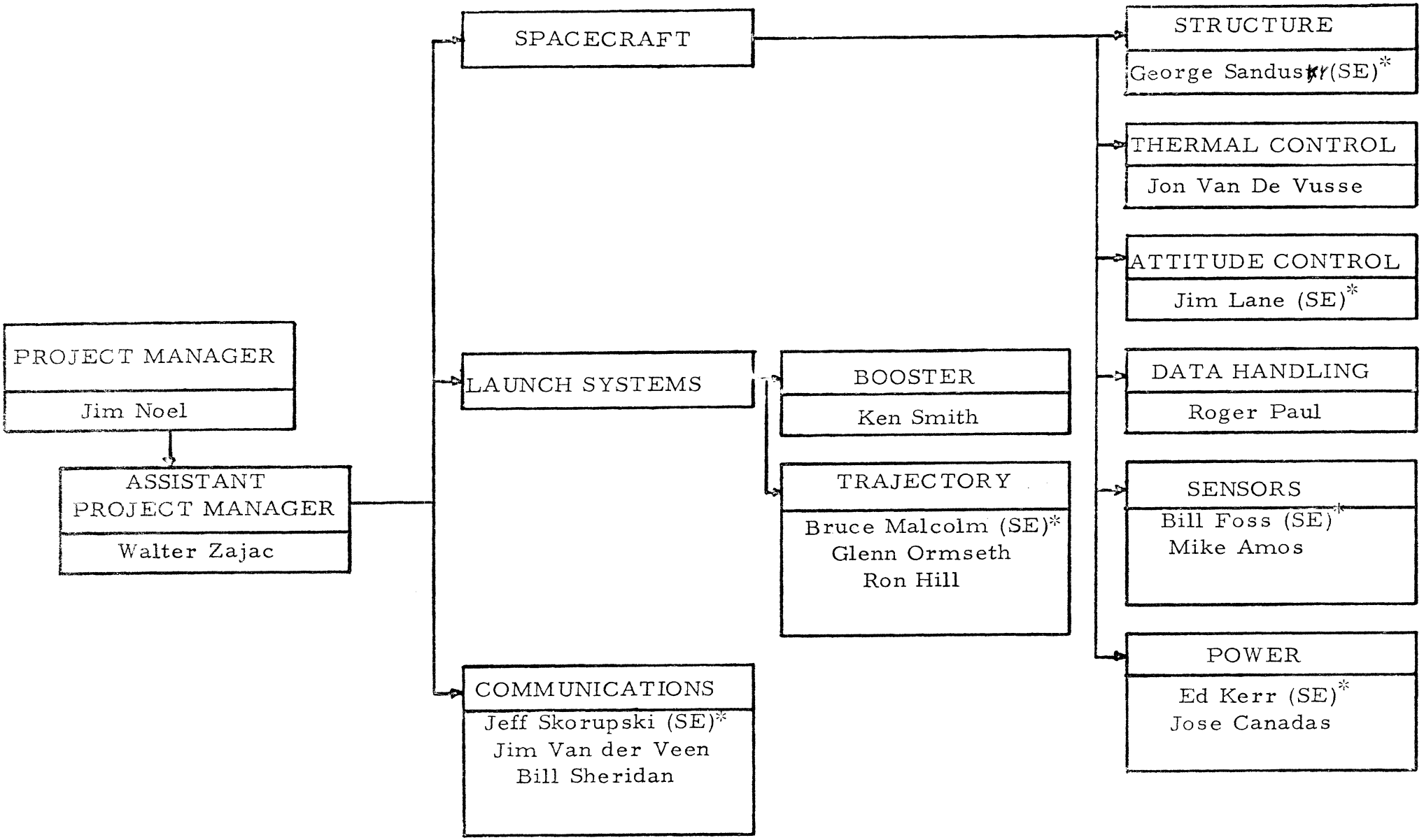

Project Personnel Chart *SE-System Engineer